2014-01-30

Simulation Study of Steam-Solvent Phase Behaviour in Solvent Aided SAGD Process and Its Effect on Oil Recovery

Ji, Dongqi

UNIVERSITY OF CALGARY

Simulation Study of Steam-Solvent Phase Behaviour in Solvent Aided SAGD Process and Its Effect on Oil Recovery

by

Dongqi Ji

A THESIS

SUBMITTED TO THE FACULTY OF GRADUATE STUDIES

IN PARTIAL FULFILMENT OF THE REQUIREMENTS FOR THE

DEGREE OF MASTER OF SCIENCE

DEPARTMENT OF CHEMICAL AND PETROLEUM ENGINEERING

CALGARY, ALBERTA

JANUARY, 2014

Abstract

In solvent aided Steam-Assisted Gravity Drainage (SAGD), steam-solvent injection, which is a different process from that of a pure-steam process, significantly affects the steam-solvent phase behavior near the vapor-liquid interface.

In this thesis, the phase behavior of the steam-solvent-bitumen system is studied in detail through simulation. It is discovered that solvent is dissolved in oil by gas-oil equilibrium near the vapor-liquid interface, rather than the mixing of bitumen and solvent condensate. The dissolved solvent is convectively delivered to the oil sand through the gravity drainage process, rather than the process of diffusion or dispersion. The effects of the solvent injection concentration and injection pressure on steam-solvent-bitumen behavior are analyzed. In addition, this study proposes a steam-solvent injection strategy to improve solvent aided SAGD performance through analysis of solvent concentration, pressure, solvent-type and solvent injection start time.

Acknowledgements

I would like to show my utmost gratitude and thankfulness to my supervisor Dr. Mingzhe Dong, for his helpful guidance and great support at each stage of my studies at University of Calgary.

I am also grateful to Dr. Zhaowen Li for his valuable suggestions and assistance regarding my thesis research.

I would like to thank to my group members, Mr. Ziqiang Guo, Mr. Yanghong Liu, Mr. Guanli Shu, Mr. Shams Mehdi and Mr. Wei Zhou. They are involved in the day-to-day life in the office, where we learn from each other.

Last but not least, thanks to all my friends for making my time at University of Calgary enjoyable.

Dedication

To my parents,

I wish to express my deep appreciation for their unconditional support and eternal love throughout my life.

Table of Contents

List of Tables

List of Figures and Illustrations

List of Symbols, Abbreviations and Nomenclature

Symbols

μ	Dynamic viscosity	cp
ν	Kinematic viscosity	m^2/s
T	Temperature	℃
q	Volumetric flow rate	m^3/s
$\emptyset$	Porosity	%
ΔS_o	Difference of initial oil saturation and residual oil saturation	%
k	Absolute permeability	$darcy$
g	Gravitational acceleration	m^2/s
h	Pay thickness	m
m	Oil viscosity temperature relationship parameter	Dimensionless
α	Thermal diffusivity of reservoir	m^2/s
L	Liquidity	Dimensionless
ρ	Density	kg/m^3
V	Volume	m^3
v_i	Geometric mean of mass and mole fractions of component i	Dimensionless
k_i	K-value of component i	Dimensionless
J_{ijk}	Flux of component i through j phase in k direction	m^3/s
H	Enthalpy	KJ/kg
C	Heat capacity	$J/(m^3 * K)$
G	Gravity force	N
F_i	Component force	N
v_i	Component velocity	m/s
ξ	Distance	m
D	Diffusion coefficient	m^2/s
U	Vapor-liquid interface advance velocity	m/s
C_s	Solvent concentration	$mole/m^3$

Subscripts

o	Oil
w	Water
G	Gas
s	Solvent

Abbreviations

ERCB	Energy Resource Conservation Board
SAGD	Steam-Assisted Gravity Drainage
cSOR	Cumulative Steam-to-Oil Ratio
CWE	Cold Water Equivalents
CSS	Cyclic Steam Stimulation
ASTM	American Society for Testing and Materials
GCOS	Great Canadian Oil Sands Ltd.,

CHAPTER ONE: INTRODUCTION

1.1 Overview

The International Energy Outlook (2013) reports that the worldwide consumption of petroleum and other liquid fluids is increasing quickly. The released data predicts the consumption of oil will increase from 87 million barrels per day in 2010 to 97 million barrels per day in 2020 and 115 million barrels per day in 2040. In addition, World Energy Outlook (2012) published by the International Energy Agency shows there is a tendency toward change of oil mix from conventional oil to unconventional oil from 1990 to 2035. In 2009, conventional accounted for 80% of global oil consumption, whereas unconventional oil (heavy oil and bitumen) only supplied 3% of the total amount. Nevertheless, it is forecast that unconventional oil will supply 10% of the total oil requirement in 2035. Thus, unconventional oil is regarded as the alternative energy source for the rapidly increasing energy consumption around the world.

In the report from World Energy Council (2010), Canada is one of the largest bitumen producers at an estimated 176.8 billion barrels, in reserve. In Canada, oil sand is mainly found in the providence of Alberta. The Energy Resource Conservation Board (ERCB, 2012) also predicts that bitumen production in Alberta will make up 88% of the total oil supply from Canada in 2017. Worldwide, Alberta ranks third, after Saudi Arabia and Venezuela, for the amount of proven oil reserves, which is shown in Figure 1.1.

Figure 1.2 shows that oil sand reservoirs include Athabasca, Cold Lake and Peace River; in northeast Alberta. In 2011, bitumen production in Alberta had over 1.7 million bbl/d. It is predicted that in 2021 this amount will be 3.7 million bbl/d.

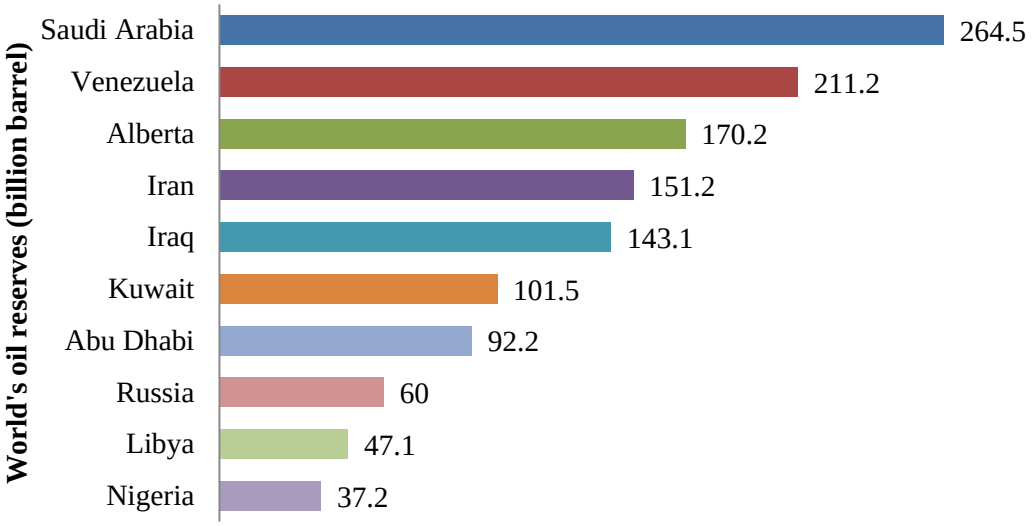

Figure 1.1: World's largest oil reserves (proven reserve) in 2011 (ERCB, 2012). The total oil reserve in Alberta is 170.2 billion bbl, of which bitumen occupies 168.7 billion bbl and conventional oil for 1.5 billion bbl.

Figure 1.2: Location of the Athabasca, Cold Lake and Peace River oil sands in Alberta (Alberta Geological Survey, 2011).

The most important property of in-situ bitumen is its significantly high viscosity. The effect of viscosity reduction by elevated temperature (Figure 1.3) is utilized in bitumen recovery. In typical oil sand reservoir conditions (typically from 7 to 11℃), viscosity of bitumen is over 1.0 million cP. When temperature is increased beyond 196 ℃, the viscosity is rapidly reduced to lower than 10 cP (Gates and Chakrabarty, 2008).

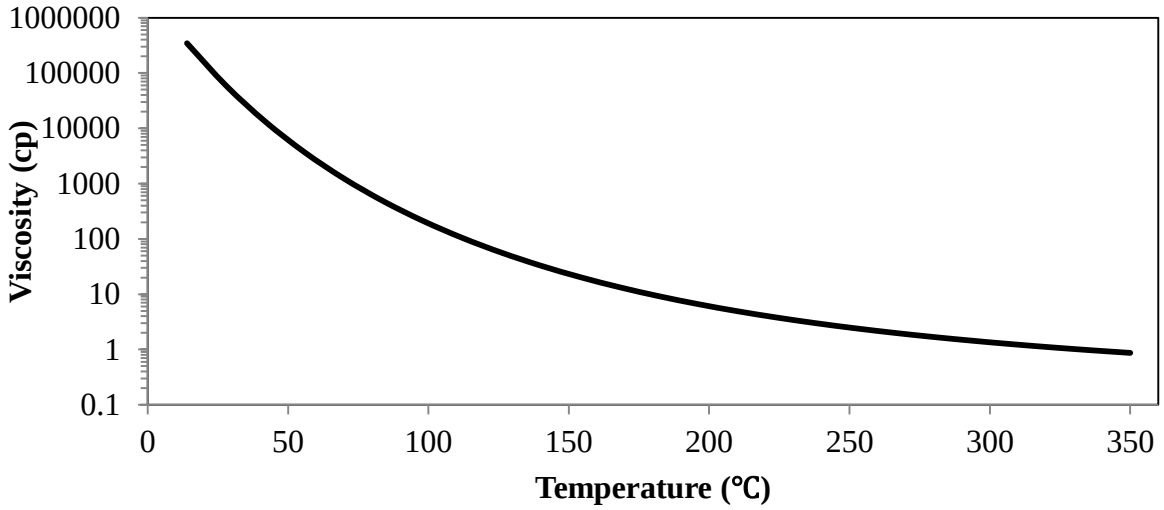

Figure 1.3: The relationship of oil viscosity and temperature (Khan et al., 1984).

In Alberta, bitumen is being recovered in two ways: for shallow oil sands (lower than 75 m), it can be mined and delivered to the refinery by truck; for the oil sand buried further beneath the surface, in-situ recovery methods are preferable in order to extract bitumen (ERCB, 2011).

Of all the in-situ thermal oil recovery methods, Steam-Assisted Gravity Drainage (SAGD), which was proposed by Butler and his colleagues thirty years ago (Butler, 1998), is considered the most promising and commercially viable method of bitumen recovery. Half of the bitumen production in Alberta is achieved through SAGD (ERCB, 2010). SAGD consists of a pair of horizontal wells drilled into formation, as the schematic shows in Figure 1.4. For typical SAGD,

a production well is located 2 m above the base of the reservoir, and an injection well is drilled parallel above the production well. The distance between the two wells is approximately 5m (Butler, 1997). Steam is introduced into the reservoir through the injection well, and a steam chamber is formed within the formation at saturated steam temperature. Steam flows into the steam chamber and condenses in the contact with the cold oil sand at the vapor-liquid interface. The latent heat of the steam transfers to the surrounding formations and mobilizes bitumen. The heated oil and condensate flow to the production well through gravity. As the oil is removed, the pore space is occupied by the injected steam (Butler, 1994).

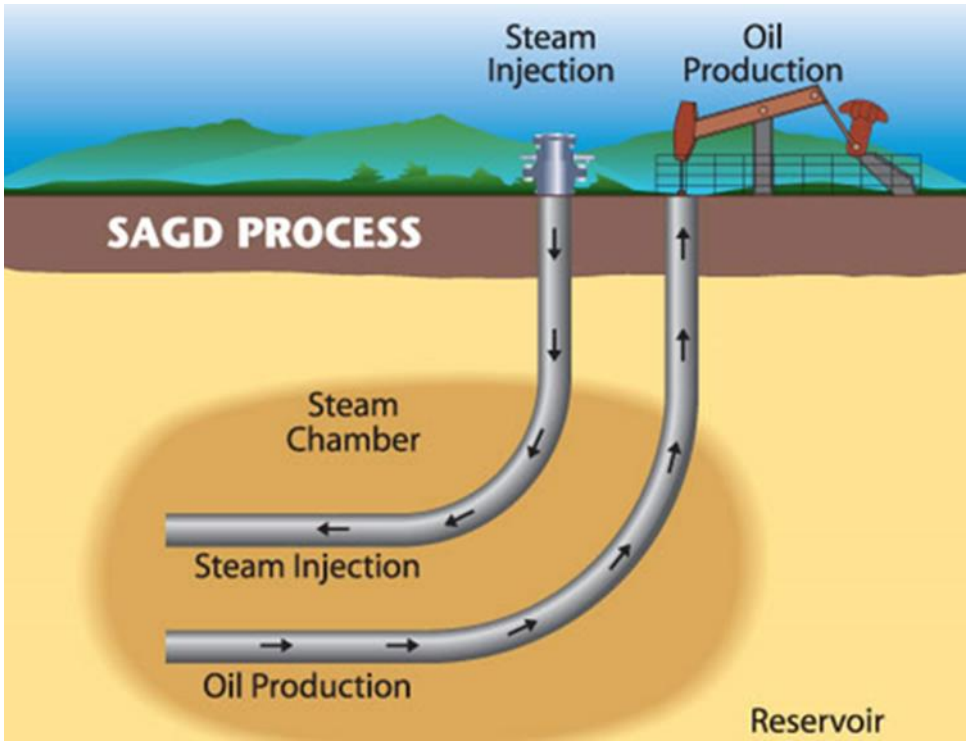

Figure 1.4: Schematics of SAGD process (Canadian Center for Energy Information, 2013).

Although SAGD is commercially implemented in Alberta, the main cost of the process is extensive steam consumption, which is generated by natural gas combustion. Typically, SAGD requires 28m^3 of natural gas and 2.5 to 4.0 barrels of water to recover 1 barrel of bitumen, as summarized in Alberta Geological Survey (2012). The main cost of the SAGD process is the extensive steam consumption and it is measured by Cumulative Steam-to-Oil ratio (cSOR) in Cold Water Equivalents (CWE). The cSOR indicates the amount of consumed steam for unit-produced bitumen. It is demonstrated that heavy oil or bitumen can be produced at 100 to 400 m^3/day with the cSOR varying from 2 to 10m^3/m^3 (Butler, 1998).

To reduce energy and water intensity, injection of a hydrocarbon additive at low concentration with steam into the reservoir is proposed by Nasr et al. (2003). Both solvent dissolution and heat dilution in bitumen viscosity reduction are utilized. At the injection well, solvent is vaporized under the condition of saturated steam and is delivered into reservoir. At the vapor-liquid interface, the solvent dissolves in oil and aids in decreasing oil viscosity. The effect of solvent dilution on oil viscosity is apparent according to Shu's correlation (1984). At 100℃, the viscosity of bitumen is approximately 200 cP. When the C6 mole fraction is higher than 0.48, the viscosity of the solvent-bitumen mixture below 10 cP can be achieved at the same temperature. As a result, the oil production rate is effectively enhanced, with a lowered water requirement, lower usage of natural gas, and emission of greenhouse gas to the atmosphere (Nasr and Ayodele, 2006).

1.2 Problem Statement

For bitumen recovery, solvent additive in injected steam is an effective method for increasing the oil production rate and decreasing steam consumption in the process. However, addition of solvent in vapor results in a more complex process. Few studies have been done on gas-oil equilibrium in the steam-solvent-bitumen system. In particular, there is little information available regarding dissolution in oil in an equilibrium state in the thermal-solvent gravity drainage process. Previous studies showed that hydrocarbon additives with similar saturation properties to steam should be used. At the vapor-liquid interface, solvent condenses with steam. Oil viscosity is reduced by the mixing of solvent condensate and bitumen (Nasr et al, 2003; Nasr and Ayodele, 2006; Li and Mamora, 2011; Ardali et al., 2011; Jha et al., 2012; Edmunds, 2013). However, Dong (2012) investigated the phase behavior of the steam-solvent system and proposed an algorithm to estimate the equilibrium temperature and solvent fraction in vapor at the vapor-liquid interface. It was shown that in a large range of solvent fraction in vapor, steam condenses first from vapor. The condensation of solvent can occur only when the solvent concentration in vapor phase is extremely high. As shown in Figure 1.5, under 2000 kPa, first condensation occurs at 213 ℃ for steam from a mixture which contains 0.03 mole fraction of C6 and 0.97 mole fraction of steam. It was also found that the solvent fraction in vapor increases as steam condenses, through heat transfer to cold oil sands. The point of lowest temperature of vapor at the vapor-liquid interface can be reached. For heavier solvents, there is a lower solvent concentration and a higher temperature at the interface compared to lighter solvents (Dong, 2012). Thus, there is a need for improved understanding of solvent dissolution in oil near the vapor-liquid interface.

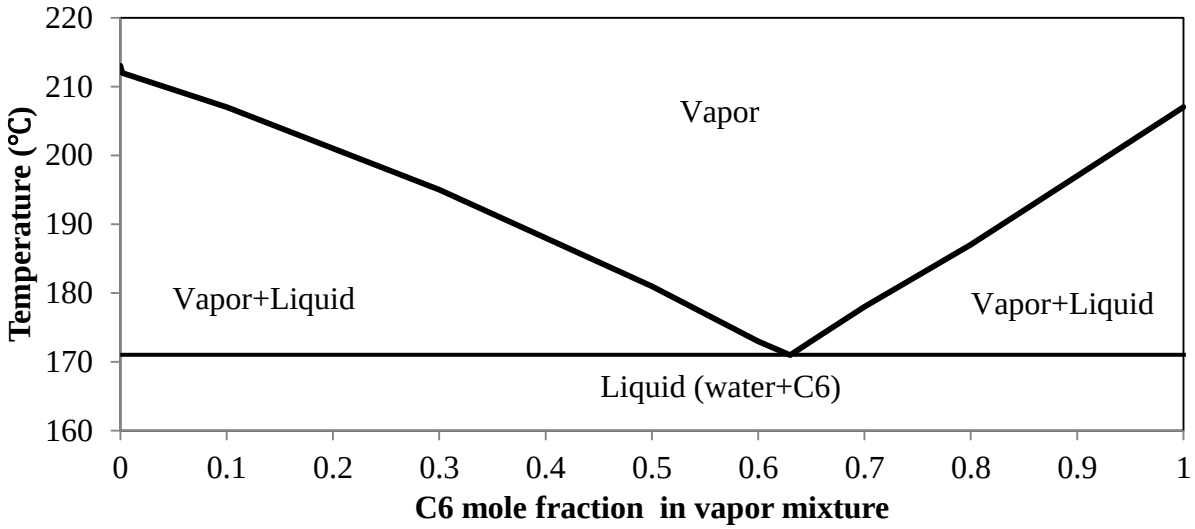

Figure 1.5: Condensation temperature of steam and solvent mixture at 2000 kPa as a function of solvent mole fraction (Dong, 2012).

Furthermore, detailed studies of the mechanism of solvent distribution in the mobile oil zone are scarce. The diffusion of solvent in bitumen was suggested as a method for transporting solvent beyond the steam chamber in previous studies (Ardali et al., 2010; Sharma and Gates, 2010; Keshavarz et al., 2013). However, solvent diffusion in oil, which is a very slow process, cannot deliver much solvent to oil sand under the fast growing steam chamber (Perkins and Johnston, 1963). Simulation studies also showed there was little effect on oil production by varying the solvent diffusion coefficient (Ivory et al, 2008). Furthermore, analysis of solvent dispersivity in oil reveals a very small effect on solvent aided SAGD production performance (Deng et al., 2010). The understanding of solvent distribution in the mobile oil zone also needs to be studied further.

Thus, a comprehensive study of the solvent-steam-bitumen system is necessary for understanding of the mechanism involved in improving SAGD by solvent addition. In this study, a method for solvent dissolution in bitumen near the vapor-liquid interface is identified. To

illustrate this process, the properties of distribution including, temperature, gas phase composition, oil phase composition, oil and water saturation, oil viscosity and oil flow rate were analyzed over the distance near the vapor-liquid interface. Figures show important phenomena occurring in the regions near the interface and their consequences for oil flow. The solvent distribution and solvent mass transfer in the mobile oil zone were also investigated, through reservoir simulation. Furthermore, the effect of operation parameters such as solvent injection concentration, steam injection pressure and solvent-type selection were studied to determine how the process is affected by changing these parameters.

1.3 Objectives of Study

The focus of this study is to gain understanding of the mechanism involved in solvent aided SAGD, based on the analysis of steam-solvent phase behavior and solvent mass transfer method. To meet this goal, specific objectives are proposed as follows:

1) Develop a numerical simulation model to exhibit the effect of solvent addition on SAGD by comparison of the solvent aided process and the pure-steam process.
2) Study the key parameters which govern solvent dissolution and transfer in mobile oil in the solvent aided SAGD process.
3) Conduct reservoir simulation to investigate the effect of operating parameters, such as solvent injection concentration, pressure, solvent-type and solvent injection start time on solvent aided SAGD.
4) Evaluate a new solvent injection strategy to improve solvent aided SAGD performance.

1.4 Organization of Thesis

This thesis consists of six chapters as follows:

Chapter Two Contains a literature survey on mechanisms, including steam chamber growth, bitumen viscosity reduction, heat transfer and oil flow in SAGD. The effects of the start-up procedure, steam trap control and pressure on SAGD performance are also reviewed. For solvent aided SAGD, steam-solvent vapor temperature and bitumen-solvent viscosity have been surveyed to understand mechanisms in the steam-solvent process. The effects of solvent-type, pressure and solvent concentration on solvent aided SAGD are also researched. Furthermore, studies of phase behavior in a steam-solvent binary system and solvent mass transfer in oil are reviewed.

Chapter Three In this chapter, a description of the SAGD process is presented. Gas saturation, oil saturation and water saturation, temperature, oil viscosity and oil flow rate are analyzed near the vapor-liquid interface to illustrate the oil flow mechanism. A description of the SAGD process is recorded in this study to establish a reference for comparison with solvent aided SAGD to illustrate our investigation.

Chapter Four In this chapter, investigation of the solvent aided SAGD process is presented. The method of solvent dissolution in oil is determined through phase behavior analysis of the steam-solvent-bitumen system. Furthermore, solvent transfer in oil is studied by the comparison of solvent diffusion and convection in the oil phase.

Chapter Five In this chapter, the effects of solvent concentration, pressure and solvent-type on the solvent aided SAGD process are identified. Performance of solvent addition during vertical steam chamber growth is also analyzed. Furthermore, an interval solvent injection strategy has

been implemented to identify its effect on bitumen production. Finally, one steam-solvent injection strategy is proposed to improve this process.

Chapter Six This chapter summarizes the major conclusions and recommendations from the studies in this thesis.

CHAPTER TWO: LITERATURE REVIEW

2.1 Thermal Oil Recovery Methods

The most popular method for bitumen recovery is the thermal process, in which steam is injected into a reservoir to heat bitumen and lower its viscosity sufficiently to enable oil flow to a production well. These thermal methods consist mainly of: Cyclic Steam Stimulation (CSS), steam flood and SAGD (Alberta's Oil Sands, 2008).

In CSS, steam is injected into a target reservoir for several weeks at the highest possible rate to minimize heat loss and then shut in the injection well for a soaking period to heat rock and fluids in the vicinity of the wellbore by partial condensation of the injected steam. After soaking, heated oil and water are produced from the depleted zone. Oil viscosity is lowered and production force is supplied by initial reservoir pressure, gravity drive, compaction and solution gas drive (Farouq-Ali, 1974). There are several recovery mechanisms that alternate with cycle numbers. Production under gravity drainage may not fluctuate much from cycle to cycle, but late cycles may be less effective when driving force is supplied by solution gas expansion. Heat loss is also a primary challenge in the CSS process (Sylvester and Chen, 1988). Increased heat loss becomes increasingly important as time passes during production and leads to gradual oil rate decline. Another cause of CSS failure is casing or tubing damage during steam injection at high pressure, especially for reservoirs deeper than 2000 ft. The higher the injection pressure, the higher the injection temperature corresponding to saturated steam properties. Thus, thermal expansion of casings and high temperatures also result in cement failure.

Steam flood is a complex displacement process which includes a series of mechanisms. Laboratory and field tests have identified these mechanisms as the following: steam drive, in-situ light oil drive, oil and water viscosity reduction, thermal permeability and capillary pressure

variations, thermal expansion, solution gas drive, emulsion drive and gravity segregation (Wu, 1977). In the steam flood process, overlay is demonstrated as a common phenomenon by previous field projects (Vogel, 1984). Most of the reports identify that steam breakthrough within one or two months after steam injection, which resulted from steam overlay. Furthermore, steam flowing to the top of the reservoir directly decreased heat efficiency through additional heat loss to overburden.

Different from CSS and steam flood methods, SAGD exhibits continuous production and high oil recovery factors. For thick and high permeability bitumen reservoirs, Butler and his colleagues proposed SAGD 30 years ago. To take advantage of temperature effects and gravity drainage, SAGD is used as an in-situ bitumen recovery method. During the injection process, production is mainly from the vapor-liquid interface, where hot steam encounters cold bitumen, based on the development of steam chamber (Albahlani and Babadagli 2008).

2.2 Mechanisms in SAGD Process

In order to have an understanding of SAGD, the mechanisms involved in SAGD are summarized in the following parts, which have been thoroughly discussed in the literatures.

2.2.1 Growth of Steam Chamber

In SAGD, steam flows through rock within the steam chamber and condenses at the vapor-liquid interface. Since most of the oil production is from the area near the sloped interface, growth and characteristics of steam chambers are critical to successful SAGD. However, there no complete observation for processes, including co-current and counter-current flow, water imbibition, oil-water emulsion and steam fingering (Albahlani and Babadagli, 2008). Generally in this process,

steam flows upwards from the base of the reservoir and oil drainage allows rise of the steam chamber (Butler, 1987). Initially, the steam chamber rises vertically and starts to grow laterally once it reaches overburden of the reservoir (Ito and Ipek, 2005). Furthermore, analysis of 4-D cross-well seismic images of steam chamber growth, steam sweep efficiency and spatial distribution of a heated reservoir showed that the geological heterogeneities have great effect on growth of the steam chamber (Zhang et al., 2007). Steam conformance of SAGD can be improved by a dynamic control algorithm. Associated parameters such as the temperature difference between injected steam and produced liquid were developed to ensure steam delivery to target regions in the reservoir (Gotawala and Gates, 2012). Recent understanding of SAGD indicated a liquid pool separates the steam chamber and the production well (Gates and Leskiw, 2005).

2.2.2 The Relationship Between Bitumen Viscosity and Temperature

Oil viscosity variance with changing temperature has great importance in thermal oil recovery processes, since viscosity determines oil phase mobility. Some studies have predicted oil viscosity change as a function of temperature through matching of numerical correlation parameters with experimental results.

The most useful correlations for viscosity-temperature, out of more than 100 published equations, are summarized in Table 2.1. The first, called the Andrade equation predicts viscosity in the range up to the boiling point of specific liquid. It can be seen in the equation that the values of a and b can be determined given two-pair values of viscosity μ_1 at temperature T_1 and viscosity μ_2 at temperature T_2. Later in 1933, Walther first proposed the idea of plotting $log_{10}[log_{10}(v)]$ versus $log_{10}T$. In the same year, he modified this correlation to $log_{10}[log_{10}(v + 0.8)]$ as a

function of $log_{10}(T)$. In this method, two values of viscosity μ_1 at temperature T_1 and μ_2 at temperature T_2 are required to determine the constant n. Furthermore, oil density under different temperatures is also required, which should be obtained through conducting experiments. For practical use, American Society for Testing and Materials (ASTM) graphs are widely used by engineers to plot the curve of viscosity-temperature based on Walther's work. The basic ASTM graph was formed by calculating $log_{10}[log_{10}(\nu + 0.7)]$ as a function of temperature, which was done by Wright in 1965. Although the ASTM graph is popular for finding oil viscosity under different temperatures, it is inconvenient for petroleum engineers since oil viscosity is presented in centistoke in the graph but not centipoise. In 1988, Svrcek and Mehrotra showed the relationship between oil viscosity and temperature in centipoise over a temperature range from 13 to 130 ℃. It is easier to determine oil viscosity with only one parameter b'. Based on measurements of bitumen in Alberta, this correlation can be extended to other bitumen to provide the relationship between viscosity and temperature.

Table 2.1: Most useful correlations for predicting oil viscosity with change of temperature.

Oil viscosity model	Comments	References
$\mu = ae^{\frac{b}{T}}$	μ in cP, T in $K = ℃ + 273.15$, a and b are constants.	Andrade (1930)
$log_{10}[log_{10}(\nu + 0.8)] = -nlog_{10}log_{10}\left(\frac{T}{T_1}\right) + log_{10}[log_{10}(\nu_1 + 0.8)]$	ν is kinematic viscosity in cs, ν_1 is known viscosity under temperature of T_1.	Walther (1933)
$log_{10}[log_{10}(\nu + 0.7)] = mlog_{10}(T + 273) + b$	ν is kinematic viscosity in cs, $T$is temperature in ℃. m and b are constants for specific oil.	Wright (1965)
$log_{10}[log_{10}(\mu + 0.7)] = b' - 3.63029log_{10}(T + 273)$	μ is kinematic viscosity in cP, $T$is temperature in ℃. b' is constant for specific oil.	Svrcek and Mehrotra (1988)

2.2.3 Effect of Oil Viscosity Heterogeneity

In reality, oil viscosity naturally varies in heavy oil reservoirs. Oil viscosity tends to increase with increased deposition depth of crude oil in one formation. For instance, oil samples from Clearwater B formation in east central Alberta show various viscosities with changes in depth (Erno et al, 1991). It was also confirmed by Li et al. (2008) that oil viscosity at the top of reservoir was much lower than the viscosity at the bottom. Through reservoir simulation, SAGD performance deteriorated with viscosity variation (Gates et al, 2008). However, numerical analysis showed that the effect of vertical viscosity gradients on cumulative oil recovery was not significant (Chen and Ito, 2012).

2.2.4 Heat (Energy) Transfer and Distribution

It is critical to understand heat transfer and distribution through the steam chamber to cold oil sand in the SAGD process, since oil is mobilized by delivered heat. Additionally, conformances of the steam chamber and heat loss are also monitored by temperature profiles in industry. Many studies have been done to analyze the process of heat transfer near the vapor-liquid interface of the steam chamber.

Due to the condensation of steam at the vapor-liquid interface, liberated heat from the steam was assumed to be transferred to cold oil sand only by conduction (Butler, 1997). This contested theory showed that heat was mainly transferred through convection as the condensate flowed (Farouq-Ali, 1997). This theory was also confirmed through numerical simulation that showed heat was convectively delivered to oil sand by water flow ahead of the interface (Ito and Suzuki, 1999). More accurate energy analysis argued that the condensate only occupied 18% of the heat of steam condensation according to the change in enthalpy. Since the latent heat was left in the

steam chamber, only 20% of the heat was transferred to the oil by convection (Edmunds, 1999). Another analysis also showed that heat was largely transferred by convection within the steam chamber. Beyond the chamber, both conduction and convection were occurring to deliver heat to mobilize cold oil (Wang et al., 2012).

Heat analysis ahead of the vapor-liquid interface, based on thermocouple data, showed that the heat transfer method has a close relationship with the temperature profile. Convective heat flux can make up 50% of total heat flux when the temperature is low (15 – 30 ℃). The convective heat flux becomes ignorable when the temperature is between 30 – 50 ℃. Above 50 ℃, the convective heat flux starts to increase and rises to 50% of the total flux again at 175 ℃ (Birrell, 2001). Convective heat transfer in reservoirs was also examined through the monitoring of steam quality flow profiles. By this method, SAGD is optimized by providing faster heat transfer in a lateral direction than in a vertical direction. As a consequence, convective heat loss to the top portion of the reservoir is reduced (Gates et al, 2007).

Project phase B implemented in Dover showed that after five years of operation, heat stored in the steam chamber is approximately 32.2%, outside the chamber is 34.7% and 33.1% is recycled back by oil and water production (Yee and Stroich, 2004).

2.2.5 Oil Flow in SAGD

Introduction of steam into the reservoir allows condensate and heated oil to flow downwards to the production well. The oil flow rate is predicted by studies, both experimental and mathematical. Observations of experiments showed that most of the oil flow is restricted in the region near the vapor-liquid interface. Little oil movement is found in the chamber (Butler 1994).

The oil drainage rate parallel to the vapor-liquid interface is integrated, based on oil rate analysis of unity thickness as shown (Butler, 1997):

$$q = 2\sqrt{\frac{2\emptyset\Delta S_o k g \alpha h}{m\nu_o}}$$

where q is oil flow rate to the production well, $\emptyset$ is the porosity, ΔS_o is the average oil saturation change, k is the permeability, g is the gravity acceleration, α is the thermal diffusivity of rock and fluid, h is the oil drainage height, m is the parameter and ν_o is the kinematic viscosity of oil. According to the formula, the rate of oil drainage is a function of the drainage height rather than the shape of the steam chamber or its lateral extension. For the operation of a single well pair SAGD process, the oil flow rate increases during the first period of vertical steam chamber growth. The rate reaches its highest value as soon as the chamber arrives at overburden of the reservoir and maintains this rate as the chamber grows laterally. Eventually, the rate decreases as drainage height declines (Law et al., 2000).

2.3 Operation Parameters in SAGD

The success of SAGD depends on not only reservoir conditions, but also on operation parameters, such as start-up procedure, steam trap control and injection pressure (Shin and Polikar, 2007). In order to build a reasonable model to simulate the SAGD process, these operation parameters are reviewed as follows.

2.3.1 The Start-up Procedure

Before SAGD initialization, both the injection and production wells must be pre-heated to ensure good steam quality at the oil sand surface (Nasr et al., 2000). Steam circulation is used to

establish heat communication between the two wells (Parmar et al., 2009). Under the circulation process, the oil sand between the two wells is heated (Nasr, 2000). Typically, 211.9 g/s or 18.3 tons/day (CWE) of steam is required for the start-up operation of an 800m well (Moini and Edminds, 2011).

In the start-up procedure there are three stages: first to circulate steam from long tubes to toes of both injection and production wells at the target steam rate; second, to generate a pressure gradient between the two wells to create heat convention near wellbores; third, to convert the circulation to SAGD mode until bitumen is sufficiently heated (Vincent et al., 2004). The steam circulation rate, which is the heat content rate of circulation, should be sufficient to deliver steam to the toes of wells without complete condensation. It is also observed that application of moderate pressure differences (around 250 kPa) between the two wells at mid-point or later in the process can create a uniform push and removal of bitumen along the entire length of the well. The lead time of oil production initialization by gravity drainage is increased if the spacing distance between the two wells is increased (Sasaki et al., 2001; Hamm and Ong, 1995). In addition, reservoir simulation studies showed that the existence of shale barriers near the wells affects the start-up time and oil production rate substantially (Chen et al., 2007). In order to improve the start-up process, two methods are proposed: one method is solvent injection to accelerate heat communication between the well pair; the second is introduce vertical channels between the two wells (Nasr et al., 2007).

2.3.2 Steam Trap Control

SAGD is an expensive process in which extensive energy is consumed. This is heightened when there is no barrier or resistance to steam flow into the production well. There is substantial

energy loss if injected steam is produced without sufficient contact with cold oil sands. Steam trap control was proposed and used as an operation parameter to prevent extensive steam withdrawal (Doan et al., 1999).

To prevent live steam loss from a reservoir, a liquid pool is maintained by submerging the production well (Edmunds, 1998). In practice, the monitoring of temperature differences between steam at the injection well and fluid at the production well is applied to measure the liquid pool level (Gates and Chakrabarty, 2008). In order to minimize Cumulative Steam-to-Oil Ratio (cSOR), which represents injected steam for unit produced bitumen in Cold Water Equivalent (CWE), at moderate reservoir conditions, the optimum temperature difference is between 30 to 40℃ as indicated in a 2-D simulation model (Ito and Suzuki, 1999). It was also found that the effect of the temperature difference on SAGD performance is obvious only when the value is higher than a certain level, such 20 ℃ in the Athabasca reservoir (Das, 2005). Furthermore, simulation studies based on the Athabasca geological model showed that the steam trap control should be considered along the whole length of the wellbores. It was suggested that, the temperature difference be measured at multiple locations along the wells (Gates and Leskiw, 2008). In addition, in simulation studies, a maximum steam rate at production is always used as a convenient method to mimic steam trap control in SAGD (Gates and Chakrabarty, 2008).

2.3.3 Steam Injection Pressure

As shown in the oil drainage rate equation (Butler, 1997), steam injection pressure has no direct effect on the oil flow rate. However, experimental analysis of steam injection pressure indicated that higher injection pressure results in a shorter time for steam breakthrough and a faster expansion rate of the steam chamber (Sasaki et al., 2001 and Robinson et al., 2005). Simulation

results also indicated there is a belief that vertical steam chamber growth is proportional to steam injection pressure. High pressure introduces rapid steam rise in a vertical direction (Wei and Gates, 2010). According to the relationship between oil viscosity and temperature, improved oil rate is the result of high injection pressure bringing high saturation temperature which further lowers bitumen viscosity to a favorable level (Gates and Chakrabarty, 2005).

Low injection pressure in SAGD was also examined by simulation. Two advantages of low-pressure processes are summarized: low-pressure tends to be energy efficient and results in favorable artificial lift for oil production (Das, 2005). Simulation studies also show that low-pressure decreases the oil production rate and cSOR (Kisman and Yeung, 1995). A suggestion for the injection pressure operation was proposed as follows: first, inject steam into the reservoir under high pressure until the steam chamber reaches overburden of the reservoir; then, maintain the pressure at a low level to reduce heat loss (Carol, 2006). The failure of low-pressure SAGD, operated by Shell in Peace River, showed that the buried depth of the reservoir is a critical parameter which determines the injection pressure (Collions, 2007). Field scale simulation of SAGD with top water concluded that low-pressure is preferable for oil production with water remaining in the top zone (Nasr et al., 2000). High pressure decreases the oil production rate and increases cSOR because of increased movement of oil and steam into the top thief zone (Law, 2003a). In conclusion, the economics of SAGD are more sensitive to cSOR than the oil production rate, and a low-pressure process is favorable for SAGD due to decreased heat loss and steam consumption (Edmunds and Chhina, 2001).

2.4 Mechanisms in Solvent Aided SAGD

Injection of a steam-solvent mixture into a reservoir is a complex process (Jha et al., 2012). The effect of solvent addition on pressure-volume-pressure behaviors of steam-solvent-bitumen systems is significant. Furthermore, dissolved solvent in oil reduces oil viscosity and impacts oil phase flow in the reservoir.

2.4.1 Temperature of Steam-Solvent Mixture

The temperature distribution at the vapor-liquid interface of the steam chamber is substantially lower than the temperature in a pure-steam SAGD process (Keshavarz et al., 2013). Analysis of binary system behavior of steam-solvent explained the different temperature (Dong, 2012). Assumptions are proposed for the analysis: there is no solubility between water and solvent and pressure gradient in the steam chamber is negligible. Since steam is the major component in the vapor, the temperature of the mixture can be written as:

$$T = T_{sat,H_2O}$$

where T is the temperature of the vapor mixture, and T_{sat,H_2O} is the temperature of saturated steam at its partial pressure.

Studies of enthalpy and temperature, based on a water-butane mixture showed that the contribution of butane to the total enthalpy is very small because of the low concentration and low specific latent heat of butane. The temperature regime is approximately equal to pure-steam SAGD and the temperature front advances at the same rate (Edmunds, 2013).

2.4.2 Viscosity of Solvent-Bitumen Mixture

In order to further reduce viscosity of bitumen, mixing light solvent with bitumen is proven to be an effective method (Gates and Chakrabarty, 2006). Many studies focusing on the relationship between bitumen-solvent viscosity and solvent concentrations have been done through both experimental and numerical methods. Many studies estimated the mixture viscosity using mole fraction (mass or volume fraction) analysis.

The most efficient methods for predicting viscosity of oil mixture are summarized in Table 2.2. Early in 1914, Bingham proposed a method of oil mixture viscosity calculation by using the relationship between inverse values of viscosity. Then Kendal and Monroe calculated oil mixture viscosity according to the relationship of the cubic root of viscosity values in 1917. However, the above methods cannot accurately predict oil mixture viscosity when the viscosity ratio (bitumen viscosity divided by solvent viscosity) is higher than 100, especially for heavy oil systems (Shu, 1984). One method representing changes of liquids viscosity with temperature, pressure and composition was outlined by Cragoe (1933). It was found that a certain function of liquid viscosity has a linear relationship with temperature; its reciprocal has a linear relationship with pressure. As shown in Table 2.2, L is liquidity as a function of viscosity:

$$L = \frac{1000ln20}{ln\mu - \ln(5 \times 10^{-4})} = \frac{2995.73}{ln\mu + 7.6009}$$

Based on the analysis of Cragoe, Van der Wyk proposed a generalized correlation for binary mixture viscosity of heavy oil, bitumen and petroleum fractions through utilizing empirical viscosity data and power-law mixing rules in 1936. Later in the same year, Lederer described the difficulty in obtaining energy change in oil mixture which is measured by q_m. He solved the problem by introducing a simple correlation as shown in Table 2.2. The parameters involved in this method are presented as follows:

$$n_A = \frac{\alpha V_A}{\alpha V_A + V_B}$$

$$n_B = 1 - n_A$$

$$\alpha = \frac{17.04 \Delta\rho^{0.5237} \rho_A^{0.5237} \rho_B^{1.6316}}{ln\left(\frac{\mu_A}{\mu_B}\right)}$$

where α is an empirical constant which has a value from zero to unity. ρ_A and ρ_B are densities of components A and B. $\Delta\rho = \rho_A - \rho_B$.

An improvement in predicting the mixture viscosity of bitumen and liquid dilutes by introducing a binary viscous interaction parameter B_{ij} was proposed by Mehrotra et al. in 1989 and 1992. The Cold Lake bitumen data was modeled with correlation and the results showed effective validation. The mixing rule is shown in Table 2.2. The method of calculating the geometric mean of mass and mole fractions of component i is as follow:

$$v_i = \sqrt{w_i x_i}$$

where w_i is mass fraction of component i, x_i is mole fraction of component i.

Miadonye et al. also developed a correlation to estimate viscosities of bitumen-diluent mixtures to achieve acceptable limits of regression error (2001). The overall deviation (12%) is lower than the result reported by Cragoe (23%). Furthermore, with this method, no experimental data is required to determine the parameters in the correlation.

In addition to the viscosity prediction of liquids mixture, the viscosity of gas-saturated oil is also studied. Through experiments of the saturating process, with gases such as CO_2, CH_4 and N_2 done by Mehrotra and Svercek in 1982, the viscosity of gas-saturated bitumen was identified as a function of pressure and temperature, as in the correlation shown in Table 2.2. One defect of this method is that it can only accurately predict oil viscosity under low pressure. Recently, a

viscosity correlation of hydrocarbons based on equation of state was proposed by Yarranton and Satyro in 2010. The correlating parameter β is shown as follows:

$$\beta = \frac{1}{e^{\left[\left(\frac{\rho_S^*}{\rho}\right)^n - 1\right]-1}}$$

where ρ is density of mixture, ρ_S^* is the density beyond which the fluid cannot be compressed.

In conclusion, bitumen viscosity can be effectively reduced by introducing lighter solvent into it. As a consequence, oil phase mobility is improved in reservoirs, resulting in favorable flow to the production well.

Table 2.2: Most efficient methods for bitumen-solvent mixture viscosity prediction.

Mixing viscosity model	Comments	References
$\frac{1}{\mu} = \frac{V_A}{\mu_A} + \frac{V_B}{\mu_B}$	μ is the viscosity of mixture, μ_1 is the viscosity of component 1; μ_2 is the viscosity of component 2; V_A and V_B are volume fractions of component A and B.	Bingham (1914)
$\mu^{1/3} = x_A \mu_A^{1/3} + x_B \mu_B^{1/3}$	μ is the viscosity of mixture, μ_A and μ_B are the viscosity of component A and B; x_A and x_B are mole fractions of component A and B.	Kendal and Monroe (1917)
$L_m = m_A L_A + m_B L_B$	L_m is a function of mixture viscosity; L_A is a function of component A; L_B is a function of component B.	Cragoe (1933)
$log_{10}\mu = x_A log_{10}\mu_A + x_B log_{10}\mu_B - \int \frac{q_m}{4.57T^2}$	μ is the viscosity of mixture, μ_A and μ_B are the viscosity of component A and B; x_A and x_B are mole fractions of component A and B; q_m is the molecular heat of solution. T is temperature in K.	Van der Wyk (1936)
$log_{10}\mu = n_A log_{10}\mu_A + n_B log_{10}\mu_B$	μ is the viscosity of mixture; μ_A and μ_B are the viscosity of component A and B; n_A and n_B are correlating parameters for components A and B.	Lederer (1936)
$log_{10}log_{10}(\mu + 0.8) = a_1 + a_2 T + \left(a_3 - \frac{a_4}{T}\right) P$	μ is the viscosity of mixture; T is temperature in K; P is pressure in MPa; a_1, a_2, a_3 and a_4 are correlation constants.	Mehrotra and Svercek (1982)
$log(\mu + 0.8) = \sum_i v_i log(\mu_i + 0.8) + \sum_i \sum_j v_i v_j B_{ij}$	μ is the viscosity of mixture, μ_i is the viscosity of component i; v_i is a parameter correlating to mass and mole fractions of component i; B_{ij} is a binary viscous interaction parameter;	Mehrotra (1992)
$\mu - \mu_G = c_1(e^{c_2\beta} - 1)$	μ is the viscosity of mixture, μ_G is the viscosity of gas; c_1 and c_2 are fit parameters; β is correlating parameter.	Satyro and Yarranton (2010)

2.5 Operation Parameters in Solvent Aided SAGD

In a solvent aided SAGD process, operating parameters including solvent-type selection, solvent concentration and pressure exhibit great effects on the behaviors of the steam-solvent-bitumen system. Some studies focused on these effects have been completed and are summarized in the following paragraphs.

2.5.1 Solvent-Type Selection

Farouq-Ali and Abad tested bitumen recovery from oil sands through solvent co-injection with steam (Farouq-Ali and Abad, 1976). In this process, the synthetic crude oil supplied by Great Canadian Oil Sands Ltd., (GCOS) naphtha and the 'Mobile Solvent' were used as surrogates of solvents. Experimental results showed that bitumen recovery has a close relationship with solvent-type selection and the GCOS was proven as ideally suited for the thermal-miscible process.

A more detailed investigation, with a large range of hydrocarbons from methane, ethane, propane, butane, pentane, natural gasoline, naphtha to synthetic GCOS was completed (Redford and Mckay, 1980). They concluded the use of methane has very little benefit to bitumen recovery improvement. However, solvent co-injection with, for example, propane and natural gasoline, can significantly improve bitumen recovery over a pure-steam only process. It is demonstrated that the bitumen recovery increases as the molecular weight of the additive increases. Heavier materials act as better solvents for bitumen recovery.

CO_2 was introduced as an additive to improve the pure-steam process by Redford (1982). Through co-injection of CO_2, bitumen recovery was substantially improved from the Athabasca oil sands. Solvents are generally divided into the following categories, as described by Shu and

Hartman (1988): light solvents, containing CO_2, ethane, propane and other gases; medium solvents, including naphtha; and heavy solvents, which are the hydrocarbons from C16 to C20. The effect of solvent type on the performance of solvent aided SAGD was evaluated, based on incremental recovery of heavy oil over the steam-only process and incremental recovery of heavy oil per barrel of unrecovered solvent. From the results, it is demonstrated that heavy solvents adversely affect bitumen recovery, with cumulative oil production less than the pure-steam process, and little solvent was recovered. Solvent efficiency is very similar for the medium solvents, with as much as 60% of enhanced oil recovery from the pure-steam process. The incremental recovery by light solvents is slightly lower than that of the medium solvents. It is concluded that the optimum solvent selection would be achieved through evaluation of a combination of the following, expected increase in heavy oil production, operation time, solvent efficiency and cost of solvent.

The oil drainage rate increases with the increase of injected hydrocarbon carbon number and the rate peaked with C6 (Nasr et al, 2003). A numerical simulation was done by Govind et al. (2008) and indicated that the influence of solvent type on solvent aided SAGD processes is negligible, with the solvent selection of C4, C5, C6, C7 and a mixture of C6 and C8. C4 was considered the best solvent surrogate because of relatively high solubility in oil under high pressure and a decrease of cSOR during the process. Ardali et al. studied the process of solvent addition in the SAGD process by numerical simulation in 2010 and the experimental method in 2011. These studies confirmed that solvents heavier than C4 have the potential to improve oil recovery and thermal efficiency of SAGD processes in Athabasca reservoir. Furthermore, C4 is considered the best choice for oil recovery from the Cold Lake reservoir. Li and Mamora (2011) also showed that the oil recovery factor increases with an increase of the carbon number of the solvent in the

SAGD process. C12 co-injection results in the highest oil recovery factor around 96%. The co-injection of C6 - C7 mixture exhibits a similar oil recovery factor to the co-injection of pure C6. Approximately 92 – 95% of injected solvents (C3, C4, C5, C6, C7 and mixture of C6 and C7) can be recovered from the reservoir. For C12, 18% of the injected amount is retained in the reservoir.

Studies also revealed that solvent type selection has a close relationship with heavy oil properties. For Athabasca reservoir, solvent heavier than butane can enhance oil recovery, and butane is the best option for Cold Lake reservoir recovery (Ardali et al., 2010). As described by Mohebati et al. (2012), C6 co-injection can considerably accelerate oil production rate in the Athabasca reservoir. However, C6 co-injection in Cold Lake and Lloydminster did not prove to be that effective.

2.5.2 Solvent Concentration

The effects of solvent concentration in injected stream on oil production performance have been investigated and reported in the literatures. It was stated that solvent concentration significantly affects the oil production rate (Govind et al., 2008). The oil production rate increases as the solvent concentration increases. Reduction of cSOR occurs when the exposure time of the steam chamber to overburden is reduced, and with the lowered temperature of steam-solvent vapor under high solvent injection concentration. It was also confirmed later that high solvent concentration can accelerate oil production rate up to 13.61% by weight (Jiang et al., 2012).

Oil recovery and cumulative energy required for cumulative oil volume recovered (CEOR) are the main parameters that determine the optimum solvent injection concentration for the SAGD process (Li and Mamora, 2011). From the sensitivity analysis of C7 injection concentration (0.01, 0.03, 0.05, 0.07, 0.09 and 0.12 mole fraction), the optimum concentration is varies from 7 to 9

mole%, which depends on the tradeoff between the heat effect from steam and the solubility effect from solvent.

Mohebati et al. conducted a C6 co-injection process through numerical simulation (2010). It was observed that increasing the C6 mole fraction in the injected stream higher than 0.01 mole fraction results in a small increase in the oil recovery factor and an improvement in cSOR. A gradual decrease of solvent injection concentration was proposed as a solvent injection strategy by Keshavarz et al. to achieve a relatively high oil recovery factor with minimum solvent loss within the reservoir (2013).

2.5.3 Steam Pressure

Similar to the pure-steam SAGD process, a change of steam injection pressure also shows significant effect on performance of the solvent aided SAGD process. Experiments were done to investigate the effect of operation pressure on the use of naphtha with steam (Redford and Mckay, 1980). Changing pressure at lower values from 200 to 300 psig showed little effect on final oil recovery. However, increasing pressure to 500 psig adversely reduced the oil production. It was assumed that the increased pressure drop between the pair results in the reduced oil rate.

With C6 mixed with steam, the simulations studies conducted revealed that C6 more effectively enhances the SAGD process under low pressure (1500 kPa) as opposed to a high pressure (1900 kPa) (Mohebati et al., 2010). This is because, in this process more oil is recovered for unit volume retained C6 within the reservoir under low pressure. A lower minimum pressure control at the production well can greatly improve the solvent aided SAGD process, according to simulation results (Ivory et al., 2008). Based on a history matched simulation model, decreasing the minimum pressure at the producer from 2200 to 1500 kPa, increases the average oil rate by

42.4% from 148.5 to 211.4 m^3/day, cSOR is reduced by 41.0 % from 3.07 to 1.81, and the net solvent-to-oil ratio is also decreased from 0.086 to 0.035 kg/kg.

Economic evaluation conducted by Deng (2005) showed that the C3 assisted SAGD with low injection pressure (800 kPa) is more cost efficient than the high pressure (2200 kPa) counterparts because the cost of steam or water remains the largest part of the total cost.

2.6 Applications of Steam-Solvent Process in Field

Although the studies relevant to hybrid steam-solvent processes have been extensively done, the number of field applications is limited. Field trials exhibiting varying success of solvent aided processes, have been summarized (Nasr, 2003 and Jha et al., 2012). Table 2.3 presents a brief summary of previous field trials of steam-solvent processes. Few of the pilots have been conducted over a long time in order to provide conclusive results. It is generally shown that there is a tendency toward improvement with solvent addition in the steam injection process.

Table 2.3: Brief summary of steam-solvent pilots have been implemented.

Project	Operator	Year	Solvent	Oil production performance		CSOR		Comments	References
				Before solvent injection	After solvent injection	Before solvent injection	After solvent injection		
Tia Juana	Petroleos de Venezuela S. A.	1987	Industrial and automotive diesel (4.8% by volume)	191 bbl/d	301 bbl/d	0.40 bbl/bbl	0.25 bbl/bbl	85.9% improvement in cumulative oil production	Bracho et al. (1991)
Senlac	EnCana	2002	Butane (15.0 % by weight)	1900 bbl/d	3000 bbl/d	2.60 bbl/bbl	1.60 bbl/bbl	Very encouraging process with more 70% solvent recovery	Gupta et al. (2005)
Cold Lake	Imperial Oil	2002 - 2007	Diluent (6% by volume)	1570 bbl/d	2830 bbl/d	3.45 bbl/bbl	2.56 bbl/bbl	Long term operation	Jha (2012)
Firebag	Suncor	2003	Naptha	-	-	-	-	Bitumen production rate was not increased	Orr (2009)
Christina Lake	EnCana	2004	Butane (15.0 % by weight)	630 bbl/d	1900 bbl/d	5.00 bbl/bbl	1.60 bbl/bbl	Benefits from solvent injection are lateral steam chamber expansion	Gupta and Gittins (2006)
Long Lake	Nexen	2006	Naptha (C7 to C12) (5.0 % by volume)	383 bbl/d	409 bbl/d	2.80 bbl/bbl	2.00 bbl/bbl	Approximate 6 % increase in oil rate and 7% decrease in CSOR	Orr (2009)

2.7 Phase Behavior in Steam-Solvent System

Due to different boiling points and partial pressures of steam and solvent in the vapor phase, the phase behavior of steam-solvent-bitumen system is not uniform within the steam chamber, especially in the region near the vapor-liquid interface. Only a limited number of studies have been done to analyze phase behavior change by solvent addition.

2.7.1 Condensation in Steam-Solvent System

With solvent co-injection with steam into the reservoir, the phase behavior inside the steam chamber is not uniform, as described by Li and Mamora (2010). The vapor solvent, liquid solvent and water near the vapor-liquid interface work together to impact oil phase viscosity and flow. Previous studies showed that, at the interface, solvent would condense with steam and dissolve in oil.

The phase behavior of steam and solvent in the SAGD process was studied by CMG STARS with 1.7 m in grid size (Li and Mamora, 2010). In this process, the vaporized C6 under saturated steam circumstances flows throughout the steam chamber. As the steam chamber grows vertically during the early period of the SAGD operation, a solvent vapor film is formed with high concentration at the top part of the steam chamber, because of the lower boiling point and density of C6. The vapor film is seen to impede heat transfer from the steam chamber to surrounding formations, especially during the vertical chamber growth stage. This impediment is not significant along the sloped boundary of the steam chamber after the chamber reaches overburden of the reservoir. As long as the hot vapor meets the cold oil sand, C6 condenses and dissolves in bitumen (Nasr et al, 2003; Nasr and Ayodele, 2006; Li and Mamora, 2010 and 2011; Ardali and Mamora, 2011; Jha et al., 2012; Edmunds, 2013). The transition between the steam

chamber and the surrounding reservoir can be divided into three films: film of condensate water, film of vapor C6 and film of liquid C6 in oil.

It is also revealed that different types of solvents show different phase behaviors inside the steam chamber. Light solvents, such as C3, adversely impact the SAGD process because of a thick gas film existence along the vapor-liquid interface. Heavier solvents cannot effectively be delivered to the interface because they condense near the area of wellbore. Ideal solvents should have the potential to build a thick film of solvent in oil to efficiently improve oil mobility near the vapor-liquid interface (Li and Momora, 2011).

A novel and more accurate analysis was done by Dong (2012) to investigate the phase behavior of the steam-solvent system, and an algorithm was proposed to estimate the equilibrium temperature and solvent fraction in vapor at the vapor-liquid interface. This method is reasonable since the solution gas in heavy oil is small, especially for bitumen.

The temperature of the vapor mixture depends on the partial pressure of the steam which is the major component. As the vapor mixture flows far away from the injection well, steam starts to condense through heat transfer to surrounding cold oil sand. As a consequence, the mole fraction of steam in vapor decreases, with simultaneous solvent fraction increase. During this process, the amount of solvent dissolved in oil is changing as well as the varying partial pressure and vapor concentration of solvent. At the vapor-liquid interface, temperature reaches its lowest level, under which much solvent exists in the oil phase.

A simple and reliable method for equilibrium state calculation is proposed by Dong (2012) for binary steam-solvent systems near the vapor-liquid interface. The following method was applied to plot the relationship between saturation temperature and solvent mole fraction in the vapor phase under a constant total pressure:

(1) Calculating saturation temperature for water condensation by using

$$T = \mathrm{T}_{sat,H_2O}$$

(2) Plot the steam condensation temperature versus solvent mole fraction in vapor from 0 to 1.

(3) Calculating saturation temperature for solvent condensation by using

$$T = \mathrm{T}_{sat,Solv}$$

(4) Plot the solvent condensation temperature versus solvent mole fraction in vapor from 1 to 0.

(5) Through the interaction point of the steam condensation temperature line and the solvent condensation temperature line, draw a horizontal line to separate vapor phase and liquid phase.

Figure 2.2, 2.3, 2.4 and 2.5 represent the equilibrium state of steam-C4, steam-C5, steam-C6 and steam-C7 systems. The curves are generated by CMG Winprop (2011) based on the calculation from Peng-Robinson Equation (1978) equation at total pressure of 2000 kPa. For example, the detailed phase behavior within the steam-C6 system is shown in Figure 2.4. The two curves at the top of the figure are temperature corresponding to the concentration of C6. The left one indicates steam condensates when C6 concentration is low. It is shown that, in a large range of solvent fraction in vapor, steam condensed first from vapor. The mole fraction of steam in vapor deceases during the process of condensation, as well as the gradual decrease of temperature. Solvent fraction in vapor increases as steam condenses through heat transfer to cold oil sands. The condensation of solvent can occur only when the solvent concentration in vapor phase is extremely high at 0.63 mole fraction. At this point, both steam and C6 start to condense

simultaneously at constant temperature until the vapor becomes liquid. At the bottom of the figure, the horizontal line indicates the temperature below which there is no vapor phase.

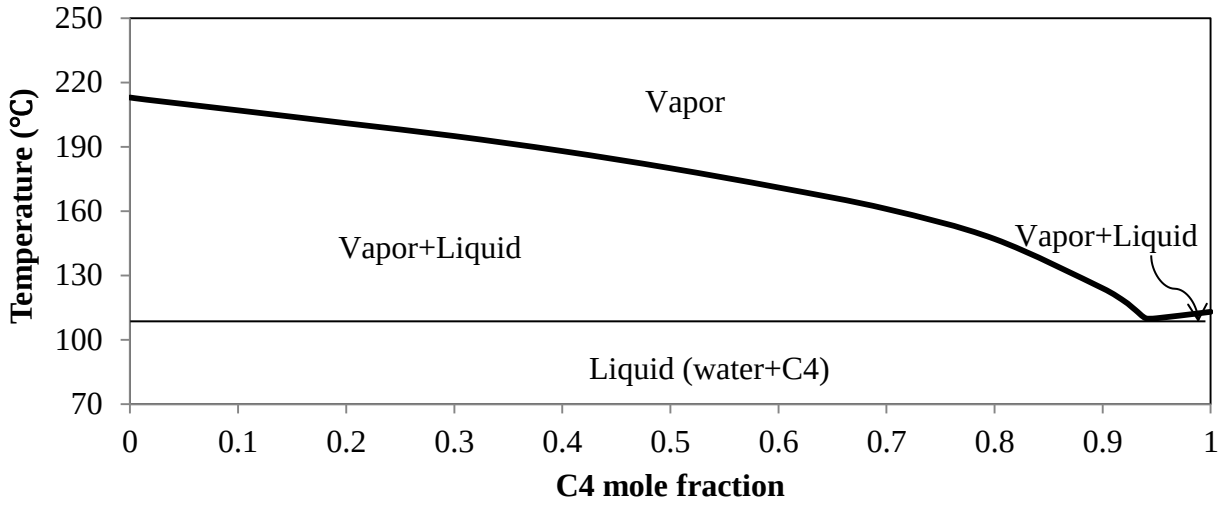

Figure 2.1: Condensation temperature of steam and C4 mixture under 2000 kPa as a function C4 mole fraction in vapor (Dong, 2012).

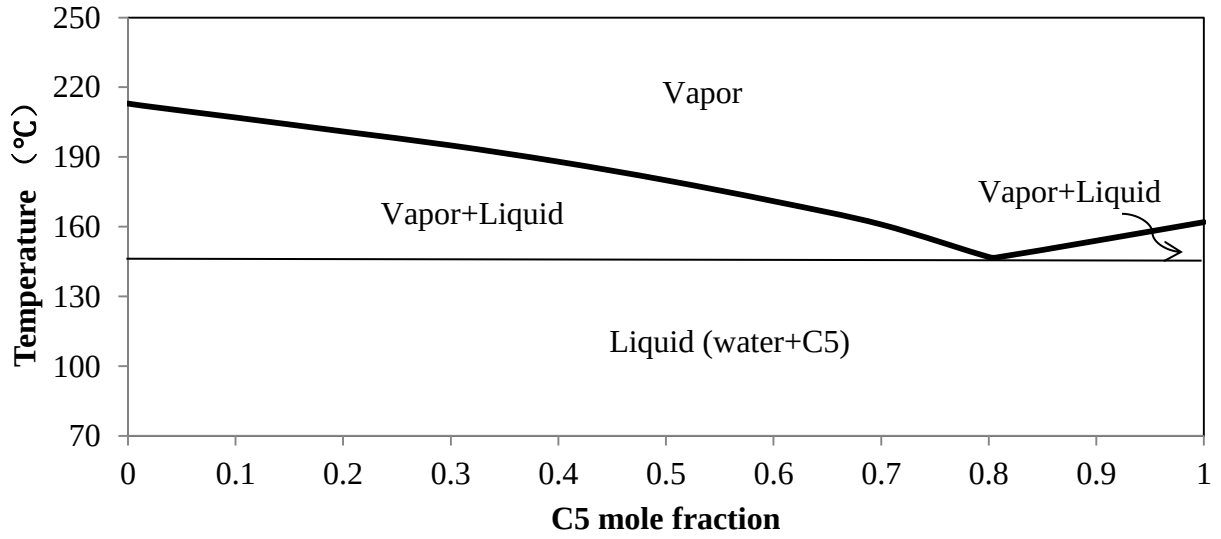

Figure 2.2: Condensation temperature of steam and C5 mixture under 2000 kPa as a function C5 mole fraction in vapor (Dong, 2012).

For different types of solvents, there are some changes in phase behavior. As the solvent becoming heavier, the required solvent concentration in vapor for solvent condensation decreases. As shown in Figures 2.2 and 2.3, there is no condensation for C4 or C5 until their mole fractions reach 0.94 and 0.81, respectively. For C6 and C7, the level is still high at 0.63 and 0.45 respectively, as shown in Figure 2.4 and 2.5 respectively.

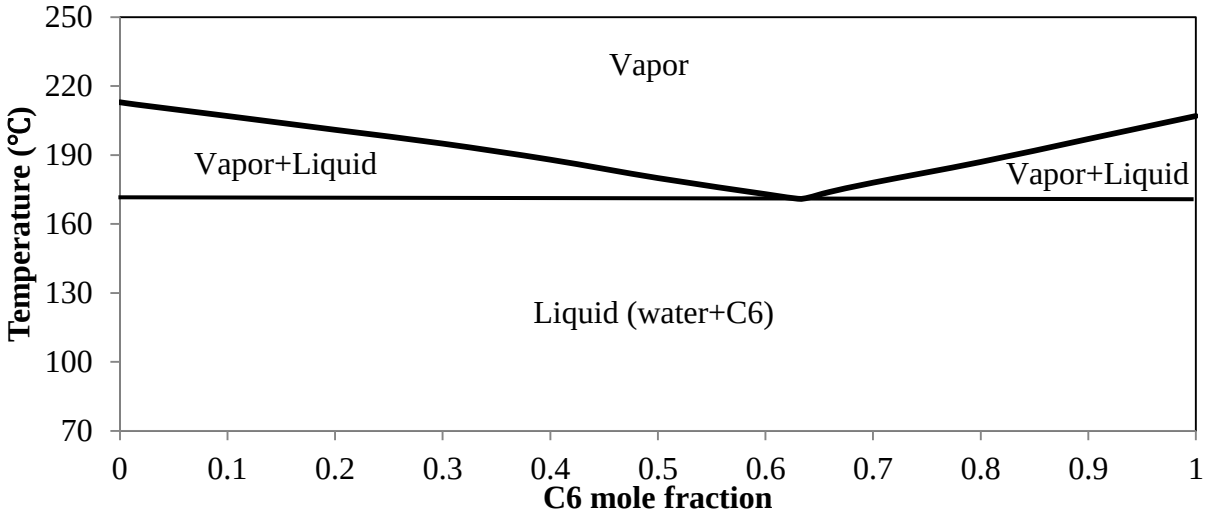

Figure 2.3: Condensation temperature of steam and C6 mixture under 2000 kPa as a function C6 mole fraction in vapor (Dong, 2012).

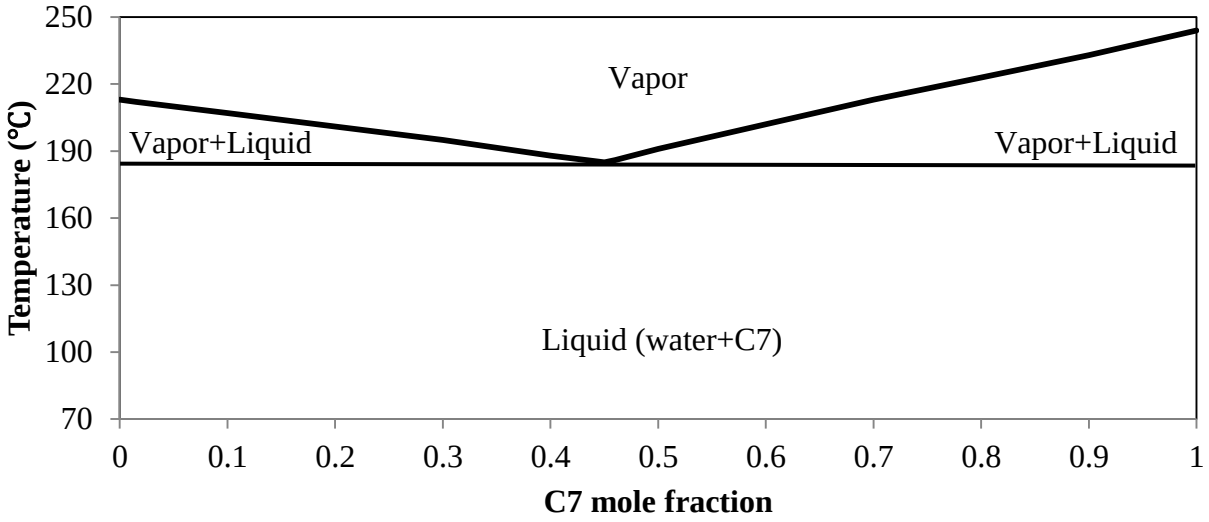

Figure 2.4: Condensation temperature of steam and C7 mixture under 2000 kPa as a function C7 mole fraction in vapor (Dong, 2012).

The effect of total pressure on steam-solvent phase behavior is illustrated in Figures 2.6, 2.7, 2.8 and 2.9. The phase behavior with various total pressures are plotted for the phase behavior of steam-C4, steam-C5, steam-C6 and steam-C7.

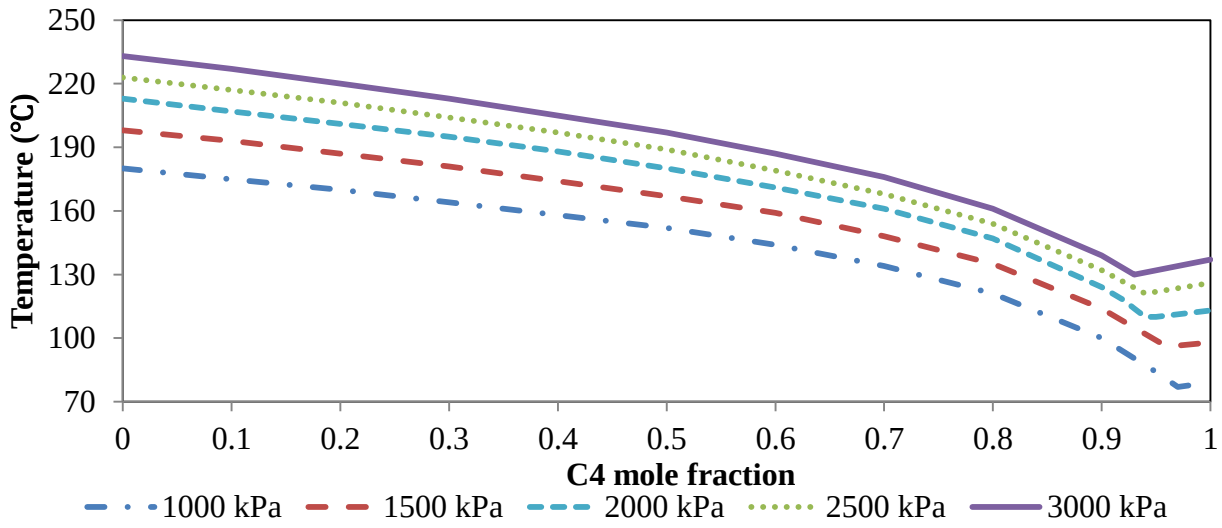

Figure 2.5: Condensation temperature of steam and C4 mixture with various total pressures as a function C4 mole fraction in vapor (Dong, 2012).

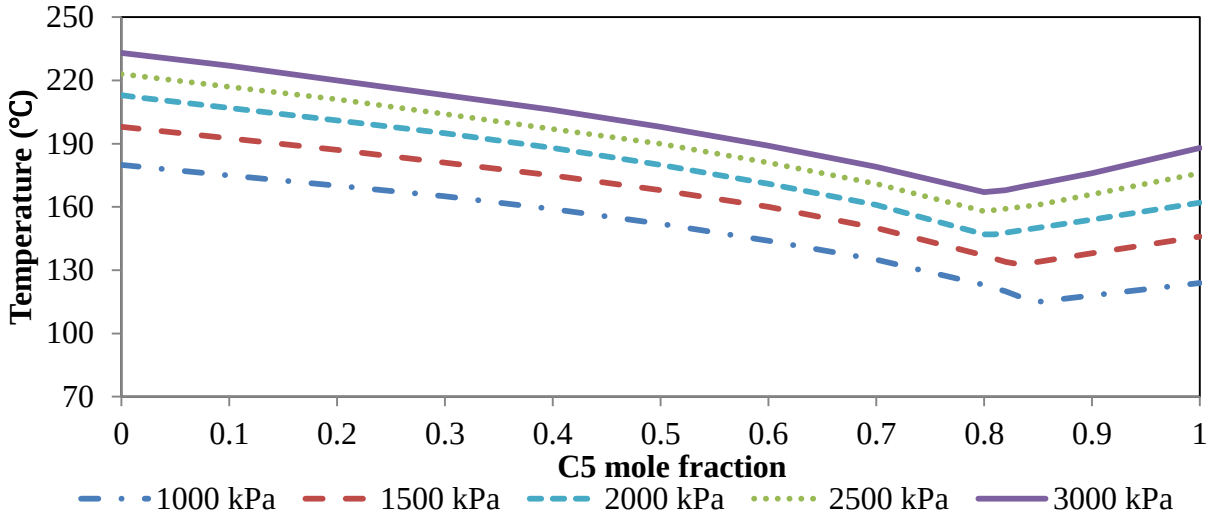

Figure 2.6: Condensation temperature of steam and C5 mixture with various total pressures as a function C5 mole fraction in vapor (Dong, 2012).

By comparing Figures 2.6, 2.7, 2.8 and 2.9, we see that increasing total pressure decreases the required minimum concentration for solvent condensation. For example, as shown in Figure 2.8, the required concentration decreases from 0.66 to 0.61 when pressure increases from 1000 to 3000 kPa for steam-C6 system.

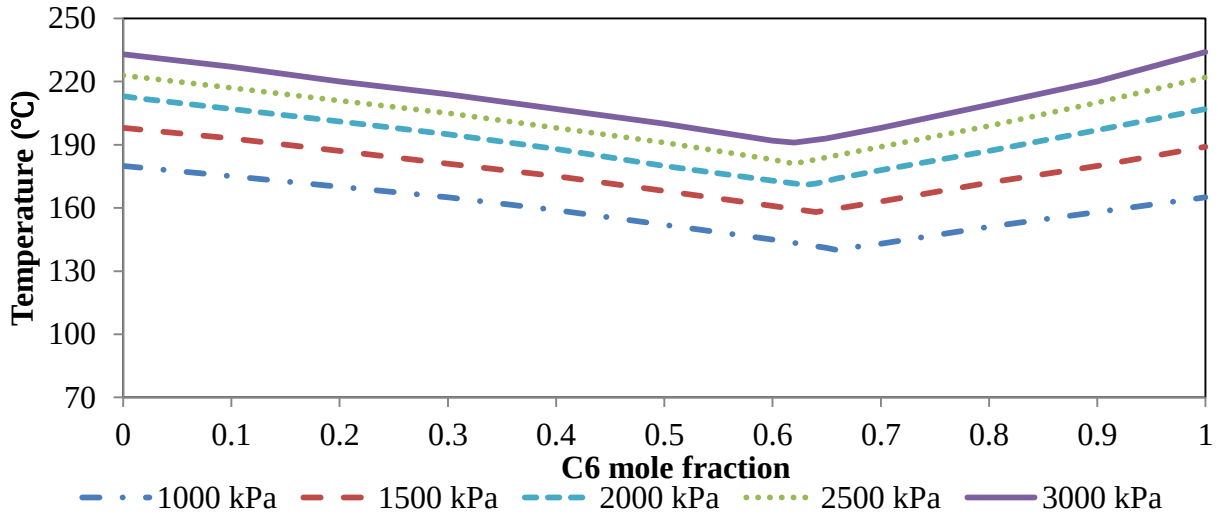

Figure 2.7: Condensation temperature of steam and C6 mixture with various total pressures as a function C6 mole fraction in vapor (Dong, 2012).

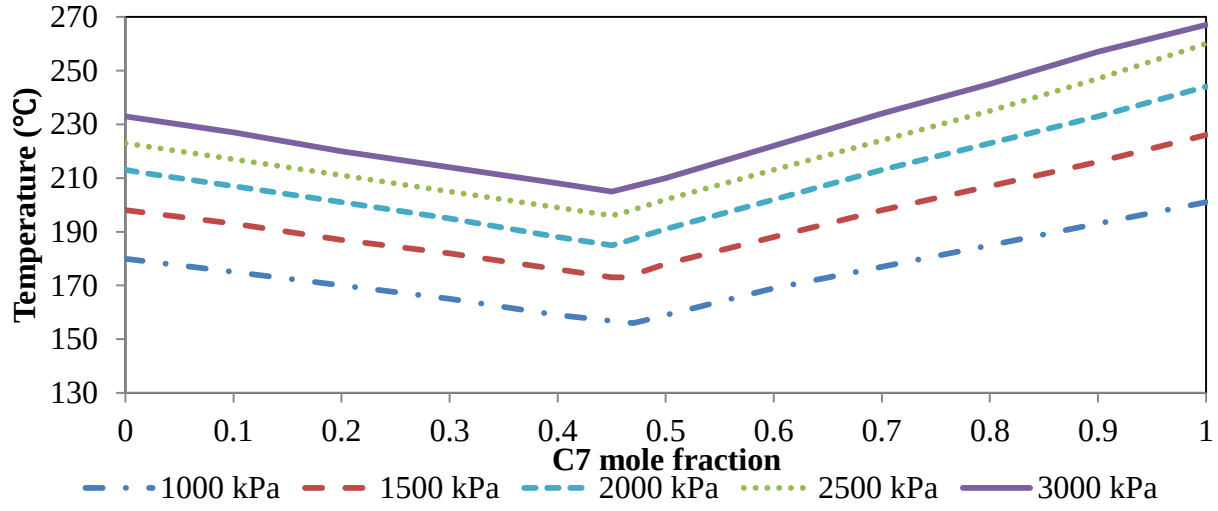

Figure 2.8: Condensation temperature of steam and C7 mixture with various total pressures as a function C7 mole fraction in vapor (Dong, 2012).

The temperature at the vapor-liquid interface is lower than the pure-steam SAGD by the separation of bubble and dew points of solvent-steam mixture (Dong, 2012). As it was described, under 2000 kPa, first condensation for steam occurs at 210.9 ℃ in the mixture containing 0.97 mole fraction steam and 0.03 mole fraction C6. The continuous condensation of steam enables a gradual increase of C6 partial pressure and saturation temperature. The temperature at the boundary was estimated at 40 ℃ lower than the pure-steam process, as shown in Figure 2.10.

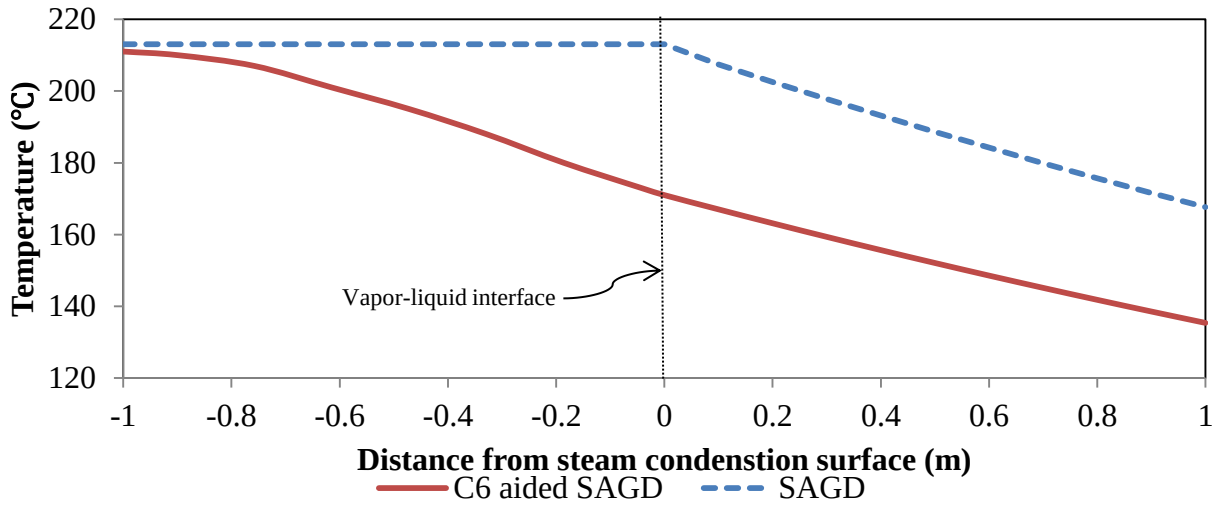

Figure 2.9: Temperature profile in distance near vapor-liquid interface of SAGD and C6 co-injected SAGD with 0.01 mole fraction C6 and 2000 kPa (Dong, 2012).

2.7.2 Solvent Mass Transfer

In solvent aided SAGD, the mobility of oil beyond the vapor-liquid interface is increased by solvent dissolution in oil. Detailed study of this mechanism of solvent distribution in mobile oil zone is scarce.

Through the studies conducted by Sharma and Gates (2010), oil viscosity reduction and enhanced oil saturation by solvent dissolution in oil effectively increase oil phase mobility. The

diffusion and dispersion of solvent in bitumen were suggested as methods for solvent transporting beyond the steam chamber in some studies.

Beyond the vapor-liquid interface to oil sand, solvent molecular diffusion and mechanical dispersion are regarded as the main methods for solvent mass transfer (Sharma and Gates, 2010). Another analysis stated that a solvent-bitumen mixing zone is formed through transverse dispersion of condensed solvent in heated oil ahead of the interface (Jha et al. 2012).

The typical diffusion coefficient of solvent in bitumen was estimated, ranging from 8.64×10^{-6} to 4.32×10^{-5} m^2/day according to the test of propane and butane diffusion in Peace River bitumen done by Das and Butler (1996). With the estimated mechanical dispersivity from 5 to 200 μm, Perkins and Johnston (1963) concluded that dispersion is greater than diffusion when fluid flows through porous media. However, solvent diffusion in oil, which is a very slow process, cannot deliver much solvent to oil sand under the fast growing steam chamber since the length scale of solvent mass transfer is two orders lower than heat transfer (Sharma and Gates, 2010). Simulation studies also showed that there was little effect on oil production by varying the solvent diffusion coefficient. A simulation model developed by Ivory et al. (2008), based on the Athabasca reservoir provided no effect of solvent diffusion coefficient on oil production, with the coefficient varying from 1.44×10^{-6} to 1.44×10^{-3} m^2/d. The results from a simulation done by Deng et al. (2010) also indicated that oil production and solvent production are less sensitive to solvent dispersion in oil even if the dispersion coefficient was increased by 2 orders (from 0.0001cm^2/min to 0.01cm^2/min). Solvent distribution in the mobile oil zone also needs to be studied again.

CHAPTER THREE: RESERVOIR MODEL

3.1 Simulation Model

In this study, a right half 2-D simulation model (Figure 3.1) is generated for simulating processes of SAGD and solvent aided SAGD. In this model, the half width is 30 m with 20 m in thickness. There is 5 m between the injection well and the production well, which is 2 m above the base of the reservoir.

In this study, CMG STARS was used as a simulator to implement the built model and investigate some mechanisms involved in both SAGD and solvent aided SAGD. Later, effects of some relevant operation parameters on the steam-solvent process were examined, which is followed by an optimized steam-solvent injection strategy.

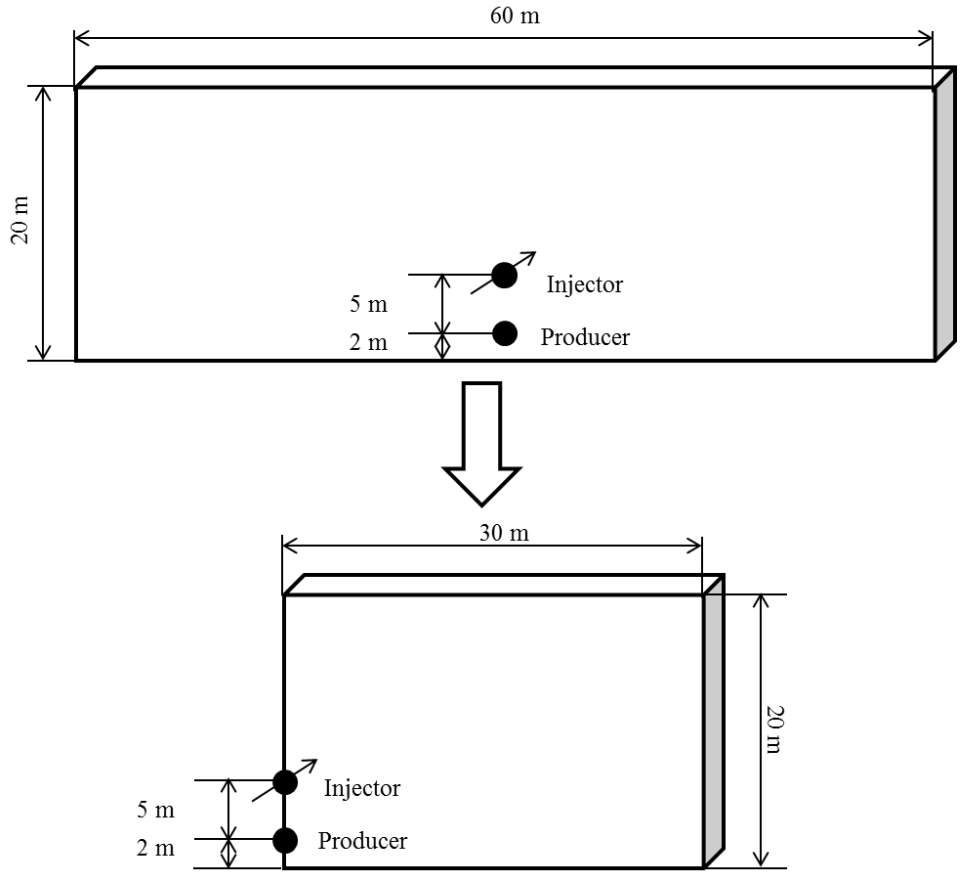

Figure 3.1: Illustration of right half reservoir model.

3.2 Grid System

The 2-D reservoir model (30 m × 20 m) is reduced to 7.5 m × 5.0 m shows in Figure 3.2. In order to investigate the effects of grid size (dimension) and grid connection type (nine-point or five-point) on the oil recovery, simulation studies have been done shown by the summary of the oil recovery factor at 120 days (end of production) in Table 3.1. Grid size is selected at 0.05 m, 0.10 m, 0.20 m and 0.40m, respectively. The solvent diffusion coefficient in oil varies from 4.32×10^{-7} to 4.32×10^{-3} m^2/day. The dispersivity changes from 0.00002 to 0.002 m.

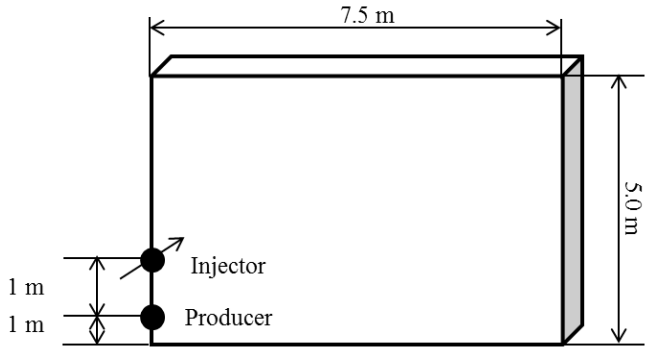

Figure 3.2: Illustration of the small reservoir model.

In Table 3.1, there is no significant change in the oil recovery factor (within 68% and 72%) with variance in the grid size (0.05 m, 0.10 m and 0.20 m). Additionally, the grid connection type (nine-point or five-point) has little impact on the oil recovery factor, either. Furthermore, the changes in solvent diffusion coefficient or dispersivity show similar the oil recovery factors. In a word, the grid size or the connection type has little impact on the oil recovery.

In order to accurately and efficiently simulate the steam-solvent injection process, a Cartesion grid system was generated with dedicated refinement. In lateral and vertical directions, there are 150 and 100 grids respectively. Furthermore, the model contains one 500 m long grid in the direction of the horizontal well to mimic oil production rate in the field.

Table 3.1: Summary of oil recovery factor of the cases with different grid size, connection type, diffusion coefficient and dispersivity.

Case				Oil recovery factor (%, at 120 days, end of production)
Grid size (m)	Grid connection type	Diffusion[1]/Dispersion[2]		
0.05	Nine-point	Diffusion coefficient (m^2/day)	4.32×10^{-7}	68
			4.32×10^{-5}	68
			4.32×10^{-3}	70
		Dispervisity (m)	0.00002	68
			0.0002	68
			0.002	68
	Five-point	Diffusion coefficient (m^2/day)	4.32×10^{-7}	67
			4.32×10^{-5}	67
			4.32×10^{-3}	69
		Dispervisity (m)	0.00002	67
			0.0002	67
			0.002	67
0.10	Nine-point	Diffusion coefficient (m^2/day)	4.32×10^{-7}	69
			4.32×10^{-5}	69
			4.32×10^{-3}	70
		Dispervisity (m)	0.00002	69
			0.0002	69
			0.002	69
	Five-point	Diffusion coefficient (m^2/day)	4.32×10^{-7}	68
			4.32×10^{-5}	68
			4.32×10^{-3}	70
		Dispervisity (m)	0.00002	68
			0.0002	68
			0.002	69
0.20	Nine-point	Diffusion coefficient (m^2/day)	4.32×10^{-7}	72
			4.32×10^{-5}	72
			4.32×10^{-3}	73
		Dispervisity (m)	0.00002	72
			0.0002	72
			0.002	72
	Five-point	Diffusion coefficient (m^2/day)	4.32×10^{-7}	72
			4.32×10^{-5}	72
			4.32×10^{-3}	73
		Dispervisity (m)	0.00002	72
			0.0002	72
			0.002	72

[1] for the analysis of diffusion coefficient, the dispersivity is set at 0.0002 m.

[2] for the analysis of dispersivity, the diffusion coefficient is set at 4.32e-5 m^2/day.

3.3 Reservoir Properties

The key reservoir properties are summarized in Table 3.1. Figure 3.3 and 3.4 show water-oil and gas-liquid relative permeability curves respectively.

This model is of a single well pair and homogeneous with respect to permeability, porosity and initial oil saturation. The horizontal permeability is 4 darcies and the vertical permeability is 2.4 darcies. The relative permeability data is provided by a publication (Nasr et al., 2000). Initial water saturation and oil saturation are 0.2 and 0.8 respectively, with a porosity of 35%. The initial reservoir temperature is 10 ℃. The modeled reservoir has a depth of 300 m. Pressure is determined by the hydrostatic method, with reference pressure 1210 kPa specified at the top of the reservoir. Thermal properties and heat loss parameters of rock and fluids are the same as the data published by Butler in 1997. There are no geomechanics involved in the model. Both gas cap and bottom water zones are also neglected.

Table 3.2: Key parameters of reservoir model

Items	Values
Reference temperature (℃)	10
Reference Pressure (kPa)	1210
Reference depth (m)	300
Initial water saturation (%)	20
Initial oil saturation (%)	80
Horizontal absolute permeability (darcy)	4
Vertical absolute permeability (darcy)	2.4
Porosity (%)	35
Formation heat capacity J/(m^3*℃)	2.0E+06
Rock conductivity J/(m*day*℃)	6.6E+05
Water conductivity J/(m*day*℃)	5.4E+04
Oil conductivity J/(m*day*℃)	1.2E+04
Overburden/underburden volumetric heat capacity J/(m^3*℃)	2.4E+06
Overburden/underburden thermal conductivity J/(m*day*℃)	1.7E+05
Formation compressibility 1/kPa	7.0E–06

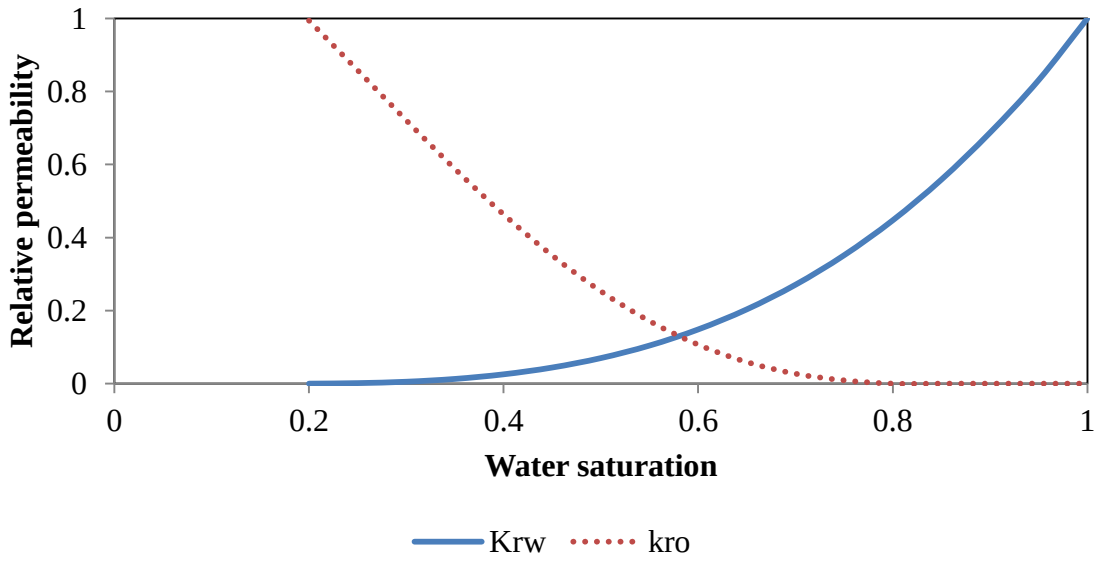

Figure 3. 3: Water-oil relative permeability. k_{rw} is water phase relative permeability, k_{ro} is oil phase relative permeability.

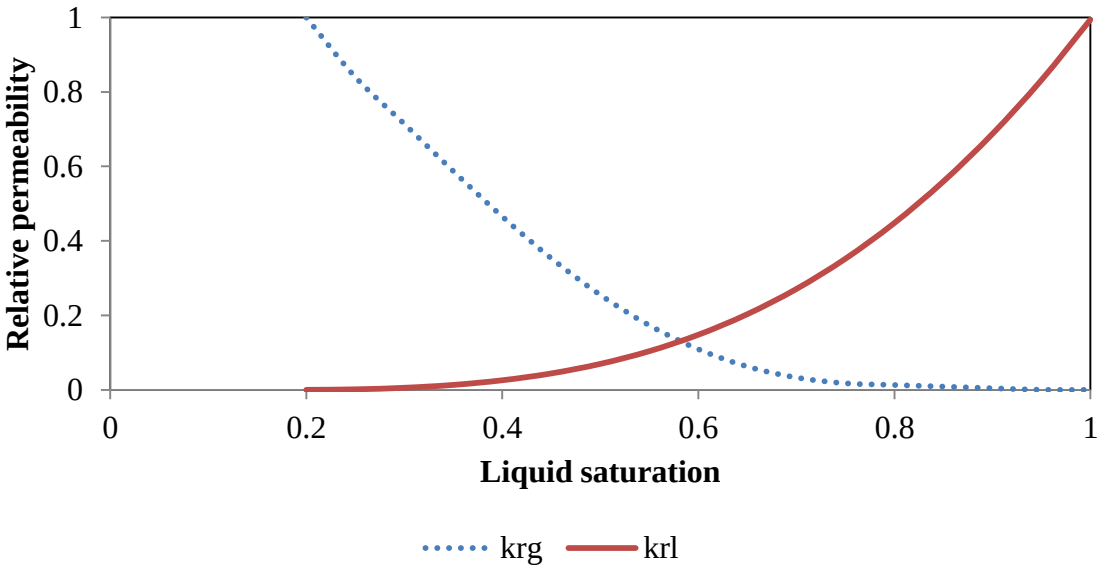

Figure 3.4: Gas-liquid relative permeability. k_{rg} is gas phase relative permeability, k_{rl} is liquid phase relative permeability.

3.4 Fluid Properties

The relationship between bitumen viscosity and temperature is tuned by CMG Winprop based on experiment results (Khan et al., 1984) through a similar method to that used by Yazdani and Maini (2010). In Figure 3.5, the curve of bitumen viscosity varies as temperature changes are plotted. It is shown that, under 10 ℃, which is the original temperature of the reservoir, bitumen viscosity is over 1 million cP. At 200 ℃, which is the usual temperature at vapor-liquid interface in the SAGD process, the viscosity is as low as 10 cP.

In Table 3.2, calculation correlations for solvent (C3, C4, C5, C6, C7 and C8) properties are summarized in detail. The relationship between solvent viscosity and temperature, solvent solubility, solvent diffusion in oil, oil mixture viscosity, vaporization heat of gases and heat capacity of gases is shown.

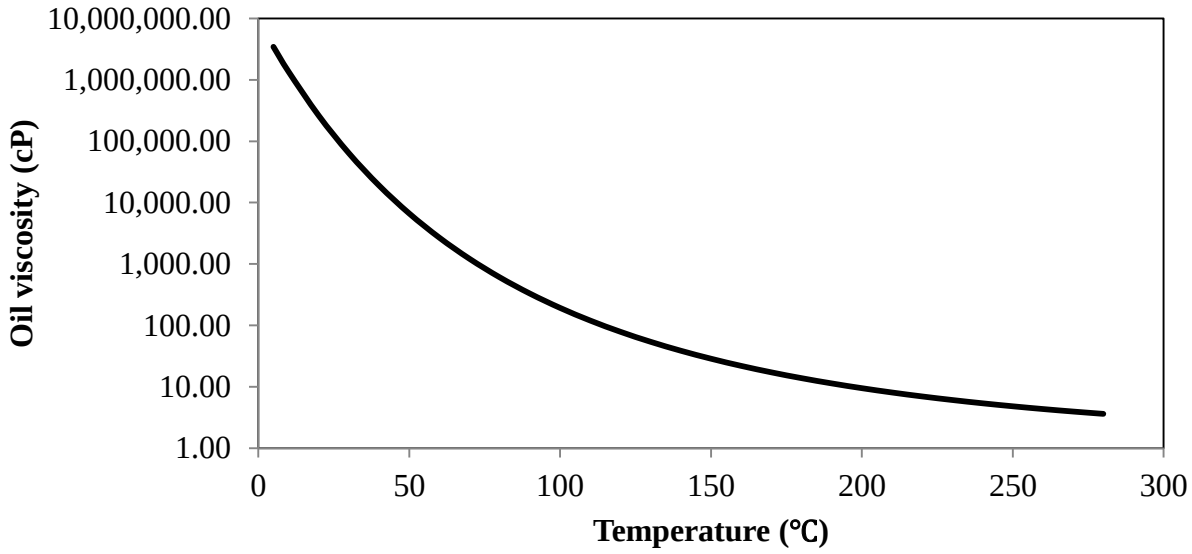

Figure 3.5: Bitumen viscosity change as a function of temperature.

Table 3.3: Properties calculation correlations (CMG STARS, 2011).

Properties	Correlations	Parameters
Solvent viscosity	$\mu = ae^{\frac{b}{T}}$	a (cP) / b (°C) C3: 0.0214257 / 512.72 C4: 0.0219066 / 612.12 C5: 0.0191041 / 722.23 C6: 0.0177073 / 835.35 C7: 0.0132383 / 1005.6 C8: 0.0131242 / 1090.7
Solvent solubility	$k = (\frac{k_{v1}}{P})e^{\frac{k_{v2}}{T-k_{v3}}}$	k_{v1} (kPa) / k_{v2} (°C) / k_{v3} (°C) C3: 9.0085e+5 / -1872.46 / -247.99 C4: 8.5881e+5 / -2154.90 / -238.73 C5: 1.0029e+6 / -2477.07 / -233.21 C6: 1.0062e+6 / -2697.55 / -224.37 C7: 1.0442e+6 / -2911.32 / -216.64 C8: 1.1187e+6 / -3120.29 / -209.52
Solvent flux	$J_{ijk} = -(\frac{\varphi S_j D_{ij}}{F_{jk}})\nabla_k(\rho_j X_{i,j})$	F_{jk} is tortuosity for phase j in direction k, assumed at 1 for homogeneous model; $\nabla_k(\rho_j X_{i,j})$ is concentration gradient of component i in phase j in direction k.
Oil mixture viscosity	$ln\mu = \sum_{i=1}^{n} x_i \ln(\mu_i)$	-
Vaporization enthalpy	$H_{vap} = HVR(T_c - T)^{0.38}$	$HVR(J/gmol * °C^{0.38})$ / T_c(°C) H_2O: 4820 / 374.15 C3: 2883 / 96.65 C4: 3317 / 152.05 C5: 3745 / 196.45 C6: 4143 / 234.25 C7: 4520 / 267.05 C8: 4892 / 295.65
Gas heat capacity	$C_{pg} = C_{pg1} + C_{pg2} \times T + C_{pg3} \times T^2 + C_{pg4} \times T^3$	C_{pg1} ($\frac{J}{gmole \cdot °C}$) / C_{pg2} ($\frac{J}{gmole \cdot °C^2}$) / C_{pg3} ($\frac{J}{gmol \cdot °C^3}$) / C_{pg4} ($\frac{J}{gmole \cdot °C^4}$) H_2O: 32.243 / 1.924e-3 / 1.055e-5 / -3.596e-9 C3: -4.224 / 0.3063 / -1.586e-4 / 3.215e-8 C4: 9.487 / 0.3313 / 1.108e-4 / -2.822e-9 C5: -3.626 / 0.4873 / -2.580e-4 / 5.305e-8 C6: -4.413 / 0.5820 / -3.119e-4 / 6.494e-8 C7: -5.146 / 0.6762 / -3.651e-4 / 7.658e-8 C8: -6.096 / 0.7712 / -4.195e-4 / 8.855e-8

3.5 Cases

For the SAGD case (Table 3.3), steam is injected at 212 ℃ with a quality of 90%. The injection well is constrained to maximum bottom-hole pressure (2000 kPa) and maximum surface water rate (500 m^3/day) in cold water equivalents (CWE). The production well is operated at maximum steam rate of 5 m^3/day to prevent extensive steam loss. To initialize SAGD, a start-up procedure is simulated for heating both injection and production wellbores to ensure a high steam quality at the sand surface (Nasr et al, 2000).

For the solvent aided SAGD case, C6 is injected as the surrogate of solvent with steam into the reservoir, with the other parameters the same as in the SAGD case (Li and Mamora, 2011). The amount of injected C6 is measured by mole fraction to conveniently calculate phase behavior in this process. The k-values of solvent at different pressures and temperature (provided by STARS User's Manual, 2011) are used in the simulation. The diffusion coefficient of C6 in oil is approximated based on the work by Das and Butler in 1996.

Table 3.4: Operation parameters of SAGD and solvent aided SAGD cases.

Parameters	SAGD	Solvent aided SAGD
Solvent	-	C6
Solvent concentration (mole fraction)	0	0.01
Injection pressure (kPa)	2000	2000
Steam quality (%)	90	90
Maximum steam rate at injection well (m^3/day, CWE)	500	500
Minimum pressure at production well (kPa)	1800	1800
Maximum steam rate at production well (m^3/day, CWE)	5	5
Steam circulation time (day)	90	90

CHAPTER FOUR: ANALYSIS OF SAGD PROCESS

4.1 Introduction

The studies of the SAGD mechanism have been done and reported in the literatures (Butler, 1994; Edmunds and Gittins, 1993; Gates and Leskiw, 2010). A description of SAGD in this study is used to establish a reference for comparison with solvent aided SAGD.

To better understand the process of SAGD, the variations of properties (temperature, gas, oil and water saturations, oil viscosity and oil flow rate) distribution near the vapor-liquid interface are analyzed in detail. Figures 4.1.1, 4.2.1 and 4.3.1 show the selected locations at the top, middle and bottom of the reservoir respectively through the three dashed lines overlaying the oil saturation profile at cross section of the SAGD at 300 days (middle of production).

4.2 Analysis at Top of Reservoir

The top location is selected first to study the SAGD process. Figure 4.1.2 shows the schematic of zones (A, B, C and D) along the top location from left to its right (from the inner portion of steam chamber to the original cold oil sand). The four zones are described as follows:

A. Non-condensation zone: In this zone, pores of oil sand are filled with steam, residual oil and water. There is no steam condensation.
B. Steam condensation zone: As vapor moves to cold oil sand, steam starts to condense, with resultant heat transfer to the surrounding formations. Gas saturation becomes zero at the vapor-liquid interface.
C. Mobile oil zone: With the heat transferred to the cold oil sand ahead of the vapor-liquid interface, oil viscosity is reduced and the oil drains downwards by gravity. There is no gas phase in this zone.

D. Immobile oil zone: This zone is far from the steam chamber and the temperature is too low to mobilize oil.

In Figure 4.1.3, oil, water and steam saturation and temperature at 300 days have been shown along the top location. Oil viscosity and oil flow rate are shown at the same location in Figure 4.1.4.

In the non-condensation zone (A in Figures 4.1.3 and 4.1.4, 0 – 10.0 m), which has a constant temperature and pressure as steam flows, the pores of rock are filled with steam, water and residual oil as shown in Figure 4.1.3. Oil and water remain at 0.10 and 0.18 respectively. In Figure 4.1.4, there is no oil flow, as shown by the oil flow rate curve.

In the steam condensation zone (B in Figures 4.1.3 and 4.1.4, 10.0 – 10.4 m), steam condenses by the contact of hot vapor and cold oil sand. As shown in Figure 4.1.3, temperature remains constant until the vapor arrives at the vapor-liquid interface. Water saturation increases due to the accumulation of the condensate. There is a sharp decrease in gas saturation (from 0.72 to 0.00) and a sharp increase in oil saturation (from 0.10 to 0.58) in this zone. The thickness of the steam condensation zone is very narrow at only 0.4 m since steam condenses at once when the temperature is lower than the steam saturation level. Under relatively low oil saturation in this zone, the total oil flow rate to the production well is slow as shown by the area beneath the oil flow rate curve drawn in Figure 4.1.4.

In the non-gas mobile oil zone (C in Figures 4.1.3 and 4.1.4, 10.4 – 13.4 m), oil is mobilized by delivered liberated heat from steam to cold oil sand (Edmunds, 1993). Under the action of gravity drainage, condensed water is accumulated and water saturation is increased in this zone, as shown by the hump of the water saturation curve in Figure 4.1.3. As a consequence, some heat is convectively transferred to oil by condensed water flow. Oil saturation increases

gradually towards the cold oil sand as the diluted bitumen flows downward. Under low viscosity and relatively high oil saturation ahead of the vapor-liquid interface, the oil drainage rate reaches the maximum level at 9.7 m^3/day as shown in Figure 4.1.4. With the increase of oil viscosity into the cold oil sand, the oil rate decreases.

Beyond the oil flow boundary, where the temperature is too low to mobilize oil, is the immobile oil zone (D in Figures 4.1.3 and 4.1.4, 13.4 – 30.0 m). Oil remains within the reservoir without movement. The slightly higher oil saturation in Figure 4.1.4 is due to oil expansion caused by the change of temperature.

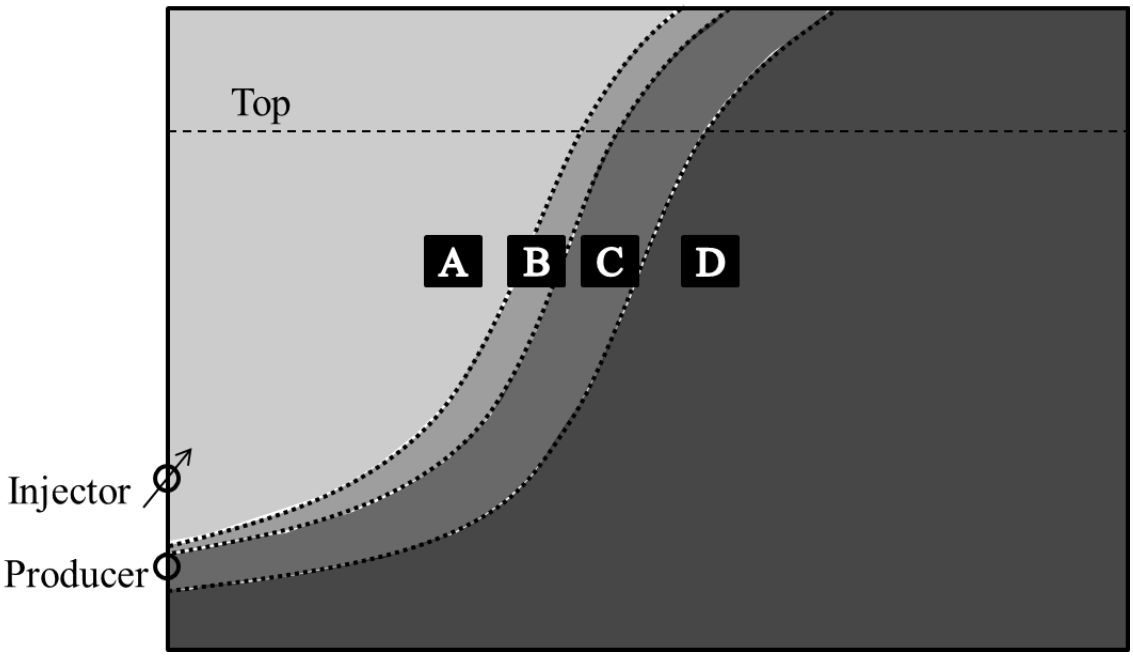

Figure 4.1.1: Four zones near the transition region illustrated by oil saturation distribution in cross-section of SAGD. The dished line is the location at top part of reservoir.

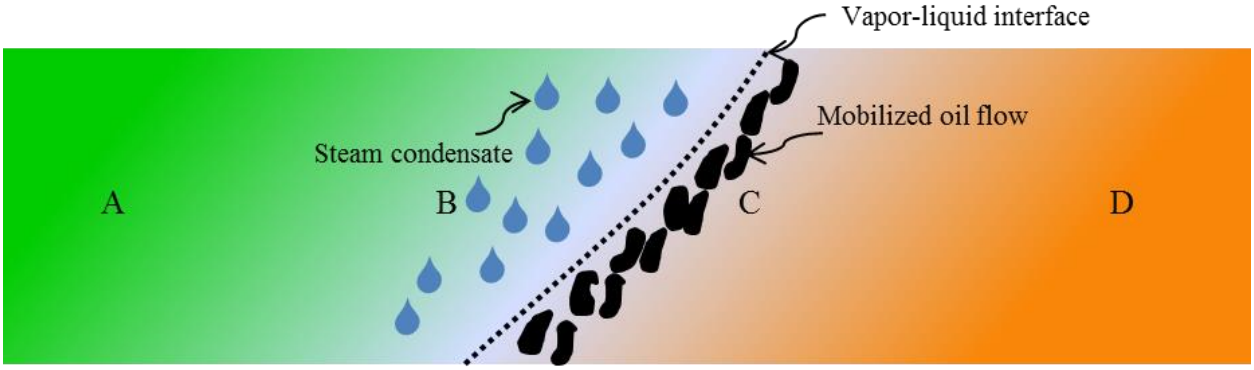

Figure 4.1.2: Schematic of four zones present along the top location in SAGD. The blue droplets represent steam condensate and the black droplets stand for mobile oil. A is the non-condensation zone. B is the steam condensation zone. C is the mobile oil zone. D is the immobile oil zone. The dashed line represents the vapor-liquid interface.

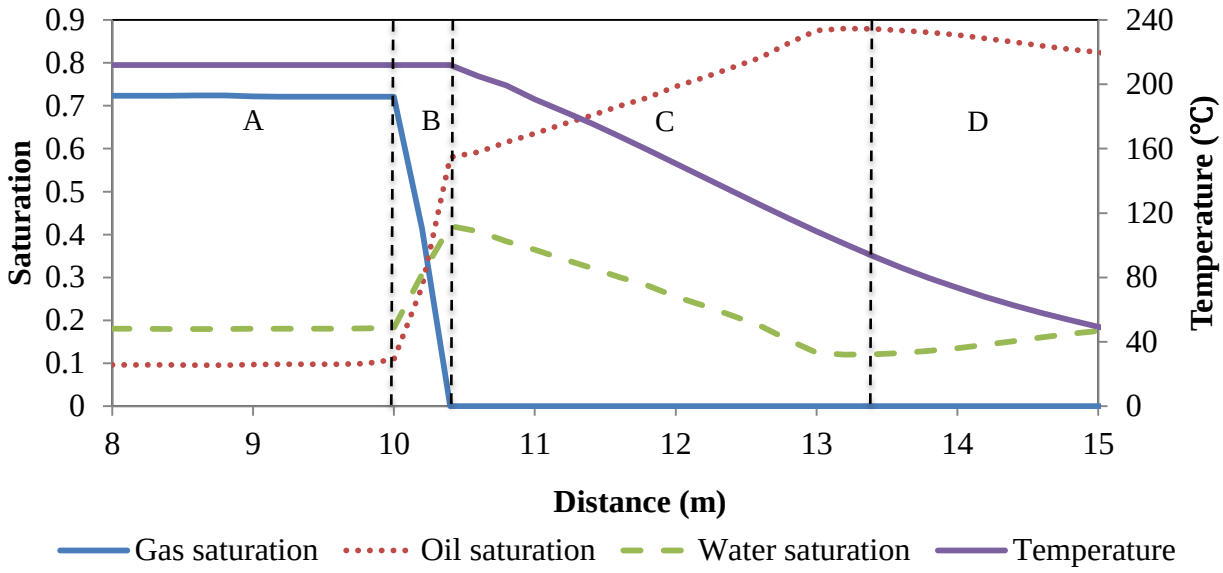

Figure 4.1.3: Gas saturation, oil saturation, water saturation and temperature at 300 days along the top location (8 -15 m) in SAGD with 2000 kPa injection pressure. A is the non-condensation zone. B is the steam condensation zone. C is the mobile oil zone. D is the immobile oil zone.

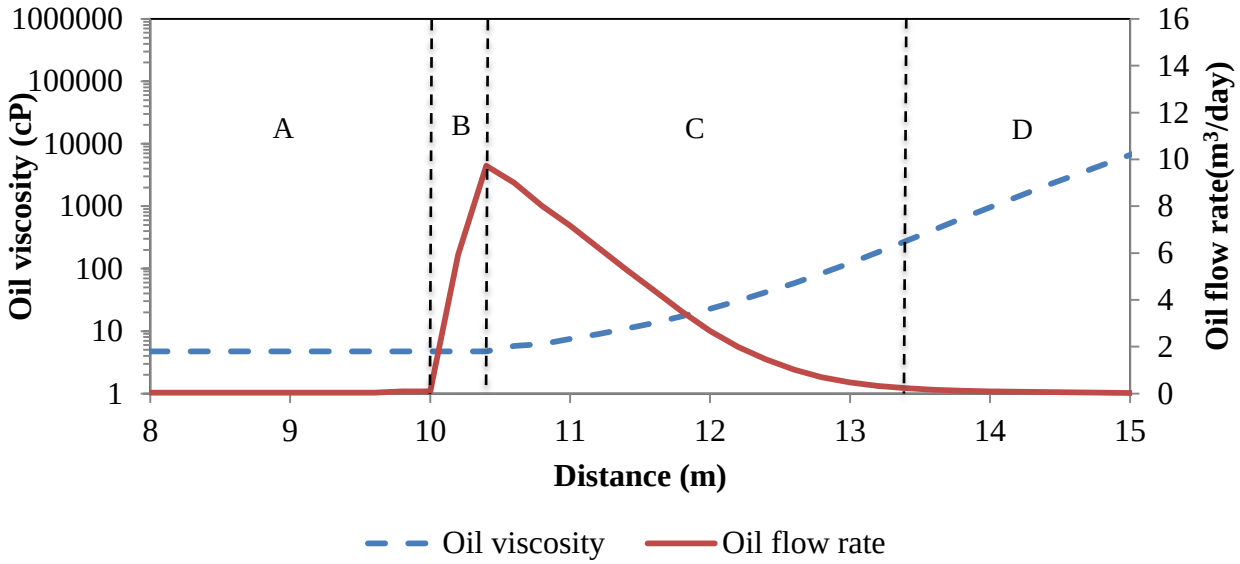

Figure 4.1.4: Oil viscosity and oil flow rate at 300 days along the top location (8 - 15 m) in SAGD with 2000 kPa injection pressure. A is the non-condensation zone. B is the steam condensation zone. C is the mobile oil zone. D is the immobile oil zone.

4.3 Analysis at Middle of Reservoir

A similar analysis to that done at the top location is done for the middle location, which is shown in Figure 4.2.1. Schematics of the processes including steam condensation, gas, water and oil flow in the non-condensation zone (A), steam condensation zone (B), mobile oil zone (C) and immobile oil zone (D) are shown in Figure 4.2.2.

In Figure 4.2.3, oil, water and steam saturation and temperature at 300 days have been shown along the middle location. Oil viscosity and oil flow rate are shown at the same location in Figure 4.2.4. In order to briefly describe the properties variance, only the differences between the middle location and the top location are discussed.

In the non-condensation zone (A in Figures 4.2.3 and 4.2.4, 0 – 6.2 m), as steam flows through the pores of rock, the properties remain at a relatively constant level, which are little changed compared to the top location.

In the steam condensation zone (B in Figures 4.2.3 and 4.2.4, 6.2 – 6.6 m), as the accumulation of heated oil flows from upwards, the increase in oil saturation (from 0.10 to 0.61) is higher than the magnitude at the top location (from 0.10 to 0.58). Under the increased oil saturation, the total oil flow rate to the production well is also increased in this zone, as in the comparison between the areas beneath the oil flow rate curve drawn in Figures 4.1.4 and 4.2.4 respectively.

In the mobile oil zone (C in Figures 4.2.3 and 4.2.4, 6.6 – 9.6 m), oil is also mobilized sufficiently by liberated heat from steam. The oil drainage rate reaches the maximum level at 13 m^3/day (Figure 4.2.4), which is faster than the rate at the top location.

Beyond the oil flow boundary is the immobile oil zone (D in Figure 4.2.3 and 4.2.4, 9.6 – 30.0 m). Oil remains within the reservoir without movement.

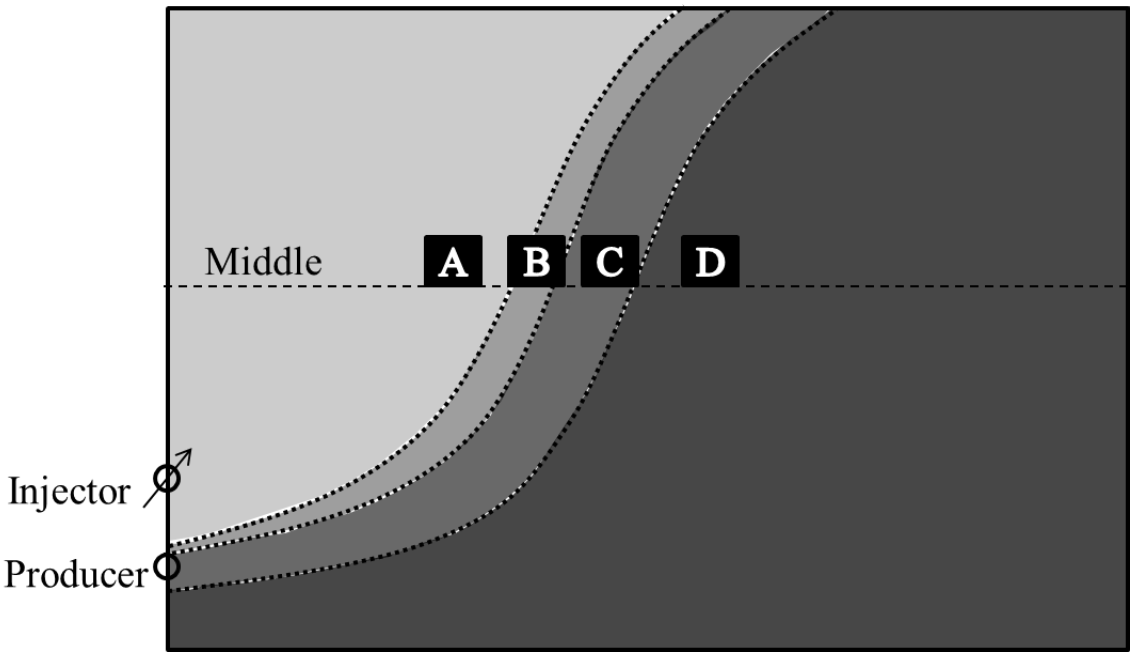

Figure 4.2.1: Four zones near the transition region illustrated by oil saturation distribution in cross-section of SAGD. The dished line is the location at middle part of reservoir.

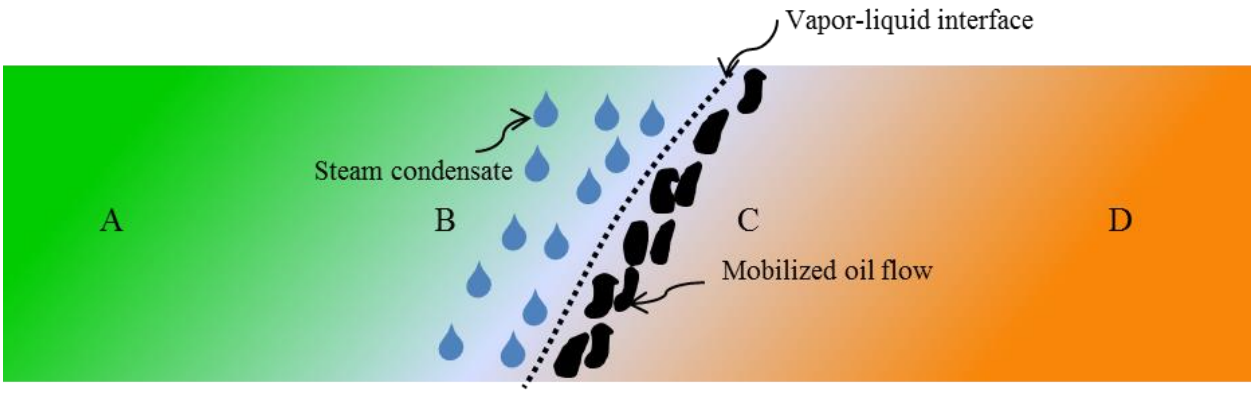

Figure 4.2.2: Schematic of four zones present along the middle location in SAGD. The blue droplets represent steam condensate and the black droplets stand for mobile oil. A is the non-condensation zone. B is the steam condensation zone. C is the mobile oil zone. D is the immobile oil zone. The dashed line represents the vapor-liquid interface.

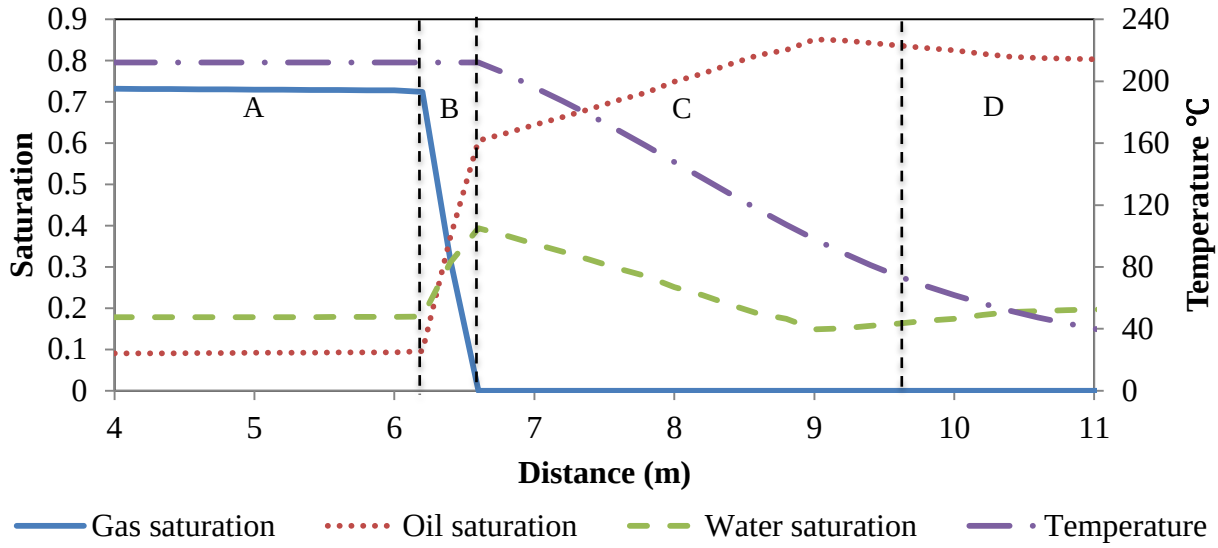

Figure 4.2.3: Gas saturation, oil saturation, water saturation and temperature at 300 days along the middle location (4 -11 m) in SAGD with 2000 kPa injection pressure. A is the non-condensation zone. B is the steam condensation zone. C is the mobile oil zone. D is the immobile oil zone.

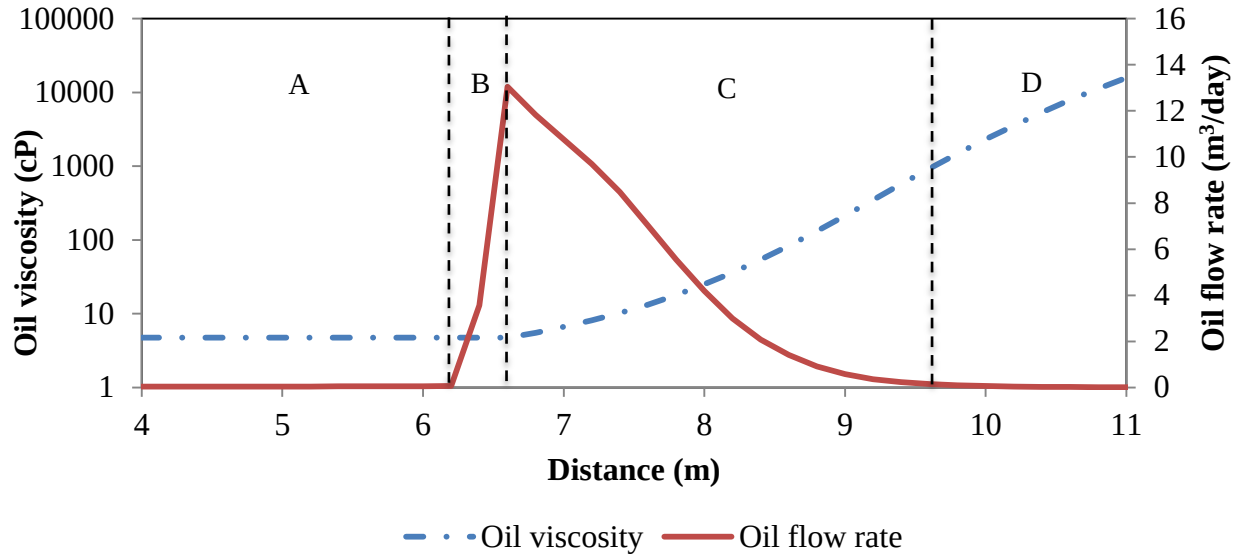

Figure 4.2.4: Oil viscosity and oil flow rate at 300 days along the middle location (4- 11 m) in SAGD with 2000 kPa injection pressure. A is the non-condensation zone. B is the steam condensation zone. C is the mobile oil zone. D is the immobile oil zone.

4.4 Analysis at Bottom of Reservoir

A similar analysis to the above two locations is done for the bottom location, which is shown in Figure 4.3.1. Schematics of the processes including steam condensation, gas, water and oil flow in zones of the non-condensation zone (A), steam condensation zone (B), mobile oil zone (C) and immobile oil zone (D) are also shown in Figure 4.3.2.

In Figure 4.3.3, oil, water and steam saturation and temperature at 300 days have been shown along the bottom location. Oil viscosity and oil flow rate are shown in Figure 4.3.4.

In the non-condensation zone (A in Figures 4.3.3 and 4.3.4, 0 – 3.2 m), properties remain at relatively similar levels as the top and middle locations.

In the steam condensation zone (B in Figures 4.3.3 and 4.3.4, 3.2 – 3.6 m), the increase in oil saturation (from 0.10 to 0.63) is higher than the magnitude (from 0.10 to 0.0.61) at the middle location, as the accumulation of heated oil flows from the top. The oil flow rate to the production well is also increased in this zone through the comparison of the areas beneath the oil flow rate curves drawn in Figure 4.2.4 and Figure 4.3.4 respectively.

In the non-gas mobile oil zone (C, in Figures 4.3.3 and 4.3.4, 3.6 – 6.8 m), the oil drainage rate reaches the highest level at 15 m^3/day, which is the fastest among the top, middle and bottom locations.

Beyond the oil flow boundary is the immobile oil zone (D, in Figures 4.3.3 and 4.3.4, 6.8 – 30.0 m). Oil cannot be removed in the reservoir.

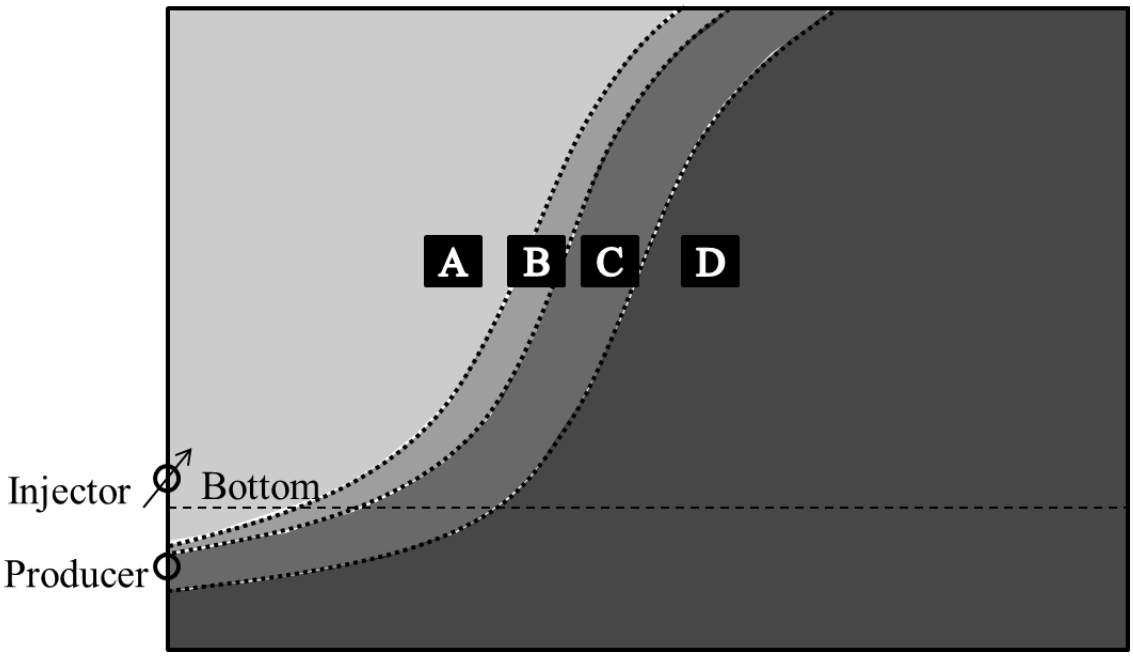

Figure 4.3.1: Four zones near the transition region illustrated by oil saturation distribution in cross-section of SAGD. The dished line is the location at bottom part of reservoir.

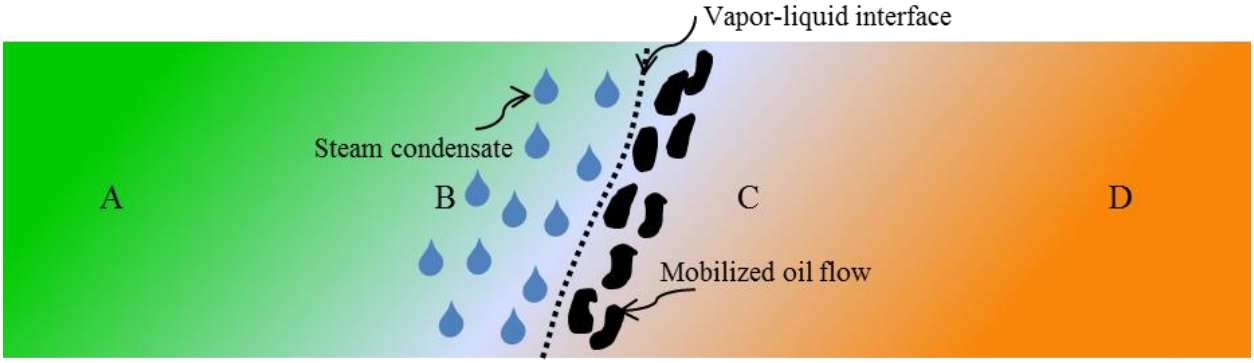

Figure 4.3.2: Schematic of four zones present along the bottom location in SAGD. The blue droplets represent steam condensate and the black droplets stand for mobile oil. A is the non-condensation zone. B is the steam condensation zone. C is the mobile oil zone. D is the immobile oil zone. The dashed line represents the vapor-liquid interface.

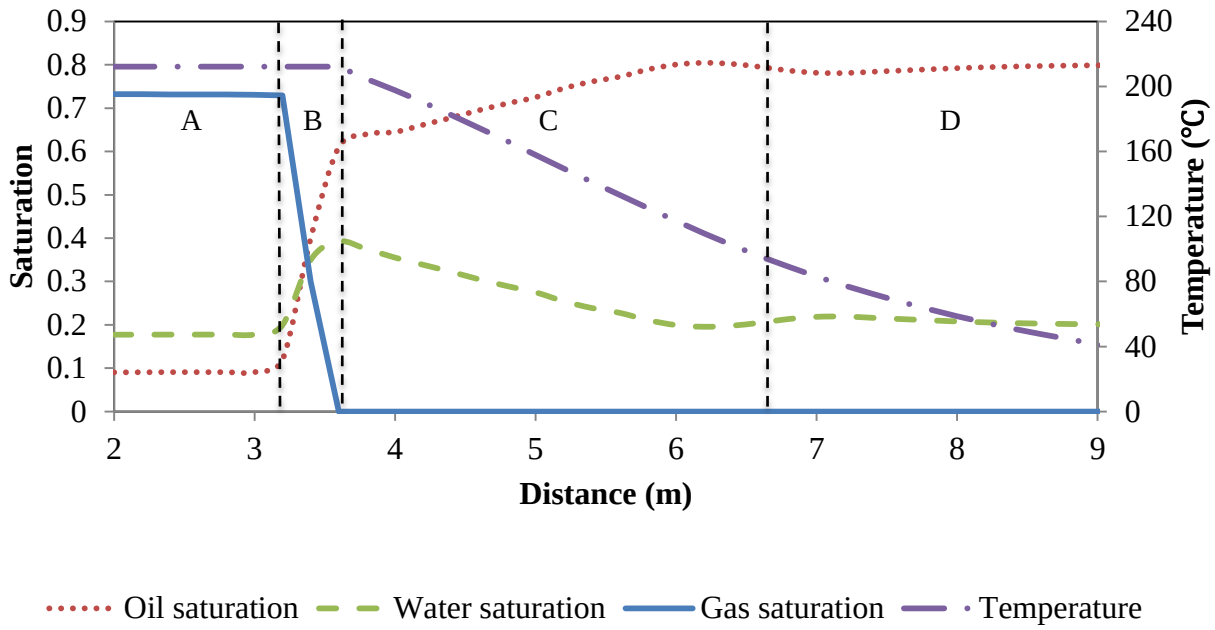

Figure 4.3.3: Gas saturation, oil saturation, water saturation and temperature at 300 days along the bottom location (2 - 9 m) in SAGD with 2000 kPa injection pressure. A is the non-condensation zone. B is the steam condensation zone. C is the mobile oil zone. D is the immobile oil zone.

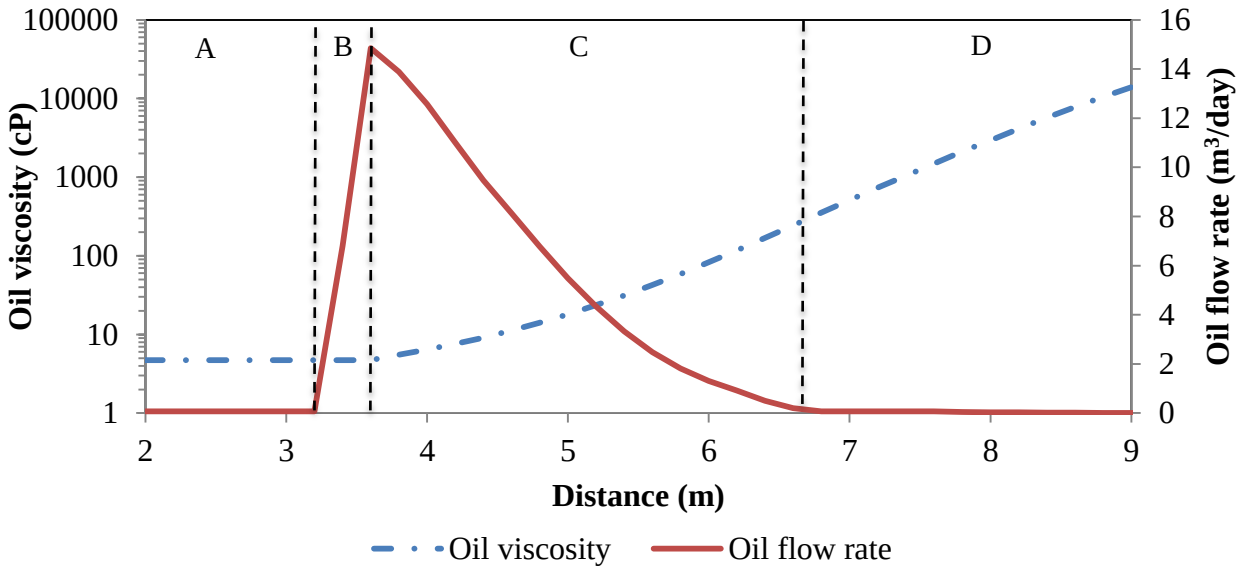

Figure 4.3.4: Oil viscosity and oil flow rate at 300 days along the bottom location (2- 9 m) in SAGD with 2000 kPa injection pressure. A is the non-condensation zone. B is the steam condensation zone. C is the mobile oil zone. D is the immobile oil zone.

4.5 Analysis of SAGD in A Vertical Direction

In Figure 4.4, steam chamber growth is revealed by properties including gas, oil and water saturation and temperature profiles in the cross-section of SAGD at 250, 300 and 340 days. From top to bottom of the reservoir, near the vapor-liquid interface, there is uniform distribution of gas saturation, oil saturation, water saturation and temperature.

Specifically, temperature at the vapor-liquid interface, the thickness of steam condensation and mobile oil zones and total oil flow rate at the top (Figure 4.1.1), middle (Figure 4.2.1) and bottom (Figure 4.3.1) locations (at 300 days) are summarized in Table 4.1.

The thickness of the mobile oil zone is important because it contains the most drained oil, as in the oil flow rate curve shown in Figure 4.3.4. Thickness of this zone is mainly determined by the temperature at the vapor-liquid interface. With higher temperatures, heat can be delivered further to the cold oil sand and enlarges the mobile oil zone. In the SAGD process, the thickness does not change much from top to bottom of the reservoir (in Table 4.1) because of the relatively constant temperature of saturated steam at the vapor-liquid interface. As the heated oil flows downwards, the drained oil accumulates at the lower part of the reservoir. The total oil flow rate is the addition of oil influx from the upper part. For example, the total oil flow rate increases from 59.2 to 104.2 m^3/day as the oil flows from top to bottom.

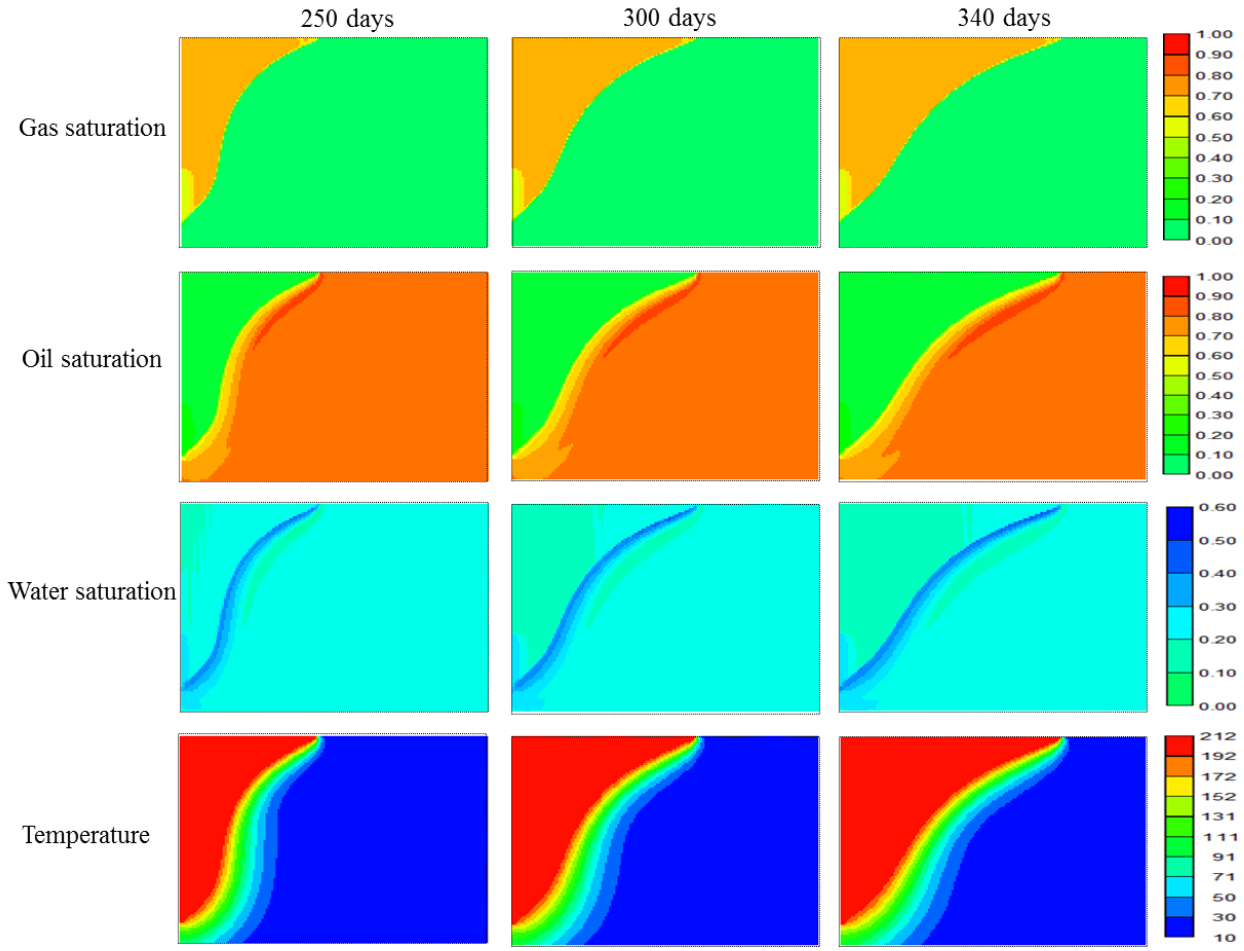

Figure 4.4: Gas saturation, oil saturation, water saturation, temperature and oil flow rate profile in cross-section of SAGD under 2000 kPa, 250, 300 and 340 days. Blank area represents 0 for each property.

Table 4.4: Temperature at the vapor-liquid interface, thickness of steam condensation and mobile oil zones and total oil flow rate at 300 days along the top, middle and bottom locations in SAGD with 2000 kPa injection pressure.

Study location	Top	Middle	Bottom
Temperature at condensation surface (°C)	212	212	212
Steam condensation zone thickness (m)	0.4	0.4	0.4
Mobile oil zone thickness (m)	3.0	3.0	3.2
Total oil flow rate (m^3/day)	59	72	104

4.6 Summary of SAGD Process

Utilizing the comparisons among the top, middle and bottom locations, and the analysis of the gas, oil and water saturations, temperature and oil flow rate variations, the process of oil drainage in SAGD can be summarized. It is shown that heat transfer, including heat conduction and heat convection, is the dominant method to mobilize oil through viscosity reduction. However, it is unclear which method is the dominated for heat delivery from hot vapor to cold oil sand. High temperature of injected vapor and efficient thermal diffusivity of the reservoir can enlarge the mobile oil zone, resulting in an increased oil production rate.

CHAPTER FIVE: ANALYSIS OF SOLVENT AIDED SAGD

5.1 Introduction

In the solvent aided SAGD case, C6 (a suitable solvent proven by Li and Momora, 2011) concentration in injected stream is 0.01 mole fraction (CWE), with other parameters the same as in the SAGD case. Figure 5.1.1 shows oil saturation at 300 days of the pure-steam SAGD case and Figure 5.1.2 shows oil saturation of the solvent aided SAGD case. Comparing the two figures, it is obvious that the swept area by vapor is greatly enlarged by the C6 addition. In other words, more bitumen can be recovered from the reservoir with the addition of C6 within a relatively short time.

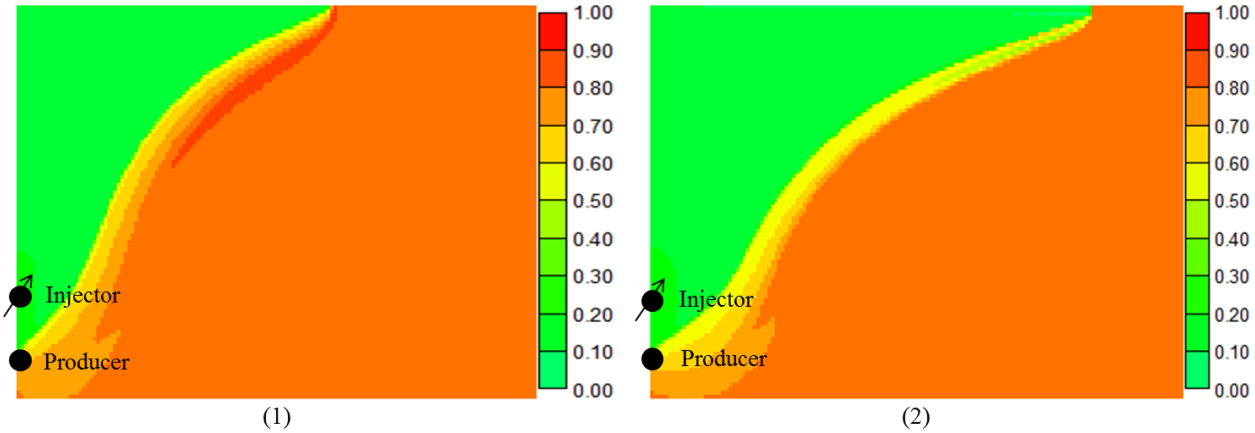

Figure 5.1: Oil saturation in cross-section of the SAGD case (5.1.1) and Oil saturation in cross-section of the solvent aided SAGD case (5.1.2) at 300 days under 2000 kPa injection pressure.

In this chapter, to better understand the roles of steam and solvent in this process, a similar analysis to that of the SAGD case is done for the solvent aided SAGD. The top, middle and bottom locations are selected as shown in Figures 5.2.1, 5.3.1 and 5.4.1 respectively. Schematics of the processes (shown in Figures 5.2.2, 5.3.2 and 5.4.2), which have different behavior with the

pure-steam SAGD, including steam condensation, gas, water and oil flow, and solvent distribution in zones of non-condensation zone (A), steam condensation zone (B), mobile oil zone (C) and immobile oil zone (D) are described as follows:

A. Non-condensation zone: In this zone, pores of the oil sand fill with steam, residual oil and water under constant temperature and pressure. There is no steam condensation.

B. Steam condensation zone: As vapor moves to the cold oil sand, steam starts to condense, with resultant heat transfer to the surrounding formations. Gas saturation becomes zero at the vapor-liquid interface.

C. Mobile oil zone: With the heat transferred to the cold oil sand and solvent dissolution in oil, mobilized oil is drained downwards by gravity.

D. Immobile oil zone: This zone is far from the vapor-liquid interface and the oil cannot be removed by gravity.

5.2 Analysis at Top Location

In Figure 5.2.3, oil, water, and gas saturation and temperature at 300 days have been shown along the top location. C6 mole fractions in the gas and oil phase are shown in Figure 5.2.4. Oil viscosity and oil flow rate are shown at the same location in Figure 5.2.5.

In the non-condensation zone (A in Figures 5.2.3, 5.2.4 and 5.2.5, 0.0 – 12.6 m), the vapor mixture of steam and C6 flows upwards and laterally at constant temperature and pressure. In Figure 5.2.3, water and oil are shown at the residual level. As shown by Figure 5.2.4, most C6 remains in vapor and a very small part of C6 is dissolved in the residual oil under the action of gas-oil equilibrium. Oil is immobile as the oil flow rate curve shows in Figure 5.2.5.

The thickness of the steam condensation zone (B in Figures 5.2.3, 5.2.4 and 5.2.5, 12.6 – 15.2 m) is greatly enlarged by co-injection of C6 when it is compared to the SAGD case (10.0 – 10.4 m). This is because, in this zone, there is a gradual steam condensation process in which only steam condenses towards the vapor-liquid interface in a large range of solvent fraction in vapor (Dong, 2012).

The temperature of the steam-C6 vapor mixture starts to decrease gradually towards the cold oil sand until it reaches the equilibrium state at the vapor-liquid interface as shown in Figure 5.2.3. In this zone, continuous steam condensation as the temperature drops is revealed by the gradually decreased gas saturation curve. The difference between the solvent aided SAGD and SAGD also includes gradually increased oil saturation through C6 dissolution in oil towards the interface. Additionally, this condensation process results in a gradual increase of C6 mole fraction in vapor as illustrated in Figure 5.2.4. At the vapor-liquid interface, the C6 mole fraction in vapor reaches the maximum value of 0.41. Correspondingly, the C6 mole fraction in oil, which is determined by the gas-oil equilibrium, increases gradually and reaches the highest level at 0.62.

Compared to the SAGD case, oil viscosity is further reduced in solvent aided SAGD by C6 dilution. The total oil flow rate is increased in this zone. This is proven by the area beneath the oil flow rate curve in Figure 5.2.5, which is larger than the area in the SAGD case at the same location (Figure 4.1.4).

In the mobile oil zone (C in Figures 5.2.3, 5.2.4 and 5.2.5, 15.2 – 17.6 m), the condensed water and mobilized oil containing dissolved C6 flow downwards. C6 is distributed far from the vapor-liquid interface in the mobile oil zone (Figure 5.2.4) and helps to reduce oil viscosity as shown in Figure 5.2.5.

At the vapor-liquid interface, the oil saturation curve reaches its peak due to the high mole fraction of C6 in oil. Towards the cold oil sand, oil saturation decreases caused by the gradually reduced C6 mole fraction, and then it increases to the original oil saturation.

In this zone, the oil flow rate is also significantly improved by C6 dilution, when the rate is compared to that of pure-steam SAGD case. Ahead of the vapor-liquid interface, where there is a high temperature and high C6 mole fraction in oil, the oil flow rate reaches its maximum value at 43 m^3/day.

Beyond the oil flow boundary (D in Figures 5.2.3, 5.2.4 and 5.2.5, 17.6 – 30.0 m) which is the immobile oil zone, oil cannot be removed under low temperature. The C6 mole fraction in oil becomes zero without mobile oil as shown in Figure 5.2.5.

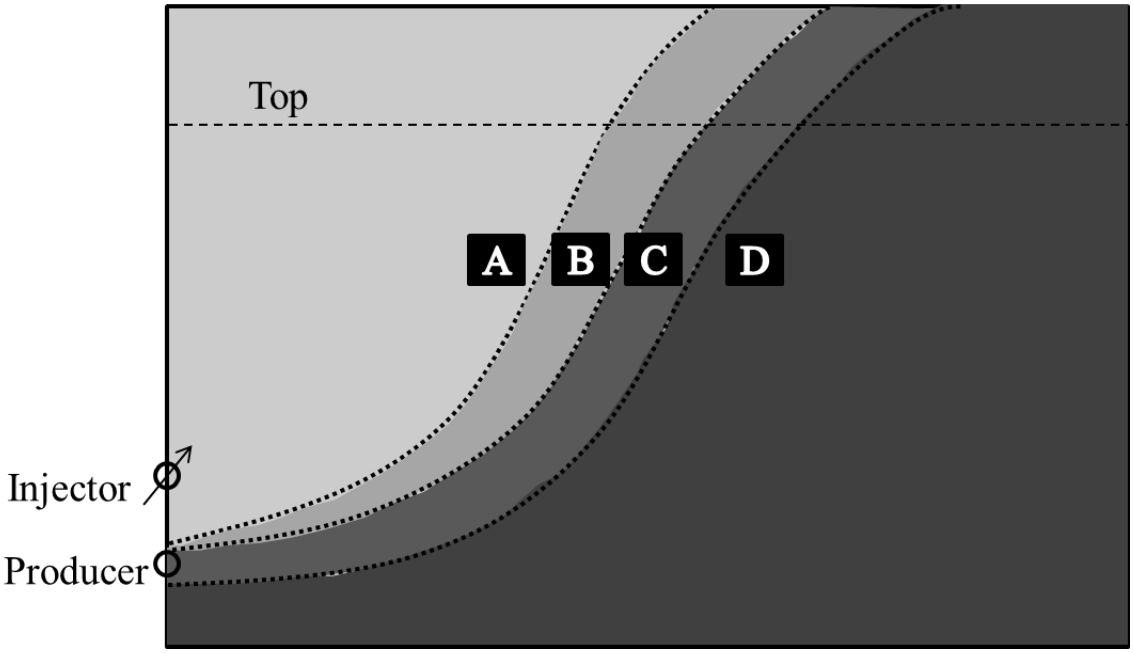

Figure 5.2.1: Four zones near the transition region illustrated by oil saturation distribution in cross-section of solvent aided SAGD. The dished line is the top location same as the SAGD case.

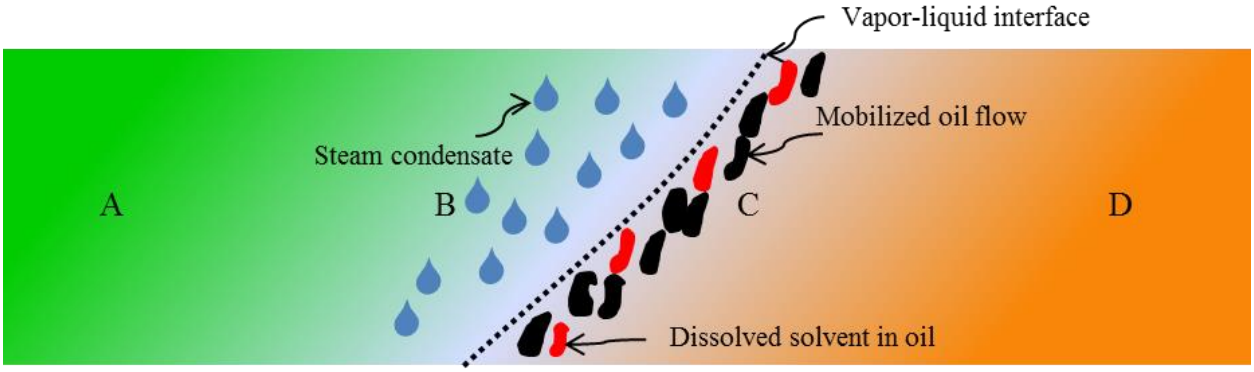

Figure 5.2.2: Schematic of four zones present along the top location in solvent aided SAGD. The blue droplets represent steam condensate, the red droplets represent solvent in oil phase and the black droplets stand for mobile oil. A is the non-condensation zone. B is the steam condensation zone. C is the mobile oil zone. D is the immobile oil zone. The dashed line is the vapor-liquid interface.

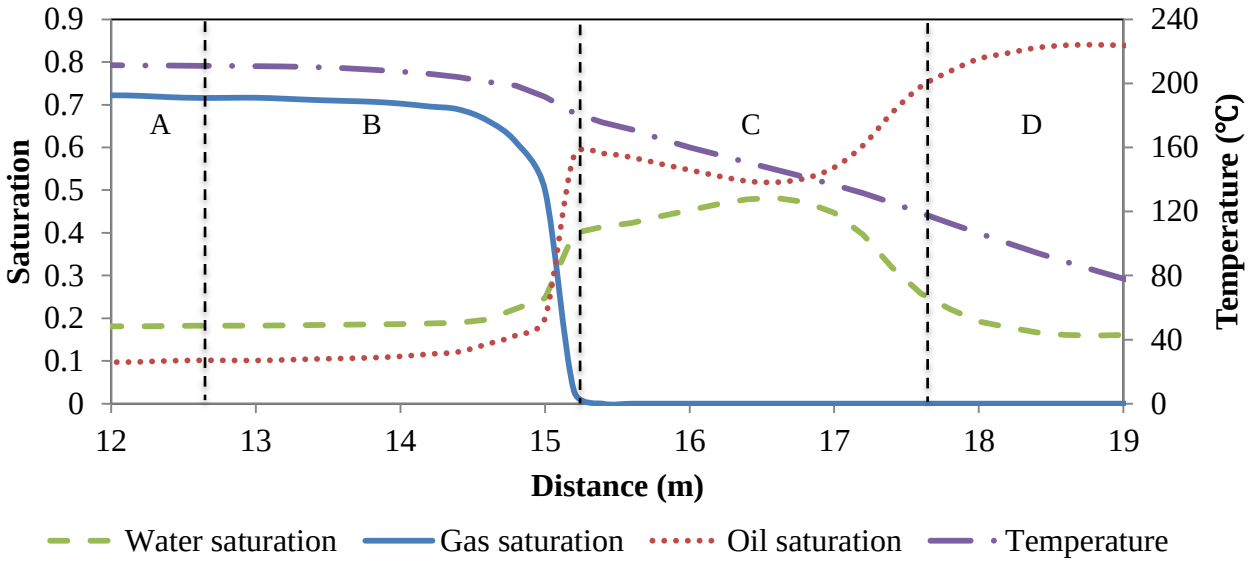

Figure 5.2.3: Gas saturation, oil saturation, water saturation and temperature at 300 days along the top location (12 -19 m) in solvent aided SAGD with 2000 kPa injection pressure and 0.01 mole fraction C6. A is the non-condensation zone. B is the steam condensation zone. C is the mobile oil zone. D is the immobile oil zone.

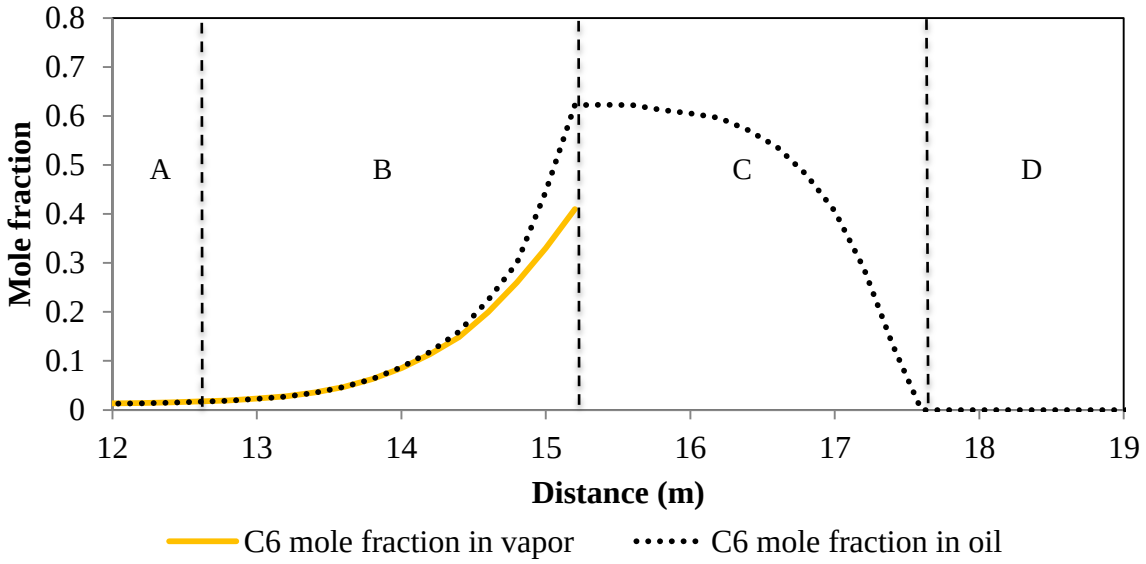

Figure 5.2.4: C6 mole fraction in vapor and C6 mole fraction in oil at 300 days along the top location (12 -19 m) in solvent aided SAGD with 2000 kPa injection pressure and 0.01 mole fraction C6. A is the non-condensation zone. B is the steam condensation zone. C is the mobile oil zone. D is the immobile oil zone.

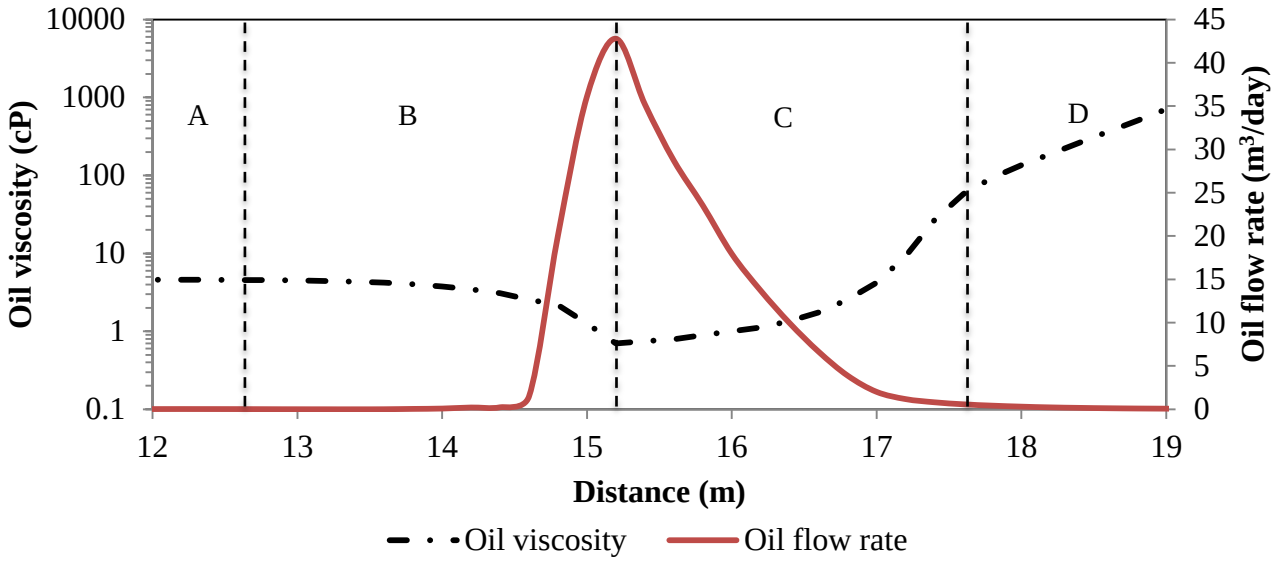

Figure 5.2.5: Oil viscosity and oil flow rate at 300 days along the top location (12- 19 m) in solvent aided SAGD with 2000 kPa injection pressure and 0.01 mole fraction C6. A is the non-condensation zone. B is the steam condensation zone. C is the mobile oil zone. D is the immobile oil zone.

5.3 Analysis at Middle Location

In order to describe the process of oil flow in the reservoir, analysis at the middle location (Figure 5.3.1) has been done. A similar analysis to that done at the top location was done for the middle location. Schematics of the processes also including steam condensation, gas, water and oil flow in the non-condensation zone (A), steam condensation zone (B), mobile oil zone (C) and immobile oil zone (D) are shown in Figure 5.3.2.

In Figure 4.3.3, oil, water, and gas saturation and temperature have been shown along the middle location at 300 days. The C6 mole fraction in gas and oil are shown in Figure 5.3.4. Oil viscosity and oil flow rate are shown at the same location in Figure 5.3.5.

In the non-condensation zone (A in Figures 5.3.3, 5.3.4 and 5.3.5, 0.0 – 7.6 m), similar to the properties at the top location, water and oil remain at the residual level and a very small part of

C6 is dissolved in the residual oil by gas-oil equilibrium. Oil cannot flow, as demonstrated by the flow rate curve shown in Figure 5.3.5.

In the steam condensation zone (B in Figures 5.3.3, 5.3.4 and 5.3.5, 7.6 – 9.2 m), its thickness is largely reduced when it is compared to the thickness at the top location (12.6 – 15.2 m). This is because, at the middle location, the amount of condensed steam decreases since there is a smaller heat loss to overburden than at the top location. As a consequence, the equilibrium state at the vapor-liquid interface can be achieved sooner with lower C6 mole fractions in vapor and oil.

As shown in Figure 5.3.3, the temperature of steam-C6 vapor mixture at the vapor-liquid interface (189 ℃) is increased when it is compared to the temperature at the top location (183 ℃) (Figure 5.2.3). At the vapor-liquid interface, the C6 mole fraction in vapor reaches the highest value at 0.38. Correspondingly, the C6 mole fraction in oil also increases gradually and reaches the highest level at 0.51.

At the middle location, oil viscosity cannot be reduced as much as that at the top location because of lowered solvent dissolution in oil. Moreover, the total oil flow rate is also decreased, as shown by comparison between the areas beneath the oil flow rate curves in Figures 5.2.5 and 5.3.5.

In the mobile oil zone (C in Figures 5.3.3, 5.3.4 and 5.3.5, 9.2 – 11.4 m), by changing the study location from the top to the middle, some differences occurred as oil and water flow downwards. From the vapor-liquid interface, oil saturation increases until it reaches the original oil saturation towards the cold oil sand. In this zone, the magnitude of oil viscosity reduction is lower (Figure 5.3.5) when compared to the top location as shown in Figure 5.2.5. Ahead of the vapor-liquid interface, the oil flow rate reaches its maximum value at 36 m^3/day, which is lower than the rate at the top location (43 m^3/day).

Beyond the oil flow boundary (D in Figure 5.3.3, 5.3.4 and 5.3.5, 11.4 – 30.0 m) which is the immobile oil zone, oil cannot be removed under low temperature.

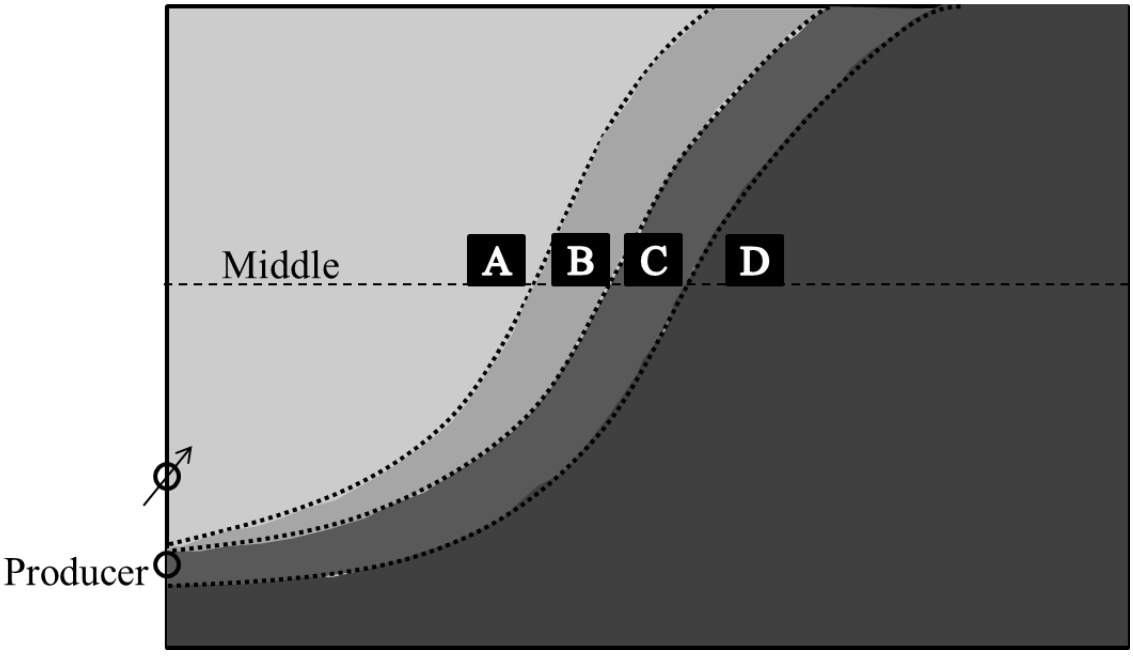

Figure 5.3.1: Four zones near the transition region illustrated by oil saturation distribution in cross-section of solvent aided SAGD. The dished line is the medium location same as the SAGD case.

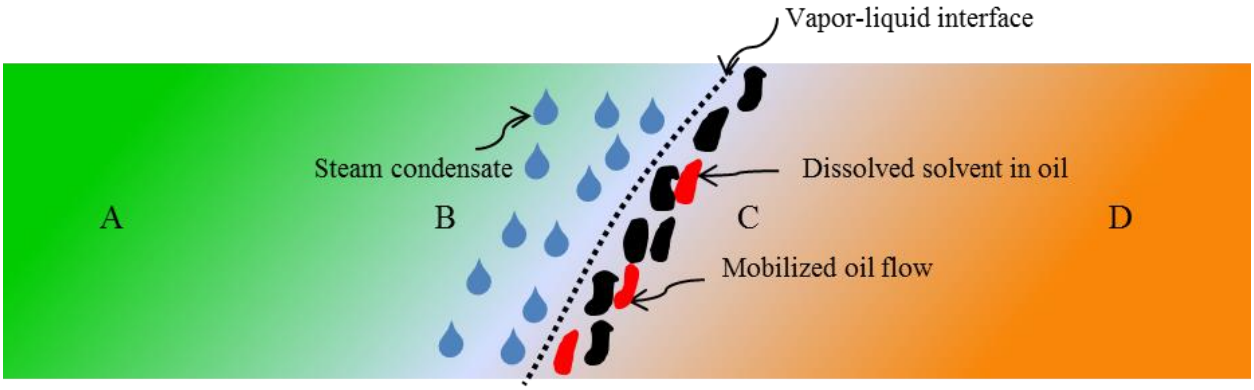

Figure 5.3.2: Schematic of four zones present along the middle location in solvent SAGD. The blue droplets represent steam condensate, the red droplets represent solvent in oil phase and the black droplets stand for mobile oil. A is the non-condensation zone. B is the steam condensation zone. C is the mobile oil zone. D is the immobile oil zone. The dashed line is the vapor-liquid interface.

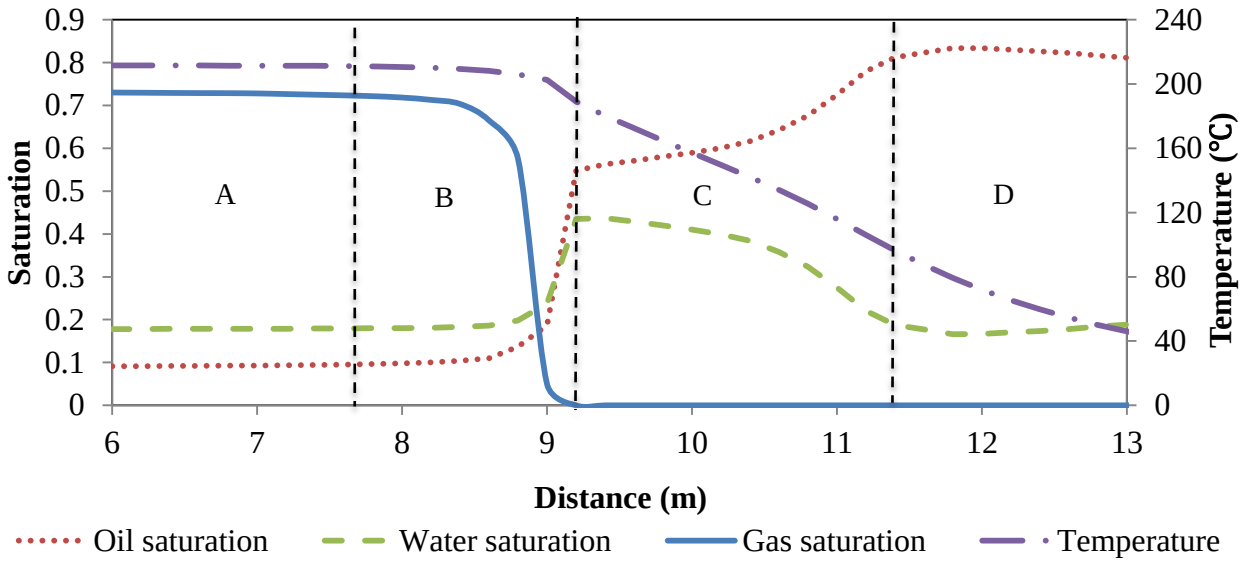

Figure 5.3.3: Gas saturation, oil saturation, water saturation and temperature at 300 days along the middle location (7 -13 m) in solvent aided SAGD with 2000 kPa injection pressure and 0.01 mole fraction C6. A is the non-condensation zone. B is the steam condensation zone. C is the mobile oil zone. D is the immobile oil zone.

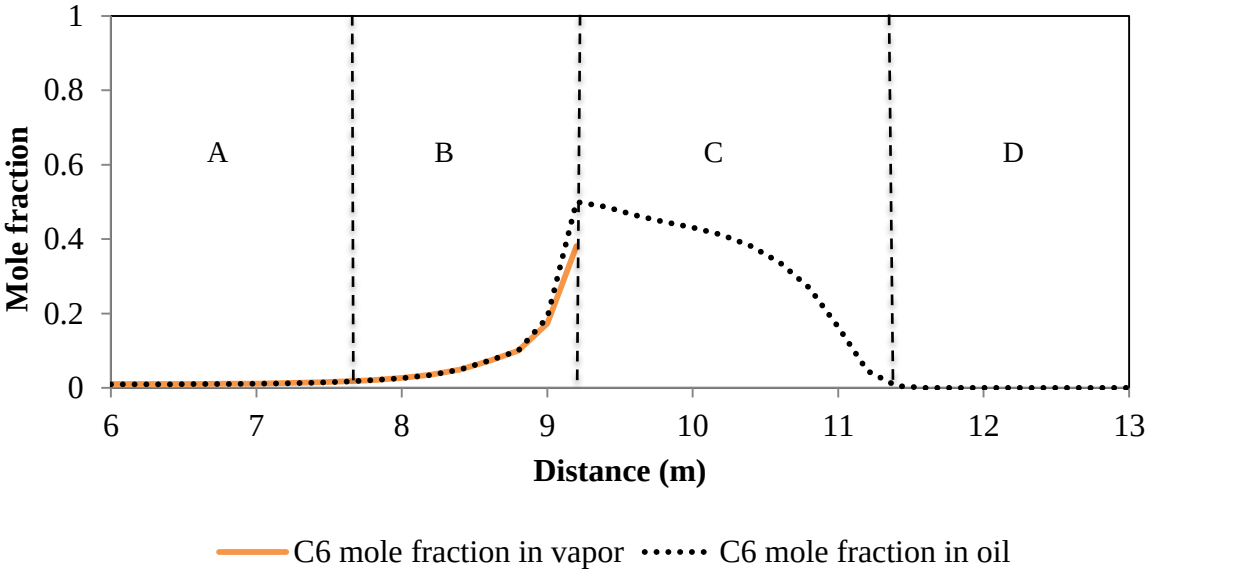

Figure 5.3.4: C6 mole fraction in vapor and C6 mole fraction in oil at 300 days along the middle location (7 -13 m) in solvent aided SAGD with 2000 kPa injection pressure and 0.01 mole fraction C6. A is the non-condensation zone. B is the steam condensation zone. C is the mobile oil zone. D is the immobile oil zone.

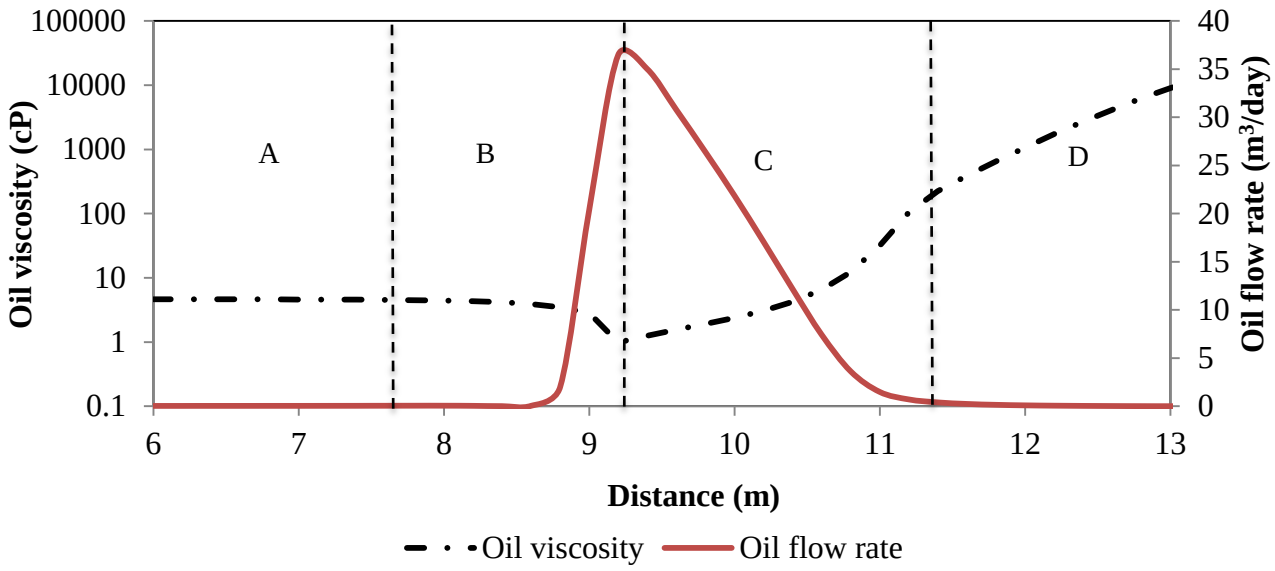

Figure 5.3.5: Oil viscosity and oil flow rate at 300 days along the middle location (7- 13 m) in solvent aided SAGD with 2000 kPa injection pressure and 0.01 mole fraction C6. A is the non-condensation zone. B is the steam condensation zone. C is the mobile oil zone. D is the immobile oil zone.

5.4 Analysis at Bottom Location

Analysis at the bottom location (Figure 5.4.1) has been done to study the behavior of steam-solvent and oil flow at the lower part of the reservoir. A similar analysis to those done at the above two locations was done for the bottom. Schematics of the processes in the non-condensation zone (A), steam condensation zone (B), mobile oil zone (C) and immobile oil zone (D) are illustrated in Figure 5.4.2.

In Figure 5.4.3, oil, water, and gas saturation and temperature have been shown along the bottom location at 300 days. Curves of the C6 mole fraction in vapor and oil are plotted in Figure 5.4.4. Oil viscosity and flow rate are shown at the same location in Figure 5.4.5.

In the non-condensation zone (A in Figures 5.4.3, 5.4.4 and 5.4.5, 0.0 – 3.8 m), water and oil remain at the residual level and a very small amount of C6 is dissolved in the residual oil under constant pressure and temperature.

In the steam condensation zone (B in Figures 5.4.3, 5.4.4 and 5.4.5, 3.8 – 4.6 m), the thickness of this zone is further reduced, compared to the thickness at the middle location (7.6 – 9.2 m). As shown in Figure 5.4.3, the temperature at the vapor-liquid interface is 201 ℃, which is higher than the temperature at the top location (183 ℃) and the temperature at the middle location (189 ℃). At the vapor-liquid interface, the C6 mole fraction in vapor is 0.20 and the C6 mole fraction in oil is 0.28. From top to bottom locations of the reservoir, the total oil flow rate is continuously decreased, as shown by comparison between the areas beneath the oil flow rate curves in Figures 5.2.5, 5.3.5 and 5.4.5 respectively.

In the mobile oil zone (C in Figures 5.4.3, 5.4.4 and 5.4.5, 4.6 – 7.2 m), the thickness is slightly increased when changing the study location from the top (12.6 – 15.2 m) to the middle (9.2 – 11.4 m) and then the bottom, because of the increased temperature at the vapor-liquid interface. Furthermore, at the bottom location, there is a slight increase in the C6 mole fraction in oil from the vapor-liquid interface to the cold oil sand, as shown by the curve of the C6 mole fraction in oil in Figure 5.4.4. The highest C6 mole fraction is located within this zone, but not the vapor-liquid interface. This is because of the accumulation of C6 delivered by drainage from the upper layers in this zone. The oil flow rate is also decreased caused by the lowered amount of dissolved C6 mole fraction in oil.

Beyond the oil flow boundary (D in Figures 5.4.3, 5.4.4 and 5.4.5, 7.2 – 30.0 m) which is the immobile oil zone, oil cannot flow.

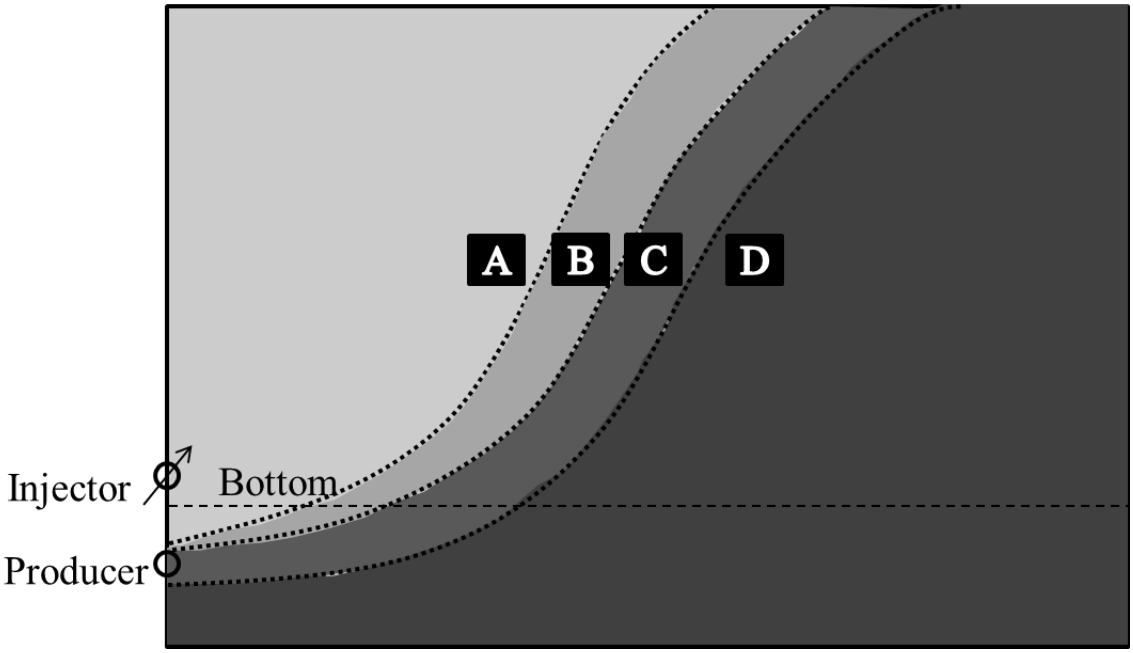

Figure 5.4.1: Four zones near the transition region illustrated by oil saturation distribution in cross-section of solvent aided SAGD. The dished line is the bottom location same as the SAGD case.

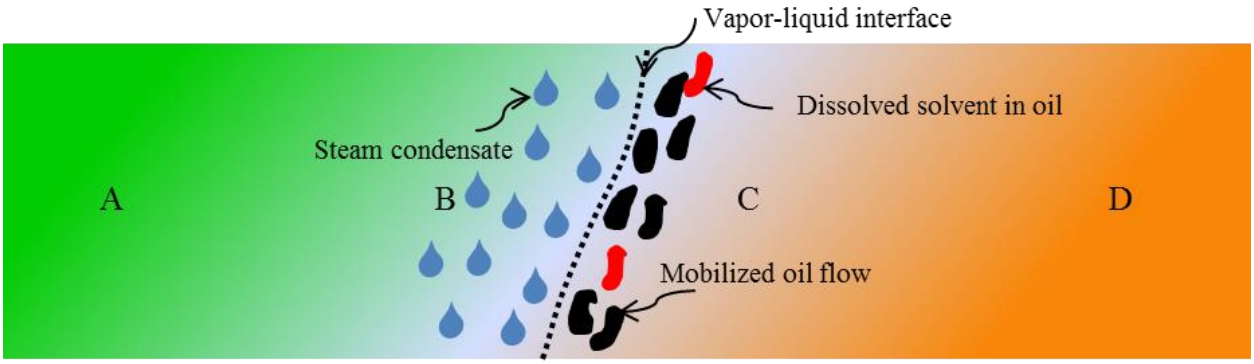

Figure 5.4.2: Schematic of four zones present along the bottom location in solvent aided SAGD. The blue droplets represent steam condensate, the red droplets represent solvent in oil and the black droplets stand for mobile oil. A is the non-condensation zone. B is the steam condensation zone. C is the mobile oil zone. D is the immobile oil zone. The dashed line is the vapor-liquid interface.

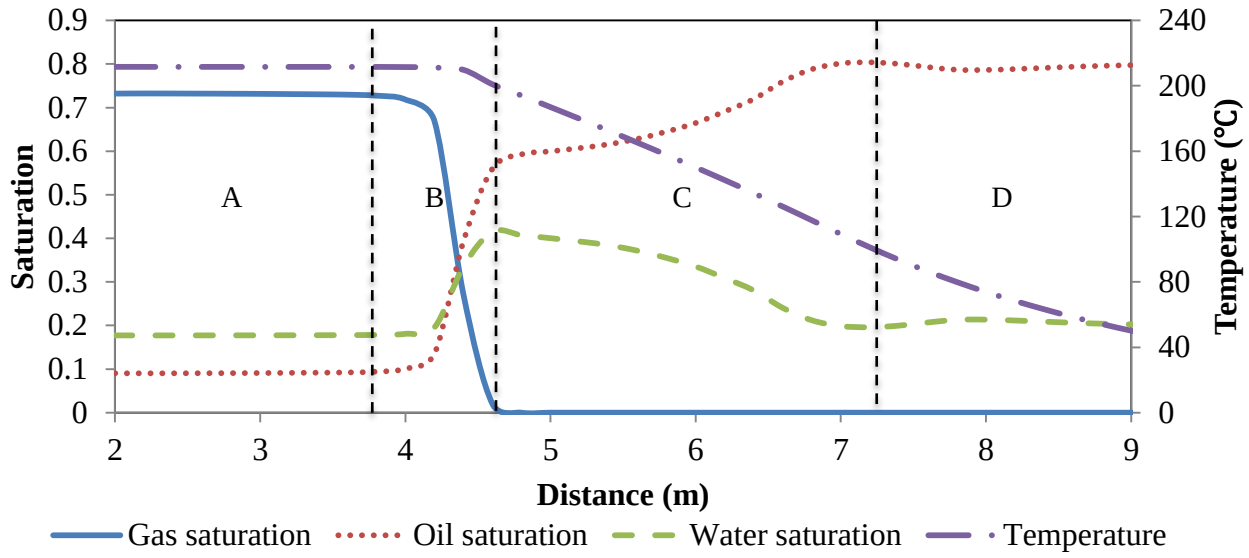

Figure 5.4.3: Gas saturation, oil saturation, water saturation and temperature at 300 days along the bottom location (2 -9 m) in solvent aided SAGD with 2000 kPa injection pressure and 0.01 mole fraction C6. A is the non-condensation zone. B is the steam condensation zone. C is the mobile oil zone. D is the immobile oil zone.

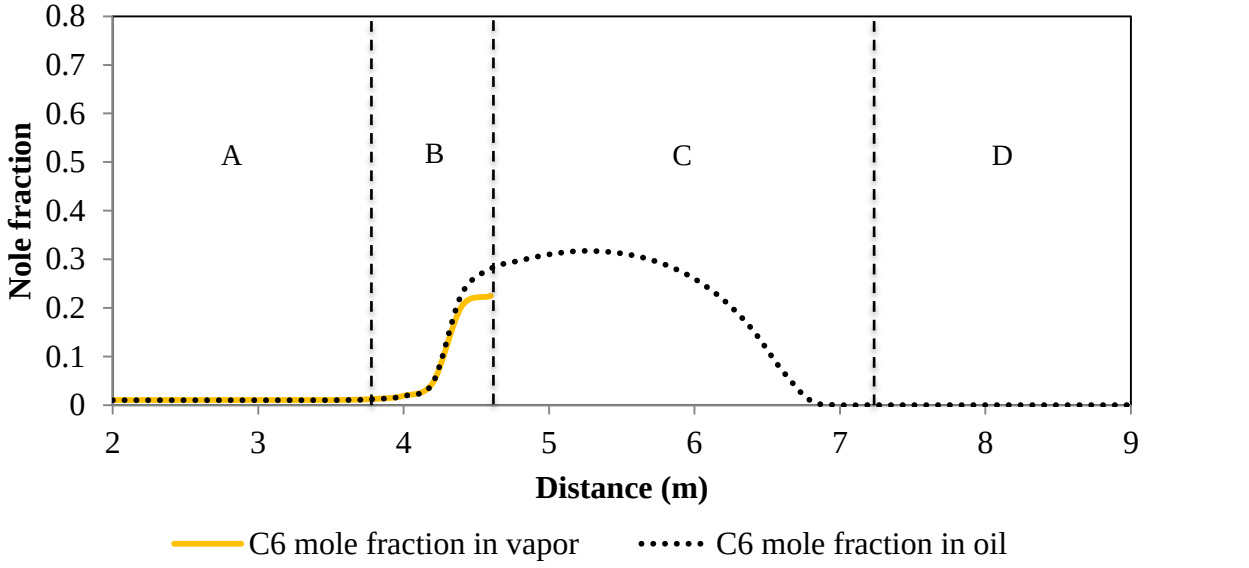

Figure 5.4.4: C6 mole fraction in vapor and C6 mole fraction in oil at 300 days along the bottom location (2 - 9 m) in solvent aided SAGD with 2000 kPa injection pressure and 0.01 mole fraction C6. A is the non-condensation zone. B is the steam condensation zone. C is the mobile oil zone. D is the immobile oil zone.

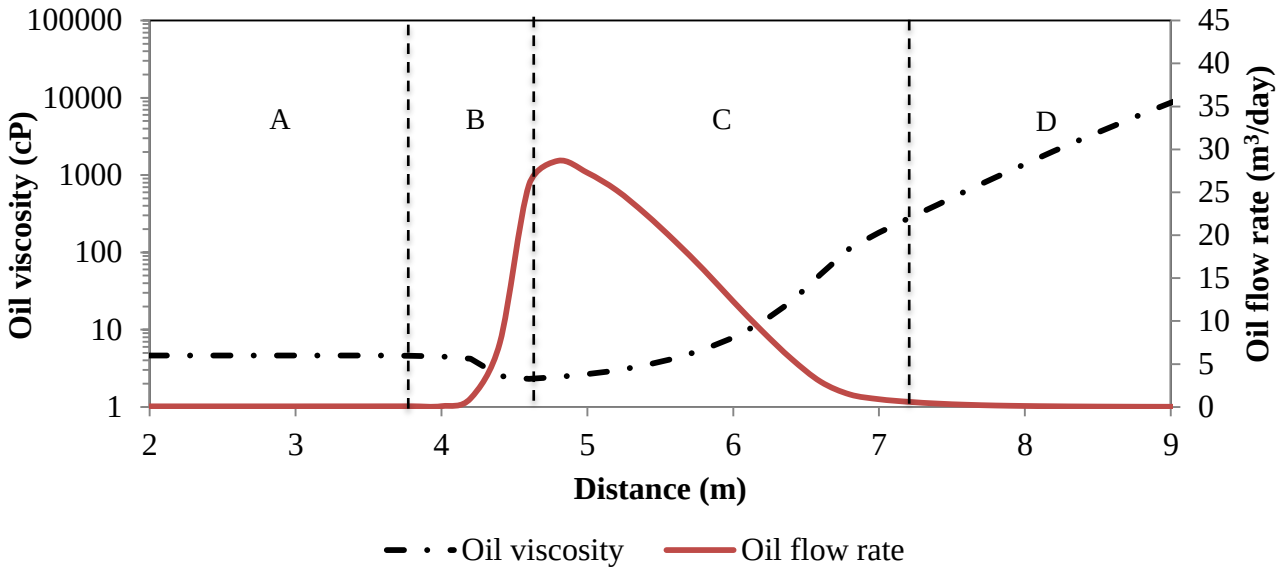

Figure 5.4.5: Oil viscosity and oil flow rate at 300 days along the bottom location (2 - 9 m) in solvent aided SAGD with 2000 kPa injection pressure and 0.01 mole fraction C6. A is the non-condensation zone. B is the steam condensation zone. C is the mobile oil zone. D is the immobile oil zone.

5.5 Analysis of Solvent Aided SAGD in A Vertical Direction

Comparing Figures 5.1.1 and 5.1.2, using C6 co-injection, the lateral steam chamber growth rate is accelerated primarily at the top part of the reservoir. To understand this process, gas, oil and water saturation, C6 mole fraction in oil, temperature and oil flow rate are shown in Figure 5.5 for the solvent aided SAGD case at 250, 300 and 340 days respectively. Furthermore, properties including C6 mole fractions in vapor and oil at the vapor-liquid interface, thickness of steam condensation and mobile oil zones and oil flow rate along top (Figure 5.2.1), middle (Figure 5.3.1) and bottom (Figure 5.4.1) locations of the reservoir at 300 days are summarized in Table 5.1 .

In Figure 5.5, it is shown that water saturation at the top of the reservoir is higher than that at the bottom. There is also a tendency toward C6 dissolution in oil decreasing from the top to the bottom of the reservoir.

At the top location, as the steam-C6 mixture flows into the steam condensation zone, there is much heat loss to overburden and transfer to the cold oil sand, and much steam condenses with the equilibrium state of high C6 mole fraction in vapor (0.46) and high C6 mole fraction in oil (0.70) at the vapor-liquid interface. As oil flows to the middle location, the C6 mole fraction in vapor is decreased to (0.38) and the C6 mole fraction in oil decreased to 0.51. At the bottom location, the C6 mole fraction in vapor is low (0.20) and the C6 mole fraction in oil is also low (0.28) at the interface due to little heat loss. As a result, there is more C6 in the mobile oil zone at the top than at the bottom. From top to bottom, even though the thickness of the mobile oil zone slightly increases from 2.2 m to 2.4 m due to the increase of temperature from 183 to 200 ℃, the steam chamber grows faster at the top than at the bottom because of the more significant effect of C6 dissolution in oil than the thickness of this zone.

According to the gas-oil equilibrium process under different temperatures near the vapor-liquid interface, C6 returns back from oil to vapor as the oil flows downwards in the mobile oil zone. As a result, part of the mobile oil becomes immobile when it is drained to the lower part of reservoir. For example, at 300 days, the total oil rate decreases from 267 to 187 m^3/day as the oil flows downwards from top to bottom (Table 5.1).

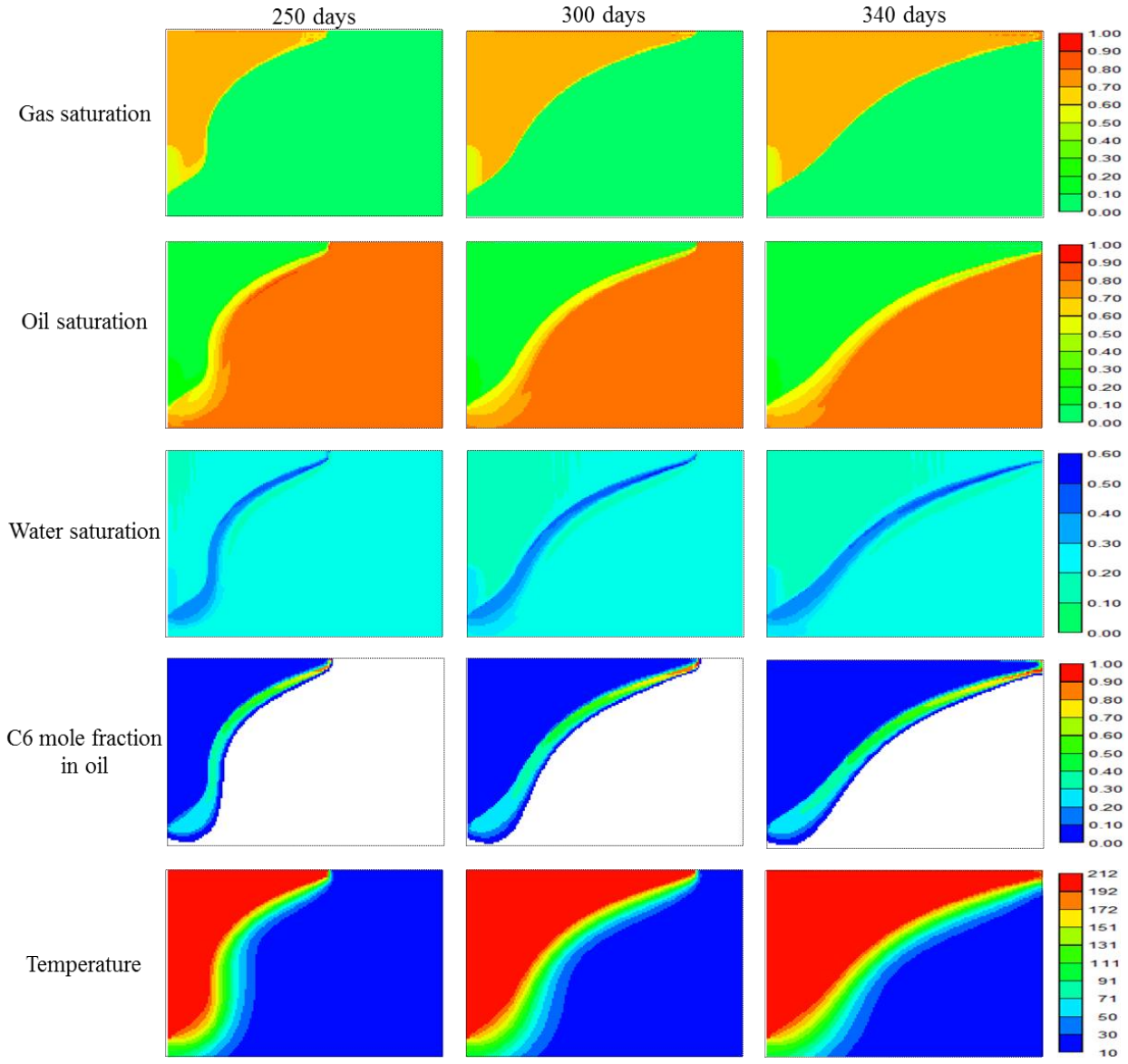

Figure 5.5: Gas saturation, oil saturation, water saturation, C6 mole fraction in oil and temperature profile in cross-section of solvent aided SAGD with 2000 kPa and 0.01 mole fraction C6, at 250, 300 and 340 days. Blank area represents 0 for each property.

Table 5.1: Temperature at the vapor-liquid interface, thickness of steam condensation zone and mobile oil zone, C6 mole fractions in gas and oil at the interface and total oil flow rate at 300 days along the top, middle and bottom locations in solvent aided SAGD with 2000 kPa injection pressure and 0.01 mole fraction C6 co-injection.

Study location	Top	Middle	Bottom
Temperature at vapor-liquid interface (℃)	183	189	201
Steam condensation zone thickness (m)	2.6	1.6	0.8
Non-gas oil mobile zone thickness (m)	2.2	2.2	2.6
C6 mole fraction in vapor at vapor-liquid interface	0.46	0.38	0.20
C6 mole fraction in oil at vapor-liquid interface	0.70	0.50	0.28
Total oil flow rate(m^3/day)	267	213	187

5.6 Analysis of Solvent Mass Transfer in Oil

In solvent aided SAGD, near the vapor-liquid interface, solvent dissolves into the oil phase through gas-oil equilibrium. As the curves of C6 mole fraction in oil show in Figures 5.2.5, 5.3.5 and 5.4.5, C6 is further transferred to the oil sand beyond the interface. Thus, the methods for solvent transfer are critically important and need to be studied.

5.6.1 Solvent Flow in the Mobile Oil Zone

The transfer of solvent in this zone can be explained by Figures 5.6.1 and 5.6.2, which illustrate a schematic description of solvent transfer from vapor further into the mobile oil zone. First, since the steam-solvent mixture is in direct contact with bitumen at the vapor-liquid interface, solvent is dissolved into the oil by gas-oil equilibrium, instantaneously (Figure 5.6.1). The solubility of the solvent in the oil is determined by the temperature of the vapor-liquid interface and the partial pressure of the solvent in the vapor phase near the interface. Second, as oil flows downward within the sloped mobile oil zone, C6 is convectively transferred further into the oil sand, establishing a solvent-rich zone. As in the force analysis, shown in Figure 5.6.2, gravity (G) on dissolved C6 can be divided into two components: one is parallel to the vapor-liquid interface (F_1); another is perpendicular to the interface (F_2). As a result, in the first instance, the dissolved

C6 has the potential to flow parallel to the vapor-liquid interface (v_1). In the second instance, C6 can be delivered by the perpendicular force (F_2) deep into the mobile oil zone (v_2), where oil has already been mobilized by heat transfer. An equilibrium state of C6 distribution is established within this zone within a short time, as shown in the curve of the C6 mole fraction in oil in Figures 5.2.5, 5.3.5 and 5.4.5. The C6 mole fraction in oil decreases as it flows towards the cold oil sand because of the decreased oil flow rate. It is also found that if there is a vertical vapor-liquid interface, C6 only dissolves into the oil at the interface without moving further into the mobile oil zone, as shown in Figure 5.6.3. This is because there is no force to enable the dissolved C6 to move further into the oil sand. In order to demonstrate the effect of gravity, Figure 5.7 shows the oil flow direction and trajectory by streamline in the mobile oil zone. As shown in Figure 5.7.1, it can be found that, when oil is flowing in the sloping mobile oil zone, there is a small angle between oil flow streamline and the vapor-liquid interface, which means that oil is flowing deeper in the mobile oil zone by gravity. However, the oil flow streamline in the vertical mobile oil zone is parallel to the vapor-liquid interface without oil flow deeper to the mobile oil zone.

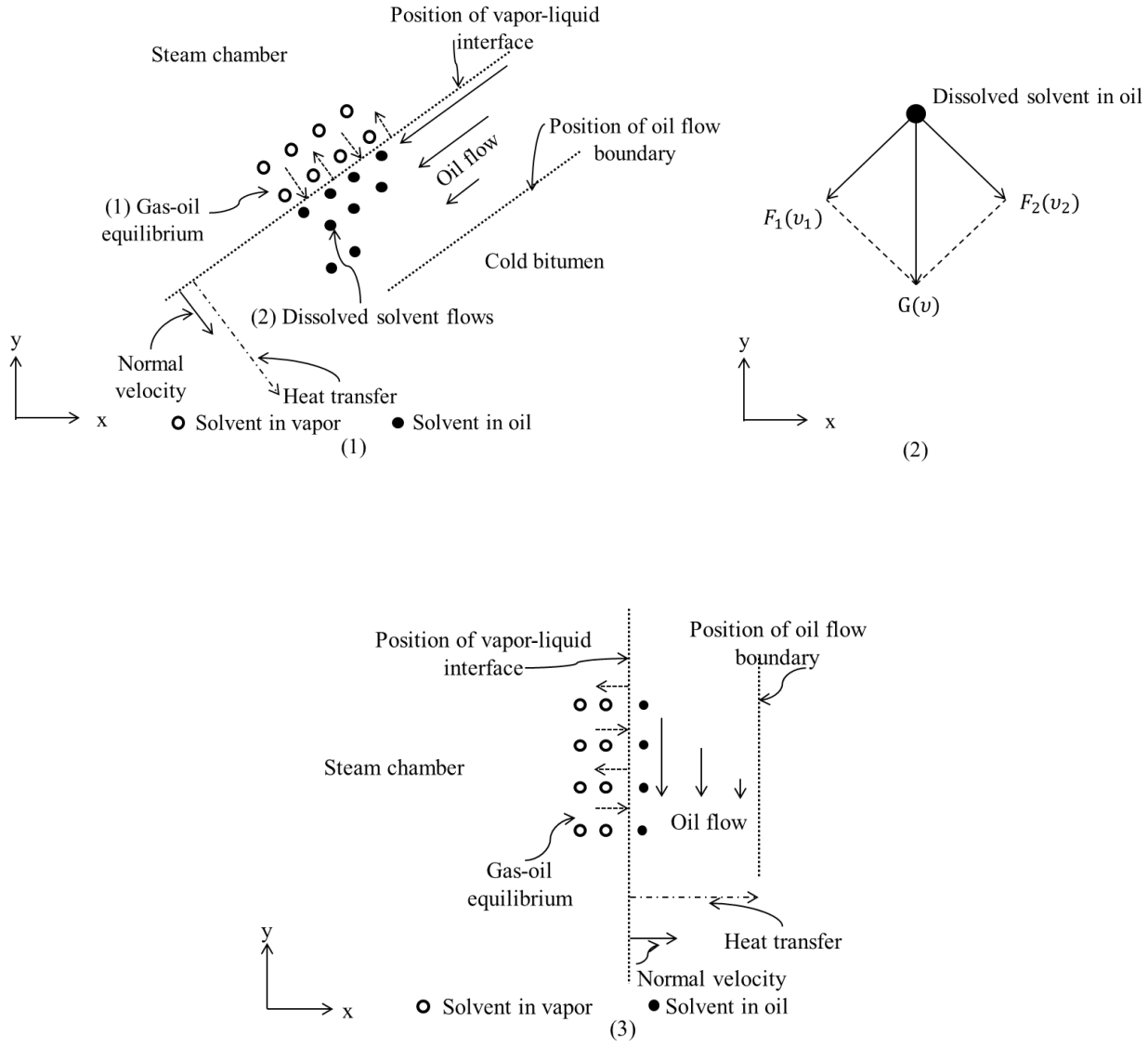

Figure 5.6: Illustration of solvent dissolution and transfer in oil. 5.6.1 is the process of solvent vapor contacting oil at a sloped interface. 5.6.2 is the movement of dissolved C6 under the analysis of force and velocity. Gravity (G) is divided into two components: F_1 and F_2. 5.6.3 is the process of solvent vapor contacting oil at a vertical interface.

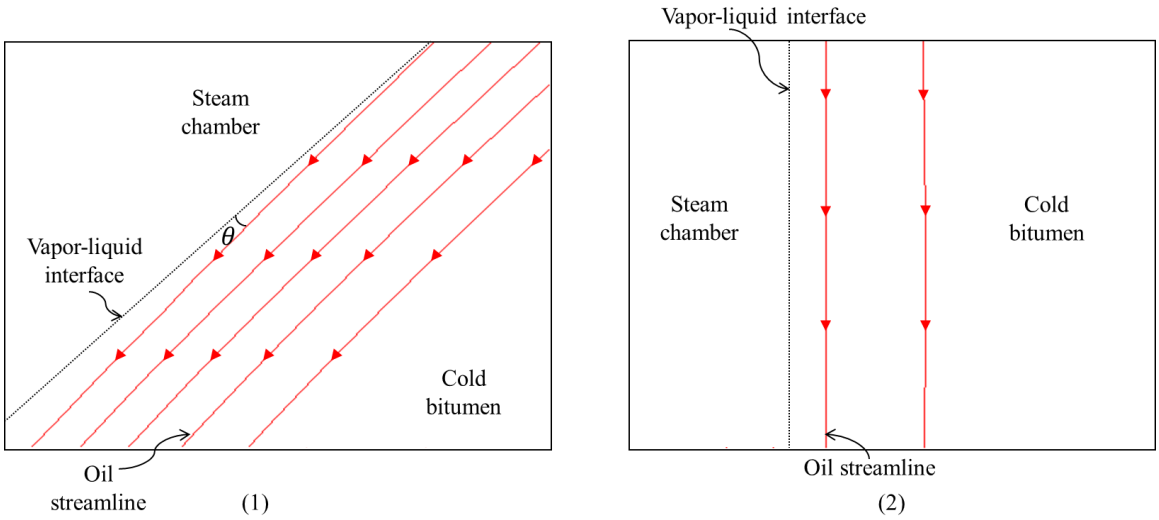

Figure 5.7: Oil flow streamline in mobile oil zone. 5.7.1 is oil flow in sloping mobile oil zone; 5.7.2 is oil flow in vertical mobile oil zone.

5.6.2 Analysis of Solvent Diffusion Process

Analysis is done to understand the effect of solvent diffusion on the process. The typical diffusion coefficient of solvent in bitumen was estimated as ranging from 8.64×10^{-6} to 4.32×10^{-5} m^2/day, according to the test of propane and butane diffusion in Peace River bitumen (Das and Butler, 1996). An estimation of the solvent diffusion distance was proposed as follows (Butler and Mokrys, 1989):

$$\xi = \frac{1}{U}\int_{C_{s,min}}^{C_{s,max}} \frac{D_s}{C_s}\, dC_s$$

where ξ is the distance the solvent diffused, U is the vapor-liquid interface advance velocity, C_s is the solvent concentration and D_s is the diffusion coefficient of solvent through oil phase.

Assume the steam chamber is moving at 0.015 m/day (U) (Butler, 1997), C_s is 0.51 at the vapor-liquid interface ($C_{s,max}$), and 0.01 at end of diffusion ($C_{s,min}$), as shown in Figure 4.3.4, and the C6 diffusion coefficient is 4.32×10^{-5} m^2/day (D_s). As a result, the diffusion distance is estimated

at only 0.01 m, which is two orders lower than the thickness of the mobile oil zone we observed (2.2 m).

In this study, a simulation was done by greatly varying the C6 diffusion coefficient in oil to see if oil recovery is greatly affected by the diffusion process. The effect of temperature and pressure on solvent diffusion in oil is reviewed and summarized in Table 5.2. It is noted that temperature or pressure can affect diffusion process, rather than extensively. When temperature changes from 50 to 90 ℃, the diffusion coefficient is increased by less than 10 times. By change in pressure from 4.0 to 8.0 Mpa, the diffusion coefficient is increased by less than 3 times.

Figure 5.4 shows the simulated oil recovery factor at 600 days (end of production) with different C6 diffusion coefficients. It is noted that the recovery factor is increased only by 2.1 % from 69.4 to 71.5 % when the C6 diffusion coefficient is increased by 10000 times (4.32×10^{-6} m^2/day versus 4.32×10^{-2} m^2/day). Figure 5.5 shows the simulated oil recovery factor at 600 days with different dispersivity. It is found that the oil recovery factor changes little when the dispersivity is increased from 0.00002 to 0.2 m. The reason for this phenomenon is practically because that diffusion or dispersion can be negligible for C6 mass transfer in this process. In addition, as the oil recovery factor shown in Table 3.1, it is little affected by large change in grid size. Thus, the numerical diffusion on solvent mass transfer is limited.

Table 5.2: Comparison of estimated diffusion coefficient for CH_4, C_2H_6, N_2 and CO_2 in Athabasca bitumen.

Gas	Pressure (Mpa)	Temperature (℃)	Diffusion coefficient (m^2/day)	References
CH_4	4.0	50	-	Upreti and Mehrotra (2002)
		90	4.98×10^{-5}	
	8.0	50	1.74×10^{-5}	
		90	9.95×10^{-5}	
C_2H_6	4.0	75	4.86×10^{-5}	
		90	6.94×10^{-5}	
	8.0	75	5.67×10^{-5}	
		90	7.99×10^{-5}	
N_2	4.0	50	5.79×10^{-6}	
		75	2.66×10^{-5}	
		90	5.79×10^{-5}	
	8.0	50	1.97×10^{-5}	
		75	5.44×10^{-5}	
		90	8.68×10^{-5}	
CO_2	4.0	50	2.78×10^{-5}	
		75	4.28×10^{-5}	
		90	4.98×10^{-5}	
	8.0	50	4.63×10^{-5}	
		75	8.68×10^{-5}	
		90	1.08×10^{-4}	
CH_4	4.0	50	-	Sheikha et al. (2005)
		90	8.45×10^{-5}	
N_2	4.0	75	3.01×10^{-5}	
		90	3.24×10^{-5}	
CO_2	4.0	75	5.32×10^{-5}	
		90	8.80×10^{-5}	
CH_4	8.0	50	1.62×10^{-5}	Sheikha et al. (2006)
		90	6.71×10^{-5}	
C_2H_6	8.0	75	1.85×10^{-5}	
		90	3.47×10^{-5}	
N_2	8.0	50	1.16×10^{-5}	
		75	3.94×10^{-5}	
		90	6.02×10^{-5}	
CO_2	8.0	50	1.27×10^{-5}	
		75	6.13×10^{-5}	
		90	1.01×10^{-4}	

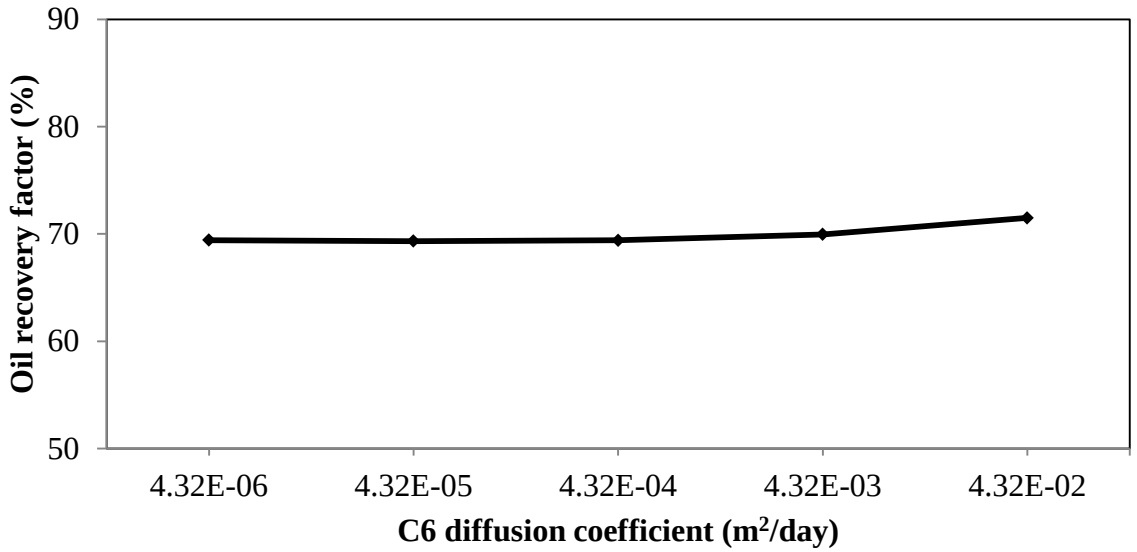

Figure 5.8: Oil recovery factor versus C6 diffusion coefficient in oil phase in solvent aided SAGD with 2000 kPa injection pressure and 0.01 mole fraction C6 co-injection at 600 days.

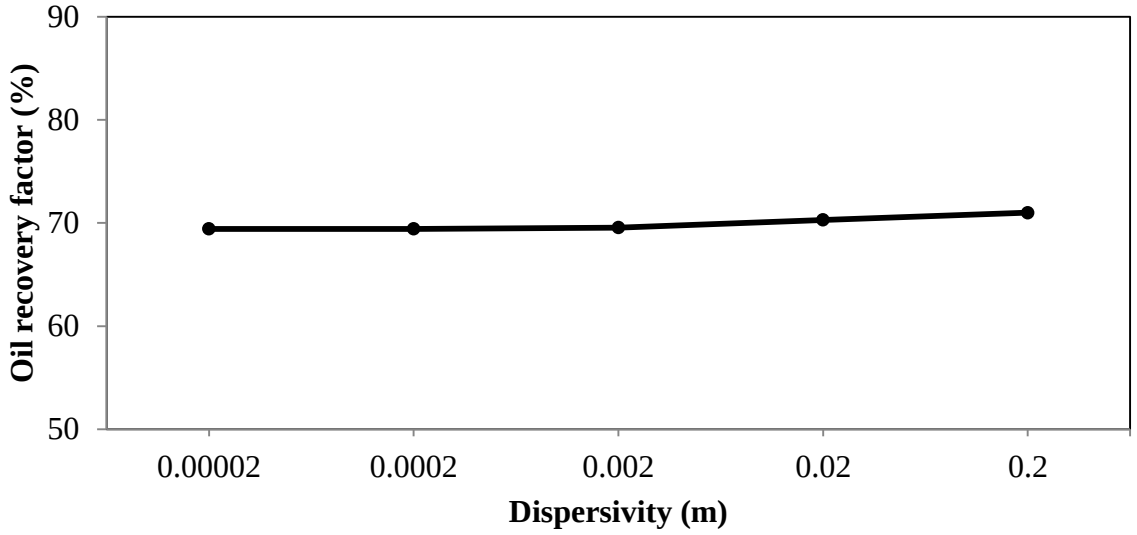

Figure 5.9: Oil recovery factor versus dispersivity in solvent aided SAGD with 2000 kPa injection pressure and 0.01 mole fraction C6 co-injection at 600 days.

5.7 Summary of Solvent Aided SAGD Process

In conclusion, in addition to heat transfer, which is one source for oil viscosity reduction in solvent aided SAGD, the oil production rate is significantly improved by further oil viscosity reduction through solvent dilution. Since there is no solvent condensation (Dong, 2012), the amount of dissolved solvent is determined by the gas-oil equilibrium near the vapor-liquid interface. Deep in the oil sand, where gas saturation is zero, the solvent is convectively delivered through the oil drainage process into the mobile oil zone. From the top to the bottom of the reservoir, the amount of dissolved solvent in oil is gradually reduced, under the action of the gas-oil equilibrium.

CHAPTER SIX: OPERATION PARAMETERS ANALYSIS FOR SOLVENT AIDED SAGD IMPROVEMENT

6.1 Introduction

The operation parameters, including solvent concentration and injection pressure, which have a close relationship with steam-solvent phase behavior, are investigated in this section. Additionally, a steam-solvent injection strategy to improve solvent aided SAGD performance is proposed through alternating solvent injection periods, solvent concentration and pressure.

6.2 Impact of Solvent Concentration on Production Performance

Solvent concentration is an important parameter which has great effect on oil production rate (Li and Mamora, 2011). In this study, C6 is injected at 0.005, 0.010, 0.020, 0.030, 0.040, 0.050 and 0.060 mole fraction in the stream with other parameters the same as the solvent aided SAGD case.

The curve of the oil recovery factor versus C6 concentration at 600 days (end of production) is plotted in Figure 6.1. It is shown that the oil recovery factor is greatly improved with an increased C6 mole fraction. Without C6 co-injection, there is only 51% bitumen recovered. When C6 concentration is 0.06 mole fraction in the injected steam-solvent stream, 80% bitumen is produced from the reservoir.

In Figure 6.2, the relationship between cSOR and C6 concentration is shown. There is a tendency toward a decrease in cSOR with increasing C6 concentration. When C6 concentration is 0, cSOR is 1.88 for this homogeneous model. With 0.06 mole fraction C6 injection, cSOR is reduced to 0.88. This is because, first under high C6 concentration, oil can be drained more efficiently by C6 dilution. Second, the temperature of vapor is reduced by lowered steam partial pressure,

which decreases heat loss to overburden, and finally, the amount of injected steam is replaced by the injected C6.

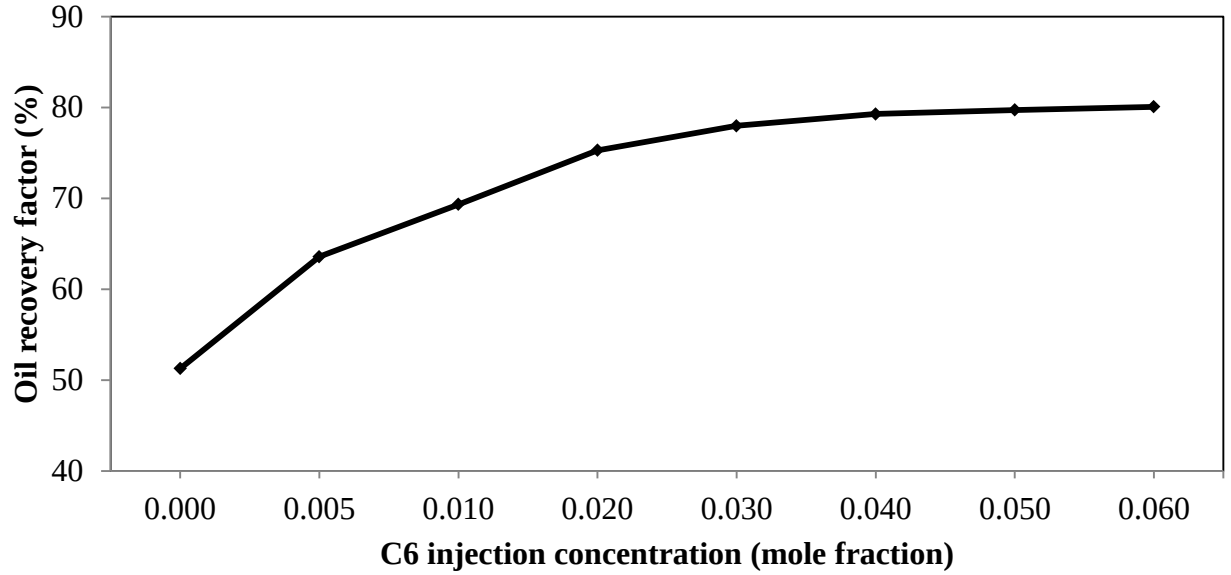

Figure 6.1: Oil recovery factor versus C6 injection concentration in solvent aided SAGD with 2000 kPa injection pressure at 600 days.

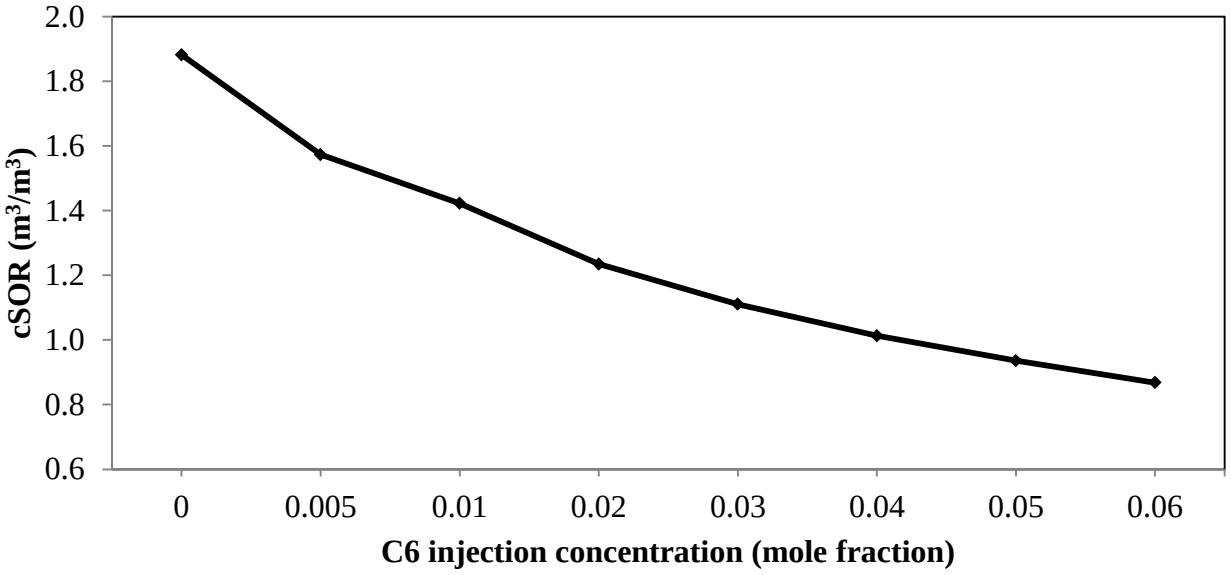

Figure 6.2: The cSOR versus C6 injection concentration in solvent aided SAGD with 2000 kPa injection pressure at 600 days.

The curve of lost C6 for unit produced bitumen with a change in C6 concentration is shown in Figure 6.3. Since solvent is usually more expensive than bitumen, it is the objective to recover as much bitumen as possible with small solvent loss in the reservoir. The value of lost C6 rises with increased C6 concentration in this process. To investigate C6 retention, studies have been done. The C6 trapped within the reservoir can be divided into two types: one is dissolved in residual oil by gas-oil equilibrium; another is trapped in the vapor phase (Keshavarz et al., 2013). Under high C6 concentration, more C6 is dissolved in oil by its high partial pressure and lowered vapor temperature. Furthermore, a large amount of C6 is also retained in the vapor phase.

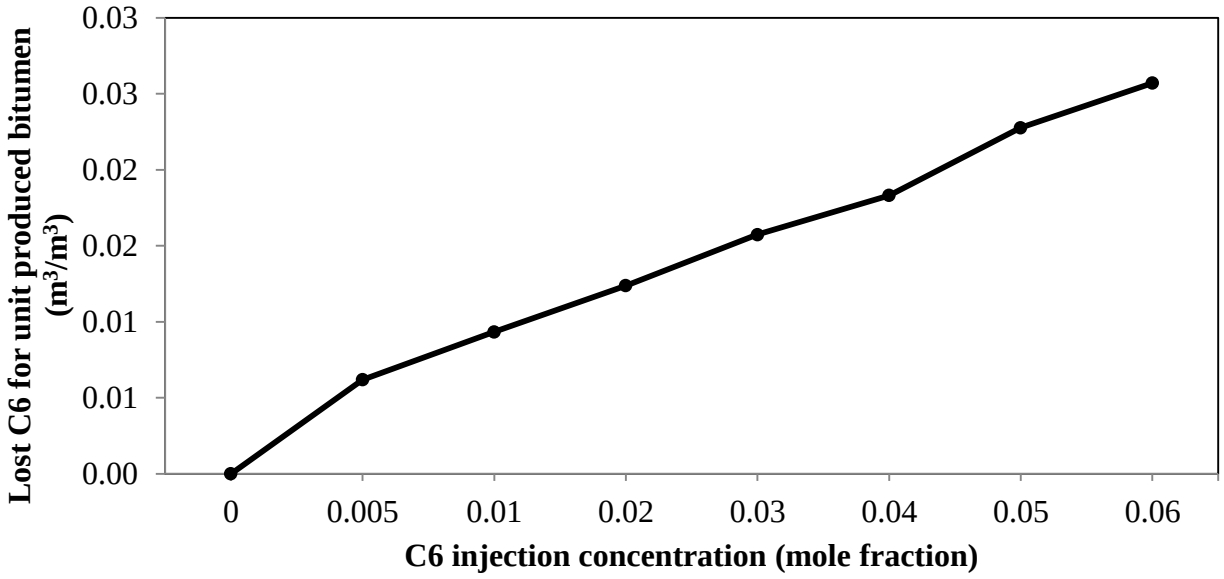

Figure 6.3: Lost C6 for unit produced bitumen versus C6 injection concentration in solvent aided SAGD with 2000 kPa injection pressure at 600 days.

Figure 6.4 shows gas saturation, oil saturation, water saturation, C6 mole fraction in oil and temperature with different C6 concentration (0.05, 0.01, 0.03 and 0.05 mole fraction) in the

cross-section of solvent aided SAGD process, at 300 days (middle of production). It is shown by the gas saturation that the swept area by vapor is enlarged under high C6 concentration, which is also revealed by the oil saturation distribution. With condensed water flowing towards, the accumulation of water in the mobile oil zone increases with high C6 concentration as the water saturation shows. It is the reason that more steam condenses under lowered vapor temperature in the steam condensation zone. This phenomenon coincides with the assumption, which is shown in Figure 2.4, proposed by Dong in 2012.

In Table 6.1, temperature at the vapor-liquid interface, thickness of steam condensation and mobile oil zones, C6 mole fractions in vapor and oil at the interface, and total oil flow rate along the middle location (Figure 5.2.5) are summarized at 300 days. The thickness of the steam condensation zone is enlarged with increased C6 concentration, since more steam condenses under the lowered saturation temperature of the vapor mixture. The thickness is increased from 0.8 to 2.4 m with the change of C6 injection mole fraction from 0.005 to 0.040. Furthermore, the C6 mole fraction in vapor at the vapor-liquid interface increases from 0.23 to 0.46 and the C6 mole fraction in oil also increases from 0.26 to 0.70. The thickness of the mobile oil zone decreases slightly from 2.4 to 2.2 m because the temperature at the vapor-liquid interface decreases from 199 to 183 ℃. When the C6 injection mole fraction varies from 0.005 to 0.040, much solvent dissolution in oil compensates for the reduced thickness of the mobile oil zone with the result that total oil flow rate increased by more than 2 times from 163 to 379 m^3/day.

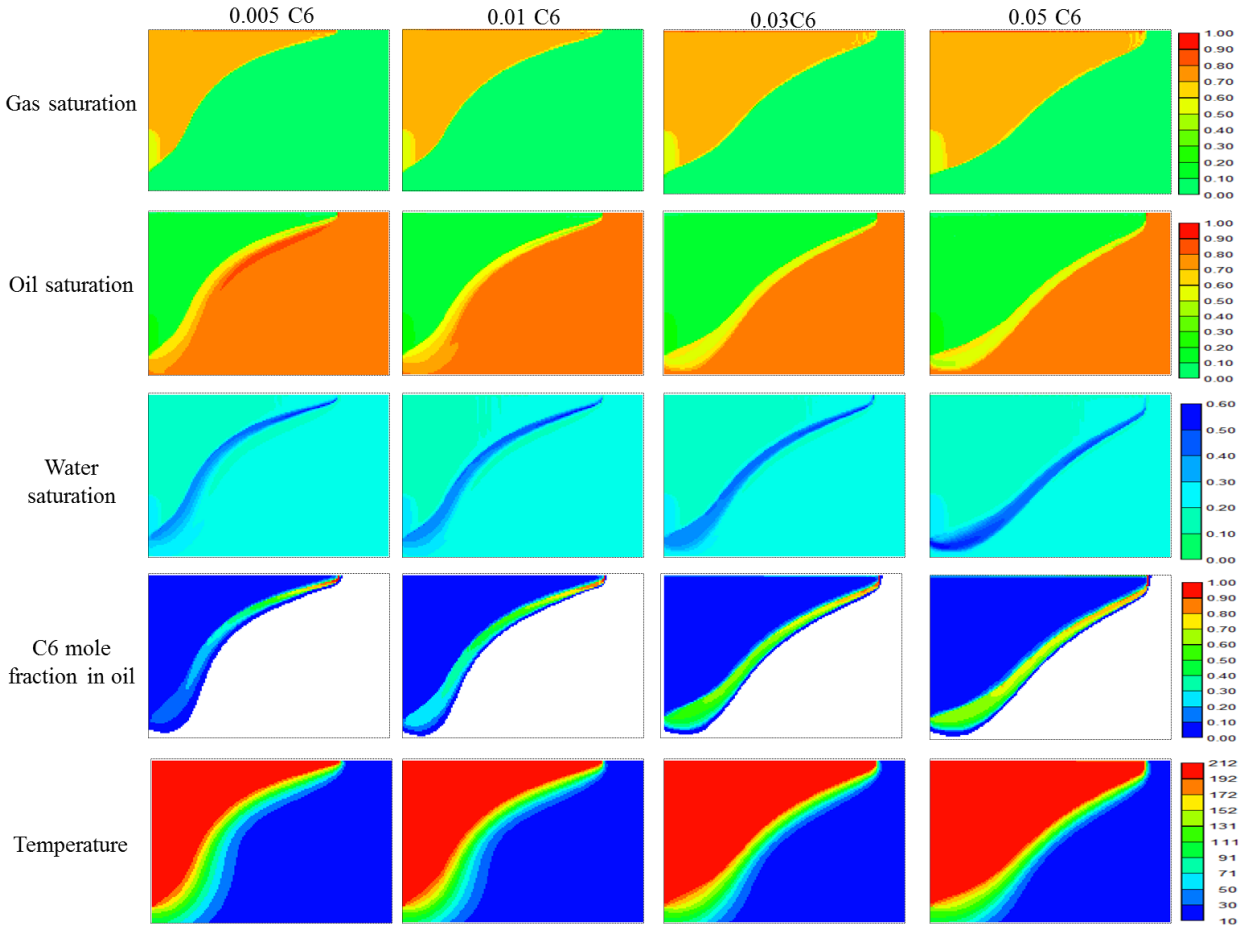

Figure 6.4: Gas saturation, oil saturation, water saturation, C6 mole fraction in oil, temperature and oil flow rate profile in cross-section of solvent aided SAGD at 300 days. C6 concentrations are selected at 0.005, 0.01, 0.03 and 0.05. Blank area represents 0 for each property.

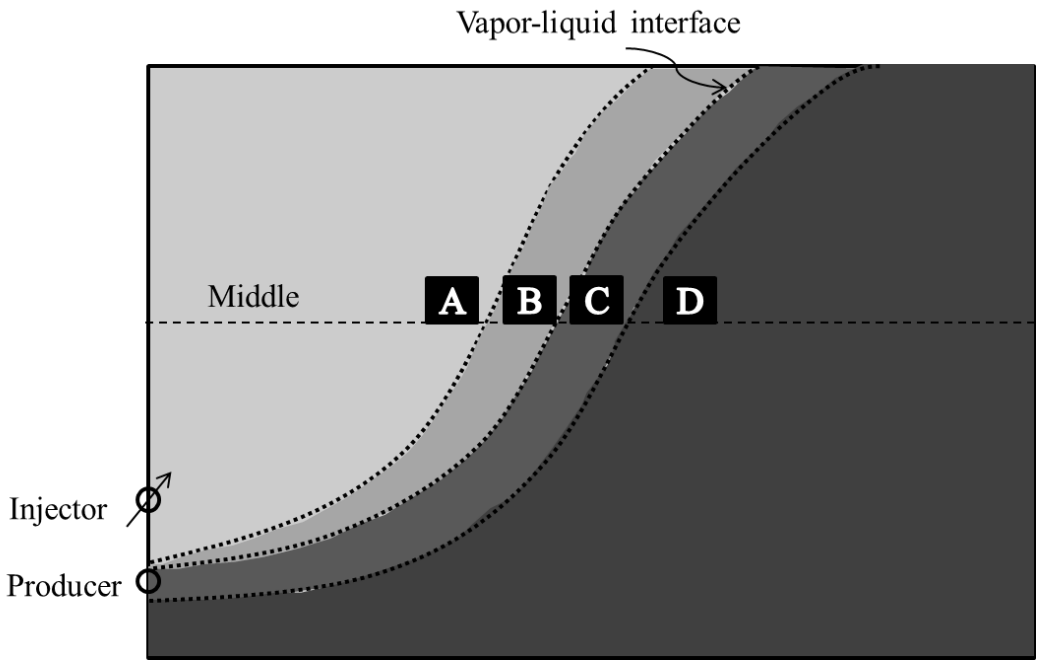

Figure 6.5: Four zones near the transition region illustrated by oil saturation distribution in cross-section of solvent aided SAGD for various solvent concentrations. The dished line is the middle location.

Table 6.1: Temperature at the vapor-liquid interface, thickness of steam condensation zone and mobile oil zone, C6 mole fractions in vapor and oil at the interface and total oil flow rate at 300 days along the middle location in solvent SAGD with 2000 kPa injection pressure and varies C6 injection concentration.

Study location	Middle						
C6 injection concentration (mole fraction)	0.005	0.010	0.020	0.030	0.040	0.050	0.060
Temperature at vapor-liquid interface (℃)	199	189	188	184	183	180	179
Steam condensation zone thickness (m)	0.8	1.6	2.0	2.2	2.4	2.6	2.6
Mobile oil zone thickness (m)	2.4	2.2	2.2	2.2	2.2	2.0	2.0
C6 mole fraction in vapor at vapor-liquid interface	0.23	0.38	0.40	0.44	0.46	0.49	0.51
C6 mole fraction in oil at vapor-liquid interface	0.26	0.50	0.64	0.65	0.70	0.76	0.80
Total oil production rate (m^3/day)	163	213	282	342	379	451	495

In Figure 6.1, when the C6 mole fraction is higher than 0.040, oil recovery factor improvement decreases because oil viscosity cannot be further reduced under very high C6 concentration in oil. Figure 6.6 shows bitumen-C6 viscosity as a function of C6 concentration under various

temperatures. For example, oil viscosity changes very little when C6 concentration increases from 0.3 to 0.7 mole fraction at a relatively high temperature (180 ℃), which is the temperature near the vapor-liquid interface. As well, since some injected steam is replaced by solvent under high solvent concentration, the decrease in injected heat also slows down the oil flow rate.

In conclusion, the oil recovery factor improvement under high C6 injection concentration is the result of increased C6 dissolution in oil in the mobile oil zone.

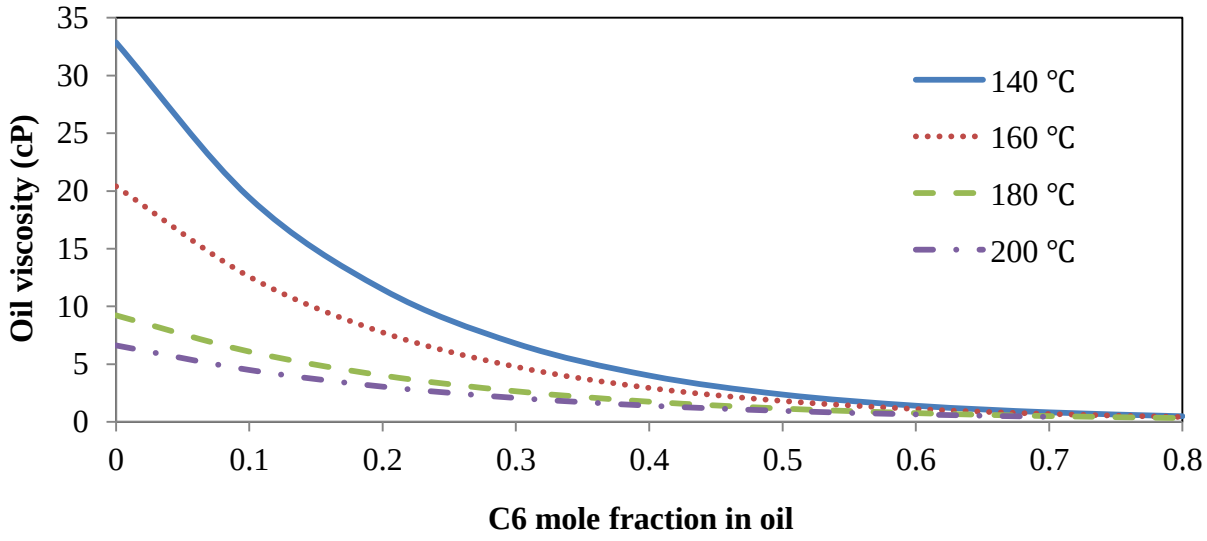

Figure 6.6: Oil viscosity versus C6 mole fraction in oil at 140, 160, 180 and 200 ℃ under 2000 kPa (Shu, 1984).

6.3 Impact of Pressure on Production Performance

Pressure is another important operation parameter since it affects steam chamber growth and oil production rate (Law et al., 2003). Four scenarios including 1600, 2000, 2400, 2800 and 3200 kPa are considered with 0.01 mole fraction C6 co-injected.

Oil recovery factor under different pressures at 600 days is shown in Figure 6.7. As it is shown, the oil recovery factor increases from 65 to 77% when the injection pressure is changed from

1600 to 3200 kPa. For cSOR, it is increased by high pressure, as shown in Figure 6.8, which shows cSOR variance with changed pressure. The relationship between lost C6 for unit produced bitumen and pressure is shown in Figure 6.9. The lost C6 remains at a relatively constant level when pressure changes from 1600 to 3200 kPa. This phenomenon can be explained by little change in C6 solubility under the change of pressure and temperature (properties of saturated steam). Under high pressure, even though the large volume of the reservoir has been swept by steam, the amount of retained C6 in the reservoir is also increased.

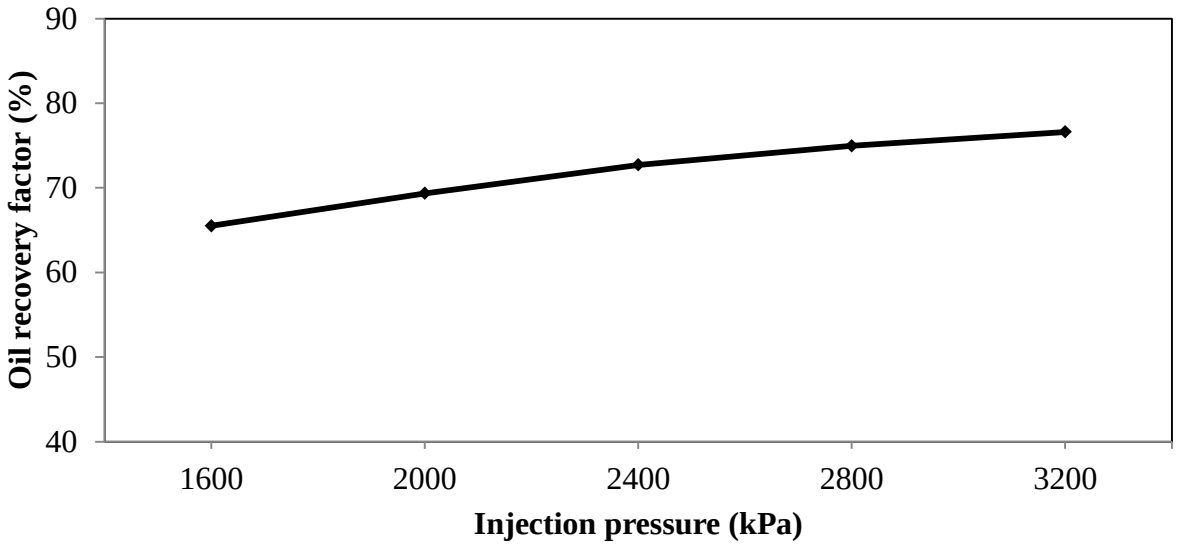

Figure 6.7: Oil recovery factor versus injection pressure at 600 days in solvent aided SAGD with 0.01 mole fraction C6.

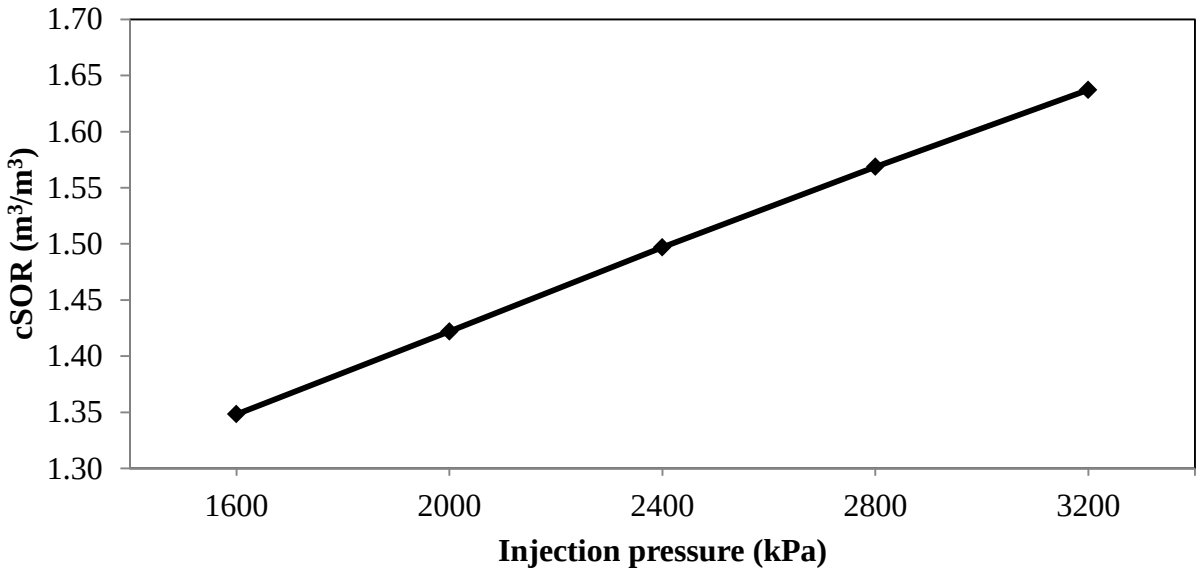

Figure 6.8: The cSOR versus injection pressure at 600 days in solvent aided SAGD with 0.01 mole fraction C6.

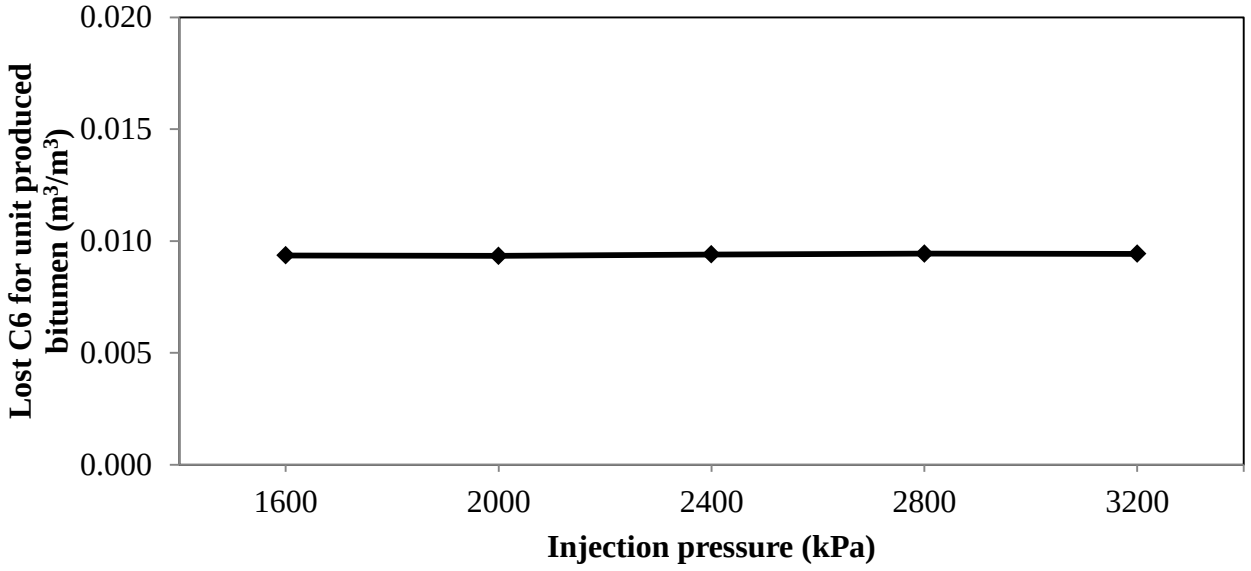

Figure 6.9: Lost C6 for unit produced bitumen versus injection at 600 days with 0.01 mole fraction C6.

Figure 6.10 shows gas saturation, oil saturation, water saturation, C6 mole fraction in oil and temperature profiles with different pressures in the cross-section of the solvent aided SAGD process, at 300 days. With an increase in pressure, as shown in gas and oil saturation, the vapor phase can occupy a larger area in the reservoir and leave less space for oil. Near the vapor-liquid interface, there is little change in water saturation and C6 mole fraction in oil. Temperature in the steam chamber increases as the pressure rises.

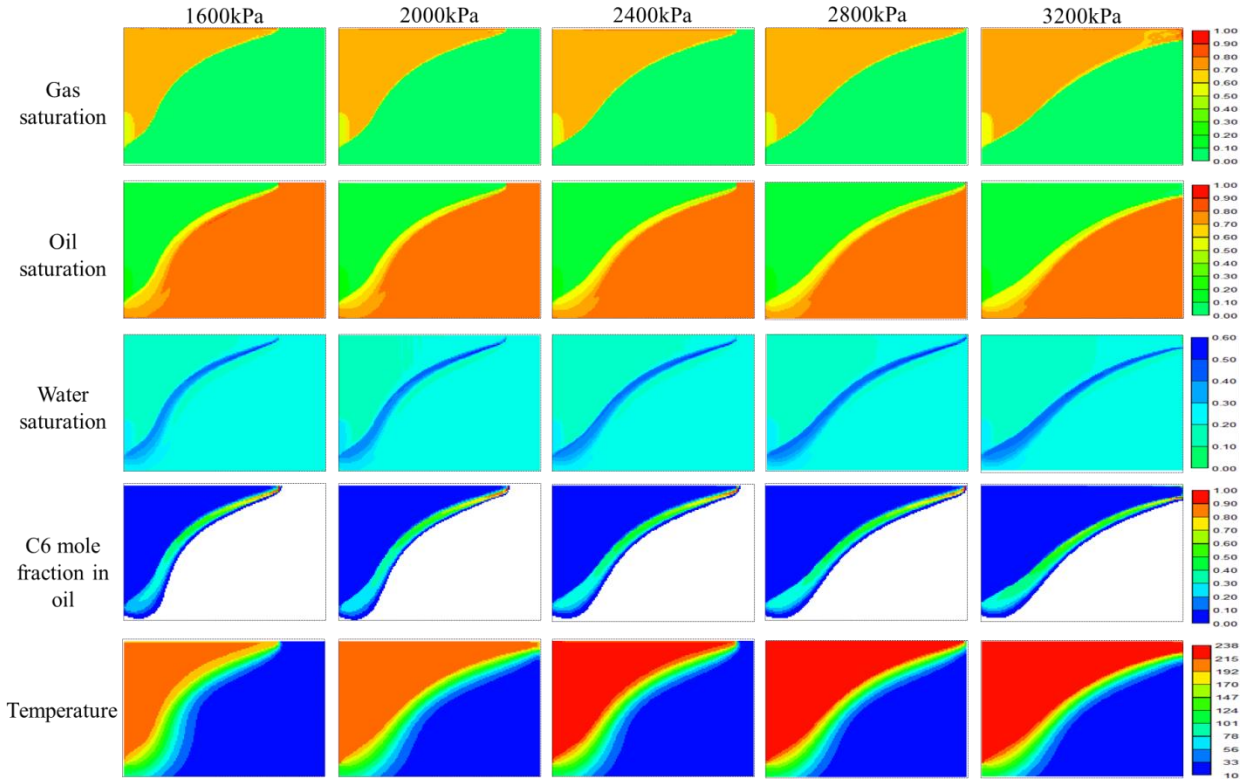

Figure 6.10: Gas saturation, oil saturation, water saturation, C6 mole fraction in oil, temperature and oil flow rate profile in cross-section of solvent aided SAGD, 300 days. Injection pressure are selected at 1600 kPa, 2000 kPa, 2400 kPa, 2800 kPa and 3200 kPa. Blank area represents 0 for each property.

To explain how the oil recovery factor is improved by high injection pressure, temperature at the vapor-liquid interface, thickness of steam condensation and mobile oil zones, C6 mole fractions in vapor and oil at the interface, and total oil flow rate are summarized in Table 6.2 along the

middle location (Figure 6.11). Since C6 is injected at the same concentration, the thickness of the steam condensation zone is similar among the various injection pressure cases with pressure increases from 1600 to 3200 kPa. Furthermore, C6 concentration in oil at the vapor-liquid interface is also similar. With injection pressure increasing from 1600 to 3200 kPa, the temperature at the interface increases from 181 to 219 ℃. As a result, the thickness of the mobile oil zone is enlarged from 2.0 to 3.0 m. The total oil flow rate is also enhanced from 186 to 308 m^3/day. It can be concluded that oil flow rate increasing under high injection pressure is the result of an enlarged mobile oil zone and lowered oil viscosity.

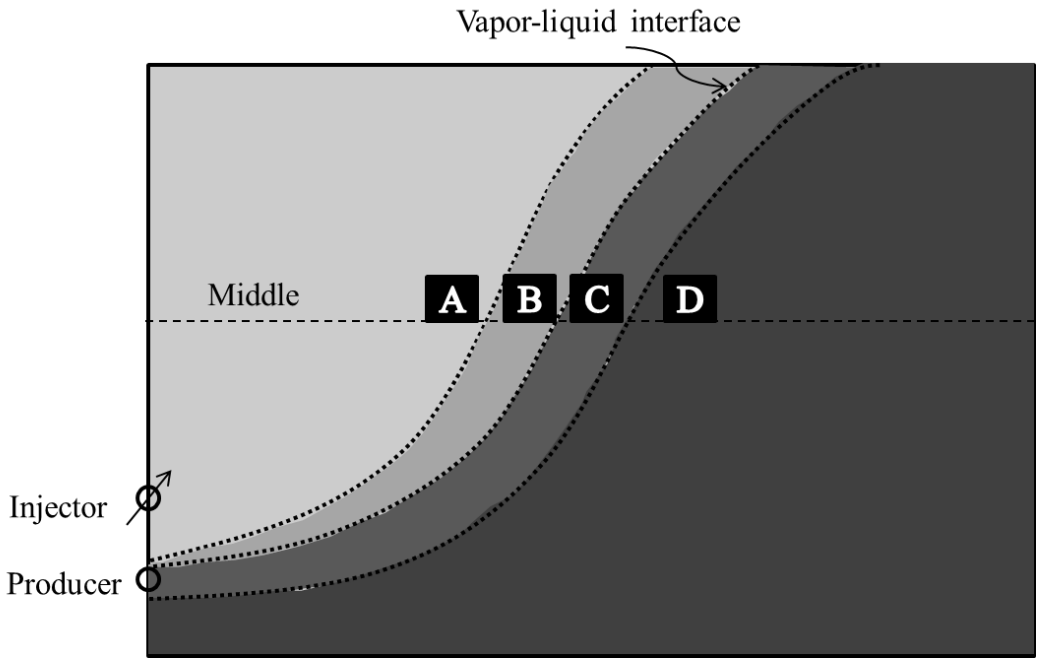

Figure 6.11: Four zones near the transition region illustrated by oil saturation distribution in cross-section of solvent aided SAGD for various pressure. The dished line is the middle location.

Table 6.2: Temperature at the vapor-liquid interface, thickness of steam condensation and mobile oil zones, C6 mole fractions in gas and oil at the interface and total oil flow rate at 300 days along the middle location in solvent aided SAGD with varies injection pressure and 0.01 mole fraction C6 co-injection.

Injection pressure (kPa)	1600	2000	2400	2800	3200
Temperature at vapor-liquid interface (℃)	181	189	203	211	219
Steam condensation zone thickness (m)	1.6	1.6	1.6	1.6	1.6
Non-gas oil mobile zone thickness (m)	2.0	2.2	2.4	2.8	3.0
C6 mole fraction in vapor at vapor-liquid interface	0.36	0.38	0.32	0.35	0.38
C6 mole fraction in oil at vapor-liquid interface	0.46	0.50	0.50	0.52	0.54
Total oil flow rate(m^3/day)	186	213	244	271	308

6.5 Impact of Solvent-Type on Production Performance

As discussed in the previous chapter, the only source for vapor solvent dissolution in oil is from the gas-oil equilibrium process. In solvent aided SAGD, the solubility of solvents, which is very important, determines the amount of solvent dissolved in oil and the production performance.

6.4.1 Pure-Solvent Injection with Steam

Cases are run with several kinds of solvents in solvent aided SAGD to analyze how the solvent type affects this process. The co-injected solvent is chosen with C3, C4, C5, C6, C7 and C8 respectively. The other parameters are same as the C6 co-injected SAGD case.

Oil recovery factor as a relationship of the solvent type at 600 days is shown in Figure 6.4.1. It is noted that the recovery factor can only be increased when the solvent is heavier than C4.

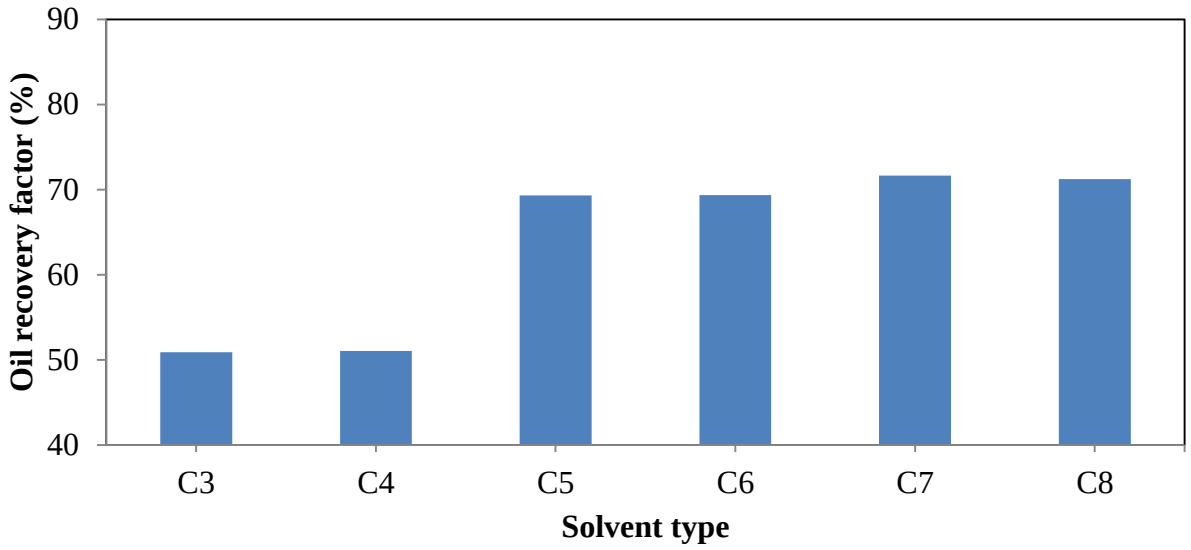

Figure 6.12: Oil recovery factor of the solvent aided SAGD with the relationship of solvent type at 600 days. Solvent is co-injected at 0.01 mole fraction under 2000 kPa.

Figure 6.13 shows gas saturation, oil saturation, water saturation, C6 mole fraction in oil and temperature profiles of the cases with different solvent-type in the cross-section of the solvent aided SAGD process, at 300 days. Due to low solubility of C3 and C4 in bitumen, the vapor sweep area is smaller than when co-injected with solvent from C5 to C8. Additionally, C3 mole fraction in oil and C4 mole fraction in oil are very low. The C3 co-injection and C4 co-injection cases have similar properties profiles and the cases of C5, C6, C7 and C8 co-injection have similar properties distribution respectively.

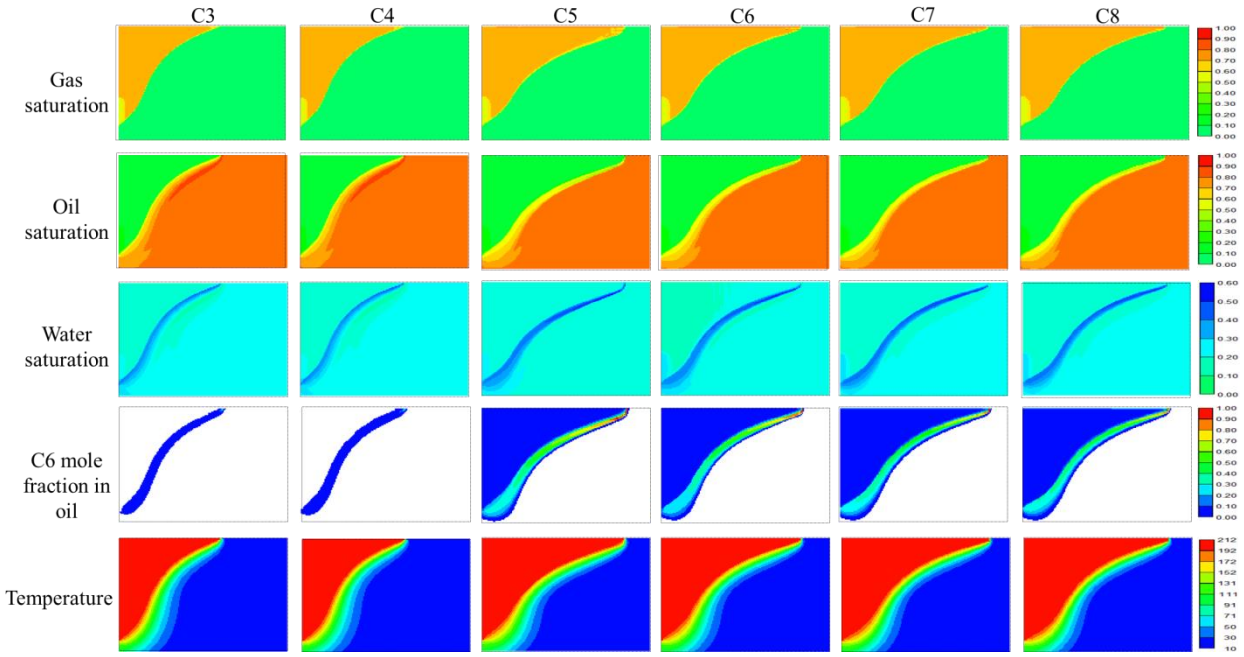

Figure 6.13: Gas saturation, oil saturation, water saturation, C6 mole fraction in oil, temperature and oil flow rate profile in cross-section of solvent aided SAGD at 600 days. Solvents are selected with C3, C4, C5, C6, C7 and C8. Blank area represents 0 for each property.

That solvents heavier than C4 are available to improve oil production in this process can be explained by solvent solubility, which is reflected by k-value in Figure 6.4.3.

In the range of temperature (170 - 210 ℃) at the vapor-liquid interface (as summarized in Table 4.1), a low k-value of C5, C6, C7 and C8 enables a large amount of solvent dissolution in oil, which results in improved oil recovery. However, a small amount of C3 or C4 dissolved in oil contributes little for oil recovery improvement. When the solvent is heavier than C4, the oil recovery factor at 600 days is similar, due to little change in the thickness of the mobile oil zone and the dissolved C6 in this zone. For the constant solvent injection concentration (0.01 mole fraction), the temperature at the vapor-liquid interface is the same of all cases due to the same

partial pressure of steam. Thus, whether solvent addition is effective in improving SAGD depends on solvent solubility in oil.

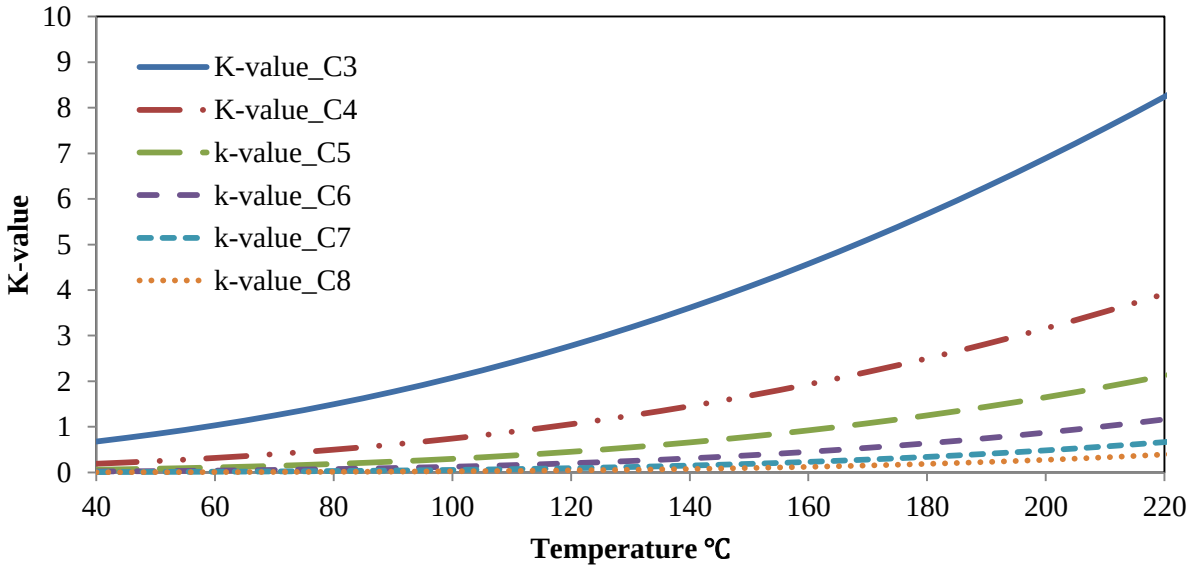

Figure 6.14: K-value of solvents (C3, C4, C5, C6, C7 and C8) from 50 to 230 ℃ under 2000 kPa. (CMG Winprop, 2011).

6.4.2 Solvent-Mixture Injection with Steam

From the previous section, analysis of pure-solvent injection with steam in the SAGD process, it is revealed that, for the bitumen type used in this reservoir model, C3 and C4 are the solvents with little ability to improve bitumen recovery. C5, C6, C7 and C8 can effectively increase bitumen recovery with similar magnitude.

In order to investigate the effects of solvent-mixture injection with steam on solvent aided SAGD performance, simulation studies have been done. C3 is selected as the ineffective solvent and C5 is the effective one. Solvent combinations are shown in Table 6.3 with 0.01 mole fraction for each solvent:

Table 6.3: Solvent combinations with 0.01 mole fraction for each one in solvent-steam mixture.

Solvent (0.01 mole fraction)	C3	C4	C5	C6	C7	C8
C3	X	X	X	X	X	X
C5			X	X	X	X

Figure 6.15 shows the oil recovery factor of the cases with various solvent combinations in the solvent aided SAGD process, at 600 days. The combination of C3-C3 and C3-C4 exhibits a similar oil recovery factor. The combinations of C3 with solvents from C5 to C8 have similar performance to single solvent process from C5 to C8. Only the combinations of solvents heavier than C4 can effectively improve the oil recovery factor.

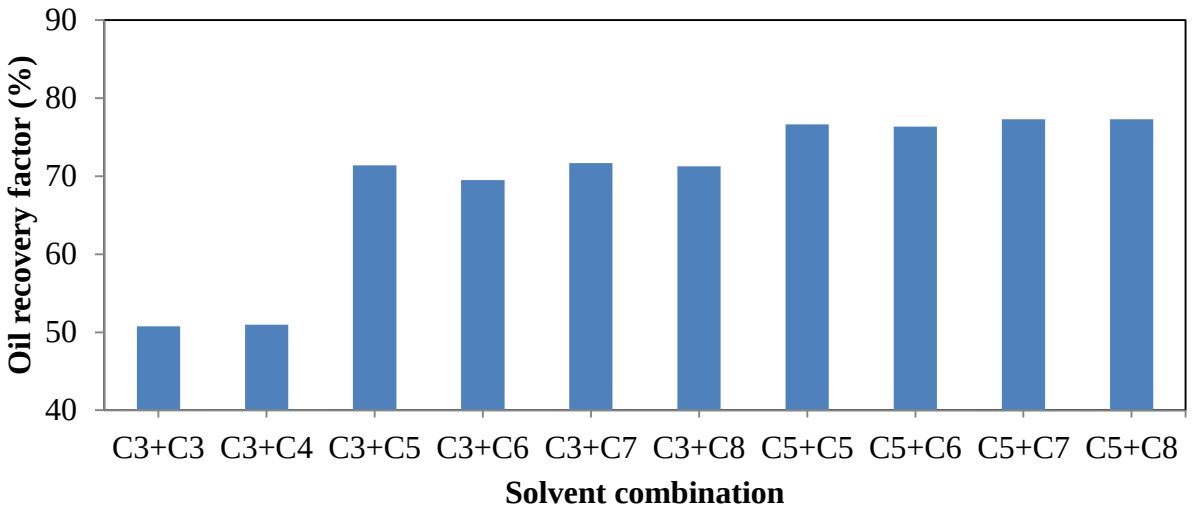

Figure 6.15: Oil recovery factor of the cases with different solvent combinations at 600days. Each solvent is injected at 0.01 mole fraction under 2000 kPa.

6.5 Impact of Solvent Injection Start Time on Production Performance

As discussed in chapter 5, convective solvent transfer in the mobile oil zone during solvent aided SAGD is the result of the sloped vapor-liquid interface. Moreover, during vertical steam

chamber growth, which is in the early stages of SAGD, the vapor-liquid interface is almost vertical. Thus, the solvent injection start time has to be investigated to study the effect of solvent on vertical steam chamber growth.

6.5.1 Effect of Solvent Injection Start Time

Cases are designed with different solvent injection start times as shown in Table 6.4. In order to study the effect of solvent addition on vertical steam chamber growth, the time of the chamber reaching overburden of the reservoir is selected as the point of potential separation of solvent injection. C5 is selected in this section, the same as the in previous chapters.

Case 1 and 2 are the processes with 2000 and 3000 kPa steam injection into the reservoir respectively, without solvent during vertical steam chamber growth. In case 3 and 4, C5 is mixed with steam at 0.01 and 0.02 mole fractions respectively under the injection pressure of 2000 kPa.

Table 6.4 Cases of different solvent injection start time.

Case	Solvent injection start time	C5 concentration (mole fraction)	Pressure (kPa)
1	After steam reaching overburden	0	2000
2	After steam reaching overburden	0	3000
3	Same as steam injection	0.01	2000
4	Same as steam injection	0.02	2000

Figure 6.15 includes gas saturation, oil saturation, water saturation, C5 mole fraction in oil and temperature profiles in the cross-section of solvent aided SAGD at 140 days, at the point where the steam chamber is reaching overburden. For case 1, vertical steam chamber growth is slow without solvent under 2000 kPa since bitumen cannot be removed quickly with relatively low temperature and pressure of steam. After the pressure is increased to 3000 kPa (case 2), the growth of the chamber is accelerated. The vapor phase arrives at the overburden at 140 days, as

the gas saturation profile shows. For case 3, in which the pressure is low (2000 kPa), vertical steam chamber growth is improved slightly by C5 addition (0.01 mole fraction), when the gas saturation is compared to the saturation in case 1. However, even when the C5 concentration is increased to 0.02 mole fraction in case 4, the growth of the steam chamber is adversely affected since the temperature of the vapor mixture is decreased by co-injected C5.

In conclusion, for vertical steam chamber growth, it is a good choice to introduce pure-steam under high pressure without solvent injection into the reservoir. During this process, high temperature of the injected steam can ensure a fast growth rate and would not cause much heat loss because almost all the energy is stored within the reservoir.

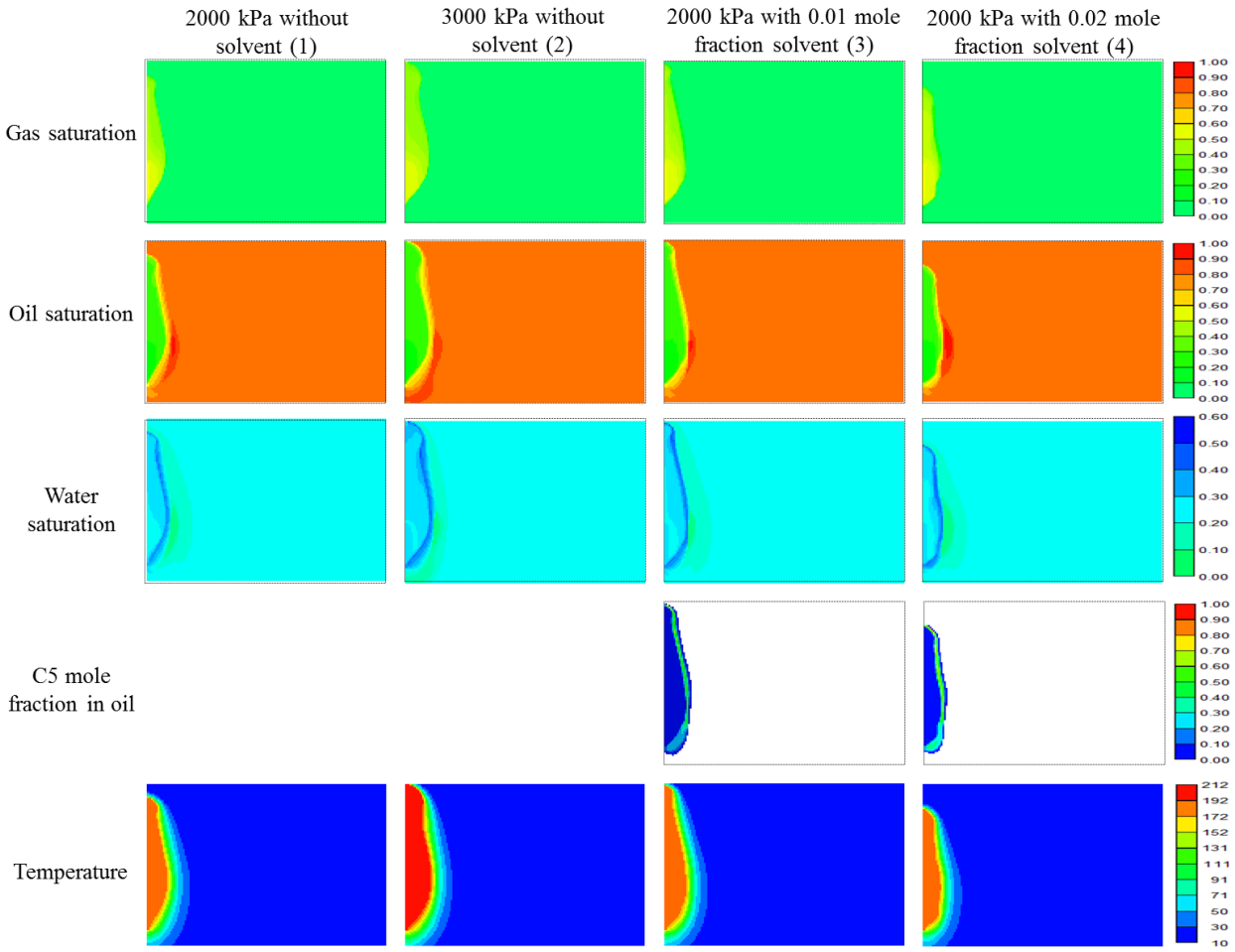

Figure 6.16: Gas saturation, oil saturation, water saturation, C5 mole fraction in oil and temperature profile in cross-section of solvent aided SAGD at 140 days. C5 is selected as surrogate of solvent. Blank area represents 0 for each property.

6.5.2 Phase Behavior in Steam-Solvent-Bitumen System During Vertical Steam Chamber Growth

During the process of vertical steam chamber growth, the vapor-liquid interface is almost vertical which is different from the sloped interface during the lateral steam chamber growth period. As a consequence, solvent distribution near the vapor-liquid interface is also changed. To illustrate the

solvent transfer process, analysis of gas saturation, C5 mole fractions in vapor and oil, and temperature variance along the middle location is done.

Figure 6.17 is the oil saturation profile of the case with C5 injection (0.01 mole fraction) simultaneously with steam. The dashed line is the middle location for properties analysis. In Figure 6.18, curves of gas saturation, C5 mole fractions in vapor and oil, and temperature are plotted along the middle location. Table 6.5 shows the temperature at the vapor-liquid interface, thickness of steam condensation and mobile oil zones, C5 mole fractions in vapor and oil at the interface and the total oil flow rate at the middle location at 140 days.

In the non-condensation zone (A in Figure 6.18, 0 – 0.8 m), steam and solvent flow at constant temperature and pressure. As the steam-solvent mixture moves ahead, steam starts to condense in the steam condensation zone (B in Figure 6.18, 0.8 – 2.0 m). C5 mole fraction vapor increases gradually and C5 mole fraction in oil also increases as a consequence. At the vapor-liquid interface (2.0 m), C5 mole fraction in oil arrives at the maximum level of 0.56. Beyond the interface, towards the cold oil sand, solvent is only distributed by 0.4 m in the mobile oil zone (C in Figure 6.18, 2.0 – 2.6 m), which is shown by the curve of C5 mole fraction in oil. At 2.4 m, the C5 concentration in oil becomes 0. The reason for this phenomenon is that C5 is transferred only through diffusion in the oil phase in the mobile oil zone and there is no force to move dissolved solvent further in the mobile oil zone.

In summary, the improvement of vertical steam chamber growth by solvent addition is not as significant as the improvement during the lateral steam chamber growth process. In order to improve the SAGD process, there is no need for solvent injection during the vertical steam chamber growth, which is at early time of SAGD process.

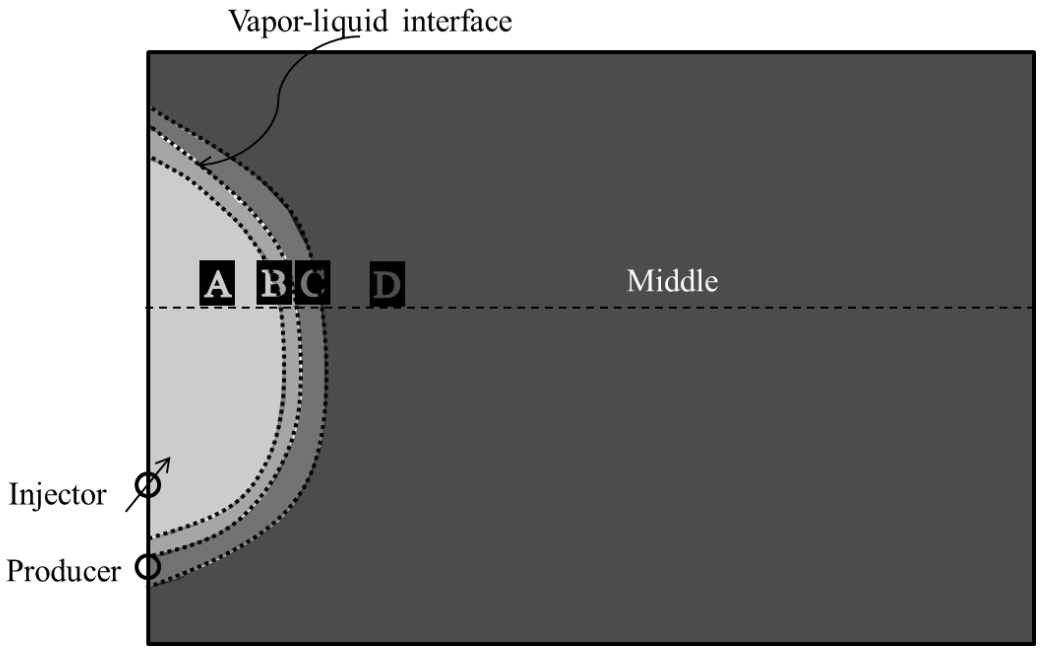

Figure 6.17: Four zones near the transition region illustrated by oil saturation distribution in cross-section of solvent aided SAGD for early SAGD. C5 is injected simultaneously with steam. The dished line is the middle location.

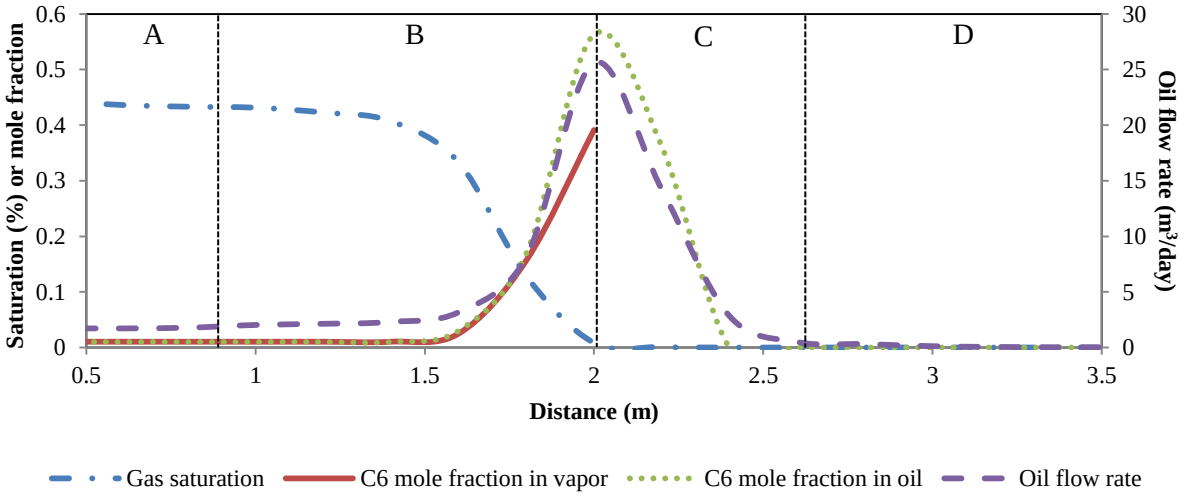

Figure 6.18: Gas saturation, C5 mole fractions in vapor and oil, and temperature at 140 days along the middle location (0.5 -3.5 m) in solvent aided SAGD with 2000 kPa injection pressure and 0.01 mole fraction C6 injected simultaneously with steam. A is the non-condensation zone. B is the steam condensation zone. C is the mobile oil zone. D is the immobile oil zone.

Table 6.5: Temperature at the vapor-liquid interface, thickness of steam condensation zone and mobile oil zone, C5 mole fractions in vapor and oil at the interface and total oil flow rate at 140 days along the middle location in solvent SAGD with 2000 kPa injection pressure and varies C5 injection concentration.

Study location	Middle
Temperature at vapor-liquid interface (℃)	203
Steam condensation zone thickness (m)	0.8
Mobile oil zone thickness (m)	0.4
C5 mole fraction in vapor at vapor-liquid interface	0.39
C5 mole fraction in oil at vapor-liquid interface	0.56
Total oil production rate(m^3/day)	51

6.6 Interval Solvent Injection

In this section, in order to achieve an effective solvent injection strategy, the effect of interval solvent injection is examined through reservoir simulation. During the interval solvent injection, steam-solvent mixture is injected into the reservoir and then it is followed by a pure-steam injection period. The ratios of steam-solvent mixture to pure-steam injection period are summarized in Table 6.6 for the cases. To make the comparison reasonable, the pure-steam injection period is 1.0 month for all cases. Figure 19 shows oil recovery factor of the different solvent injection interval cases at 600 days (end of production). The cSOR is also shown in Figure 20 at the same date.

For case 1, the oil recovery factor is the lowest, with the highest cSOR among the cases. The increase in the ratio of steam-solvent to pure-steam injection period, which means more solvent injected into the reservoir, shows a tendency for increase of oil recovery and decrease of cSOR. For case 5, in which C5 is injected with steam throughout the process, it has the highest oil recovery factor and the lowest cSOR.

In conclusion, according to the above analysis, the improvement of SAGD by solvent addition is only effective when there is solvent injection into the reservoir. If there is no solvent in the injected stream, oil production performance returns to the level of pure-steam process.

Table 6.6: Cases of different solvent injection intervals. For the pure-steam injection period, it is 1.0 moth for all cases.

Case	Ratio of steam-solvent injection period to pure-steam injection period
1	0.5
2	1.0
3	2.0
4	3.0
5*	-

* Solvent is being injected with steam throughout SAGD process.

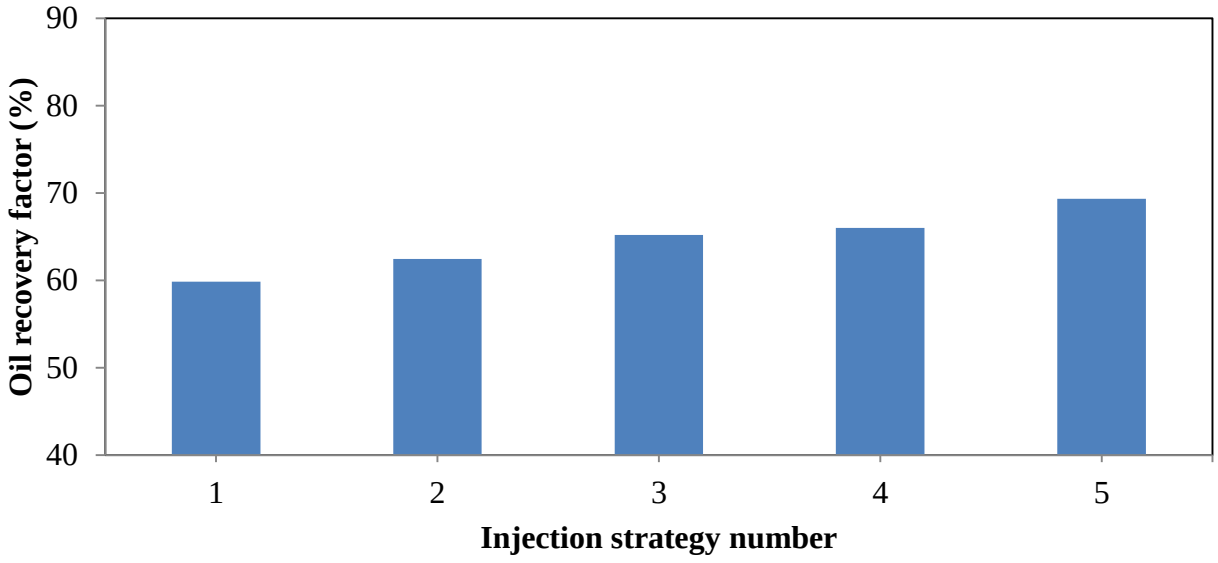

Figure 6.19: Oil recovery factor of the cases with interval solvent injection at 600 days.

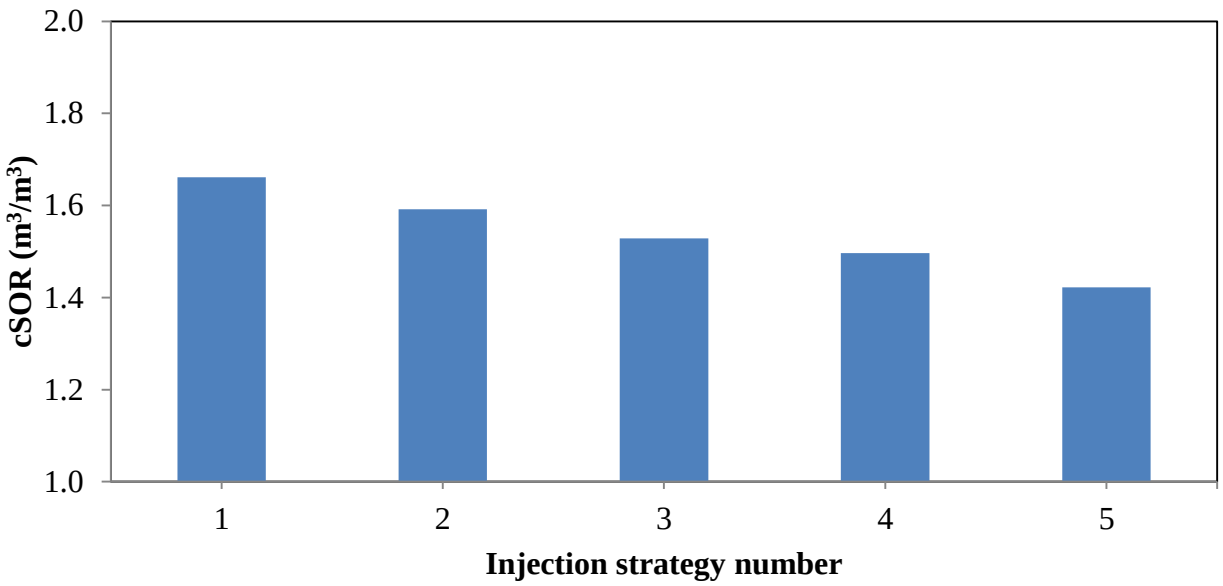

Figure 6.20: The cSOR of the cases with interval solvent injection at 600 days.

6.7 One Steam-Solvent Injection Strategy to Improve Solvent Aided SAGD

To better utilize steam and solvent and improve solvent aided SAGD production performance, the following injection strategy, which builds on the previous discussions of solvent concentration and pressure, is proposed:

Vertical steam chamber growth: Introduce steam into the reservoir under high pressure (such as 3000 kPa), until steam reaches overburden of the reservoir. High pressure increases vertical steam chamber growth without heat loss in this process. As well, solvent addition is useless since solvent cannot transfer further to the oil sand through the vertical vapor-liquid interface in this period.

Lateral steam chamber growth: After the chamber has reached overburden and starts to grow laterally, C5 is selected (the cheapest solvent which can improve the SAGD process) and injected at a relatively high concentration (such as 0.03 mole fraction) with the steam, under moderate pressure (such as 2000 kPa), during lateral growth of the steam chamber. Under high

C5 injection concentration, the oil production rate can be significantly enhanced. A moderate injection pressure can prevent much heat loss to overburden.

Continuous production: As the vapor-liquid interface is becoming horizontal near the end of production, pure-steam is injected under relatively low pressure (such as 1400 kPa) to continue the production. In this process, much of the C5 can be regained at the surface because it is retained in the residual oil by gas-oil equilibrium.

To demonstrate the advantages of the proposed injection strategy, cases were run, as summarized in Table 6.7.

Table 6.7: Injection strategies to improve solvent aided SAGD.

Operation parameters	Case				
	1	2	3	4	5*
C6 concentration (mole fraction)	0.01	0.01	0.05	0.05	0, 0.05, 0
Stream injection pressure (kPa)	2000	3000	2000	3000	3000, 2000, 1400

*5 is the new injection strategy case descripted above.

Figure 6.2.1 compares oil recovery factors at 600 days (end of production). The cSOR is shown in Figure 6.2.2 and lost C5 for unit of produced bitumen is shown in Figure 6.2.3.

For case 1, oil recovery is too low to produce adequate bitumen. In case 2, the cSOR is very high, which means much steam is consumed. Case 3 and case 4 retain much C5 in the reservoir, resulting in a huge economic cost. The new injection strategy (case 5) is the optimal given overall consideration of the oil recovery factor, cSOR and lost C5. In this strategy, the oil recovery factor is very high (76%), with a relatively low cSOR (1.1 m^3/m^3) and extremely low lost C5 for unit of produced bitumen (0.005 m^3/m^3). Since the injected solvent is much more expensive than produced bitumen, the proposed improve the solvent aided SAGD process by significantly solvent loss reduction.

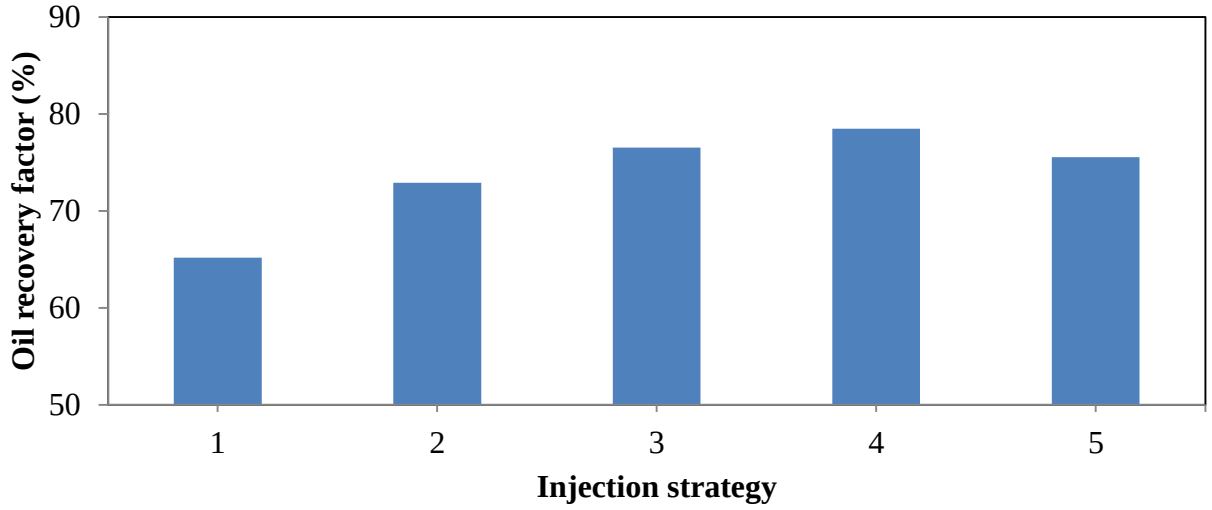

Figure 6.21: Oil recovery factor of the cases with various injection strategies. 1 represents C5 injection at 0.01 mole fraction under 2000 kPa. 2 represents C5 injection at 0.01 mole fraction under 3000 kPa. 3 represents C5 injection at 0.03 mole fraction under 3000 kPa. 4 represents C5 injection at 0.03 mole fraction under 2000 kPa. Case 5 is the the new injection strategy discussed above.

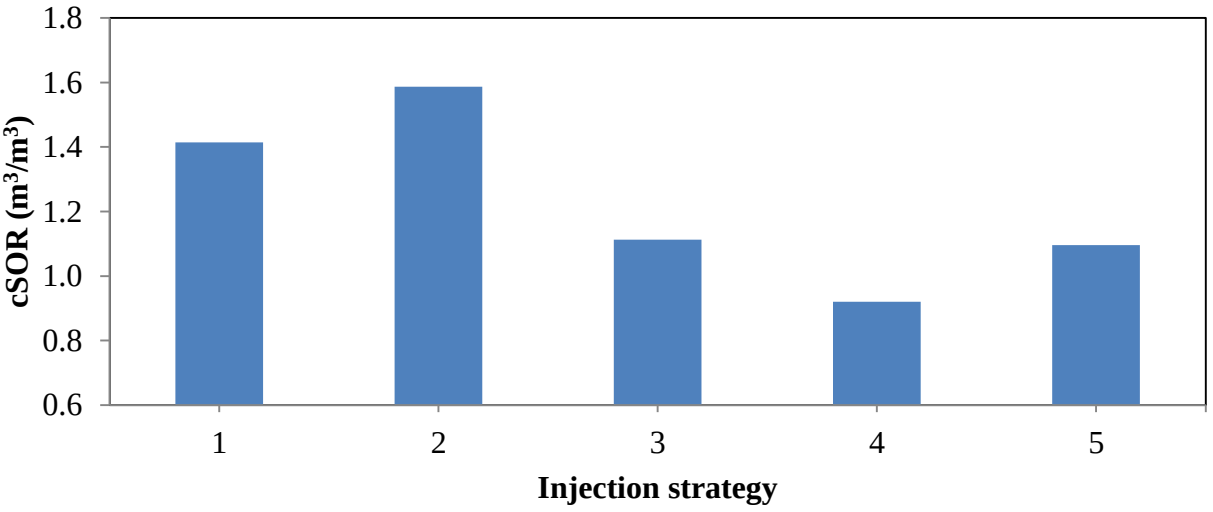

Figure 6.22: The cSOR of the cases with various injection strategies. 1 represents C5 injection at 0.01 mole fraction under 2000 kPa. 2 represents C5 injection at 0.01 mole fraction under 3000 kPa. 3 represents C5 injection at 0.03 mole fraction under 3000 kPa. 4 represents C5 injection at 0.03 mole fraction under 2000 kPa. Case 5 is the new injection strategy discussed above.

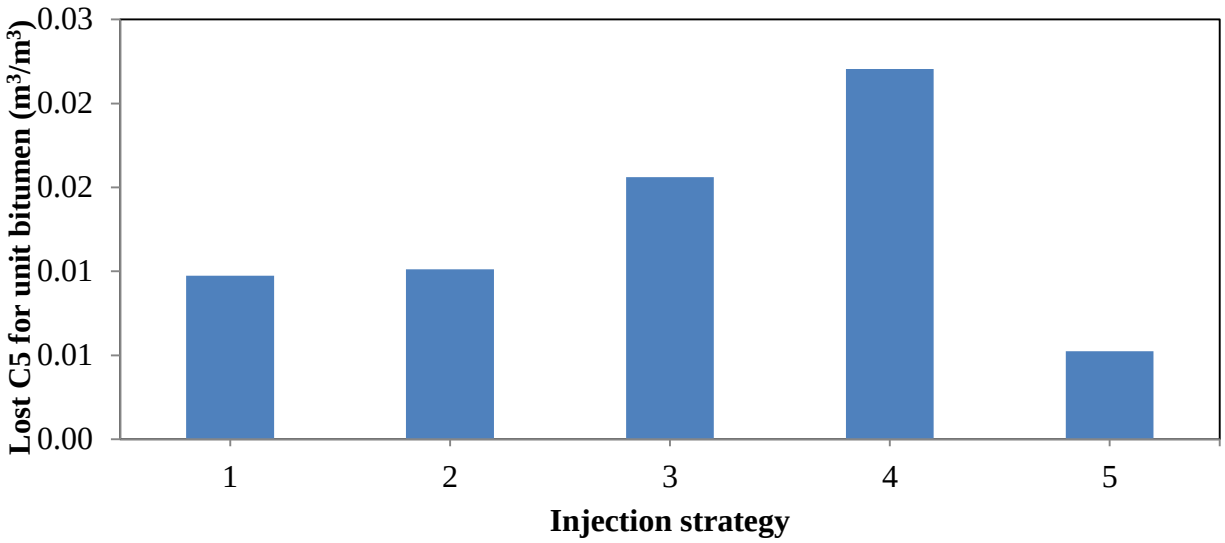

Figure 6.23: Lost C5 for unit produced bitumen of the cases with various injection strategies. 1 represents C5 injection at 0.01 mole fraction under 2000 kPa. 2 represents C5 injection at 0.01 mole fraction under 3000 kPa. 3 represents C5 injection at 0.03 mole fraction under 2000 kPa. 4 represents C5 injection at 0.03 mole fraction under 3000 kPa. Case 5 is the new injection strategy discussed above.

CHAPTER SEVEN: CONCLUSIONS AND RECOMMENDATIONS

7.1 Conclusions

For bitumen recovery, SAGD has been proven as an effective method. Steam-solvent injection can improve the SAGD process by increasing the oil production rate, decreasing steam consumption, reducing natural gas combustion and greenhouse gas emissions, in the process. However, addition of solvent with the steam complicates this process.

Research has been reported in this thesis that is focused on the analysis of phase behavior involved in the steam-solvent-bitumen system in the solvent aided SAGD process and its effects on bitumen recovery.

The following conclusions are drawn from the research:

1. In solvent aided SAGD, near the vapor-liquid interface, solvent dissolves into mobile oil zone by the gas-oil equilibrium, rather than condensation.
2. The dissolved solvent is further delivered to the mobile oil mainly through convective oil drainage in the mobile oil zone.
3. Solvent can be further transferred to mobile oil zone through a sloping vapor-liquid interface, rather than a vertical vapor-liquid interface.
4. The proposed strategy can effectively improve the solvent aided SAGD performance to achieve high economic efficiency.

7.2 Recommendations

In this research, the phase behavior of steam-solvent-bitumen system and solvent transfer in the mobile oil zone have been studied in detail. However, more work needs to be done to fill the gap between homogeneous model and real oil reservoir.

The following are suggestions for the improvement of the current work:

- More sensitivity analysis of operation parameters need to be done.
- Apply the proposed steam-solvent injection strategy to heterogeneous reservoirs.

REFERENCES

Albahlani A. M. and Babadagli T., A Critical Review of the Status of SAGD: Where Are We and What Is Next?; *SPE-113283, Presented at SPE Western Regional and Pacific Section AAPG Joint Meeting, 29 March-2 April 2008, Bakersfield, California, USA.*

Alberta's Oil Sands, Opportunity, Balance, Alberta, 2008. *Available at http://www.environment.alberta.ca/documents/oil_sands_opportunity_balance.pdf.*

Andrade E. N. The Viscosity of Liquids; *Nature, Vol. 125, pp. 309-310, March 1930.*

Ardali M., Mamora D. D. and Barrufet M., A Comparative Simulation Study of Addition of Solvents in SAGD Process; *SPE-138170, Presented at Canadian Unconventional Resources & International Conference held in Calgary, Alberta, Canada, 19-21 October 2010.*

Ardali M., Mamora D. D. and Barrufet M., Experimental Study of Co-injection of Potential Solvents with Steam to Enhance SAGD Process; *SPE-144598, Presented at SPE Western North American Regional Meeting held in Anchorage, Alaska, USA, 7-11 May 2011.*

Bingham E. C., A New Viscometer for General Scientific and Technical Purposes; *Journal of Industrial and Engineering Chemistry, Vol. 6, pp. 233-237, March 1914.*

Birrell G. E., Heat Transfer Ahead of a SAGD Steam Chamber, a Study of Thermocouple Data From Phase B of the Underground Test Facility (Dover Project); *SPE-71503, Presented at SPE Annual Technical Conference and Exhibition, 30 September-3 October 2001, New Orleans, Louisiana.*

Bracho L. G., Oquendo O. A. and Maraven S. A., Steam-Solvent Injection, Well LSJ-4057, Tia Juana Field, Western Venezuela; *SPE-21530, Presented at SPE International Thermal Operations Symposium, 7-8 February 1991, Bakersfield, California.*

Burrowes A., Marsh R., Teare M., Evans C., Ramos S., Rokosh D., Rahnama F., Kirsch M-A., Philp L., Stenson J., Yemane M., Horne J. V., Fong J., Ashrafi B., Sankey G., Alberta's energy reserves and supply/demand outlook. 2010; *Energy Resources and Conservation Board.Alberta.*

Butler R. M., Rise Of Interfering Steam Chambers; *Journal of Canadian Petroleum Technology, Vol. 26, pp. 70-75, May-June 1987.*

Butler R. M., Steam-Assisted Gravity Drainage: Concept, Development, Performance and Future; *Journal of Canadian Petroleum Technology, Vol. 32, pp. 44-50, February 1994.*

Butler R. M., Thermal Recovery of Oil and Bitumen, third edition; *GravDrain Inc. Canada; 1997.*

Butler R. M., SAGD Comes of Age!; *Journal of Canadian Petroleum Technology, Vol. 37, pp. 9-12, July 1998.*

Chen J. and Ito Y., Effect of Oil-Viscosity-Gradient Presence on SAGD; *Journal of Canadian Petroleum Technology, Vol. 51, pp. 95-105, March 2012.*

Chen Q., Gerritsen M. G. and Kovscek A. R., Effects of Reservoir Heterogeneities on the Steam-Assisted Gravity-Drainage Process; *SPE Reservoir Evaluation & Engineering, Vol. 11, pp. 921-932, October 2008.*

CMG STARS Users' Manual, version 2011.10; *Computer Modeling Group Ltd., Calgary, Alberta, Canada 2011.*

CMG Winprop Users' Manual, version 2011.10; *Computer Modeling Group Ltd., Calgary, Alberta, Canada 2011.*

Collins P. M., The False Lucre of Low-Pressure SAGD; *Journal of Canadian Petroleum Technology, Vol. 46, pp. 20-27, Jaunary 2007.*

Cragoe C. S., Changes in the Viscosity of Liquids with Temperature, Pressure and Composition; *Presented at 1st World Petroleum Congress, July 18 - 24, 1933 , London, UK.*

Das S. and Butler R. M., Diffusion Coefficients of Propane and Butane in Peace River Bitumen. *The Canadian Journal of Chemical Engineering, Vol. 74, pp. 985-992, December 1996.*

Das S., Improving the Performance of SAGD; *SPE-97921, Presented at SPE/PS-CIM/CHOA International Thermal Operations and Heavy Oil Symposium, 1-3 November 2005, Calgary, Alberta, Canada.*

Deng X., Recovery Performance and Economics of Steam/Propane Hybrid Process; *SPE-97760, Presented at SPE/PS-CIM/CHOA International Thermal Operations and Heavy Oil Symposium, 1-3 November 2005, Calgary, Alberta, Canada.*

Deng X., Huang H., Zhao L., Law D.H.-S. and Nasr T. N., Simulating the ES-SAGD Process With Solvent Mixture in Athabasca Reservoirs; *Journal of Canadian Petroleum Technology, Vol. 49, pp. 38-46,January 2010.*

Doan L. T., Baird H., Doan Q. T. and Farouq-Ali S. M., An Investigation of the Steam-Assisted Gravity-Drainage Process in the Presence of a Water Leg; *SPE-56545, Presented at SPE Annual Technical Conference and Exhibition, 3-6 October 1999, Houston, Texas.*

Dong L., Effect of Vapour–Liquid Phase Behaviour of Steam-Light Hydrocarbon Systems on Steam Assisted Gravity Drainage Process for Bitumen Recovery; *Fuel Vol. 95, pp. 159–168, May 2012.*

Edmunds N. R. and Gittins S. D., Effective Application of Steam Assisted Gravity Drainage of Bitumen to Long Horizontal Wells. *Journal of Canadian Petroleum Technology, Vol. 32, pp. 49-55,June 1993.*

Edmunds N. R., Investigation of SAGD Steam Trap Control in Two and Three Dimensions; *SPE-50413, Presented at SPE International Conference on Horizontal Well Technology, 1-4 November 1998, Calgary, Alberta, Canada.*

Edmunds N., On the Difficult Birth of SAGD; *Journal of Canadian Petroleum Technology, Vol. 38, pp. 14-24, January 1999.*

Edmunds N. and Chhina H., Economic Optimum Operating Pressure for SAGD Projects in Alberta; *Journal of Canadian Petroleum Technology, Vol. 4, pp. 13-17, December 2001.*

Edmunds N. R., Observations on the Mechanisms of Solvent-Additive SAGD Processes; *SPE-165419, Presented at SPE Heavy Oil Conference held in Calgary, Alberta, Canada, 11-13 June 2013.*

Energy Information Administration U.S., International Energy Outlook 2013; *Available at http://www.strategywest.com/downloads/ERCB_ST98_2012.pdf*

Erno B. P., Chriest J. R. and Wilso R. C., Depth-Related Oil Viscosity Variation In Canadian Heavy Oil Reservoirs; *Journal of Canadian Petroleum Technology, Vol. 30, pp. 36-41, May-June 1991.*

Farouq-Ali S. M., Current Status of Steam Injection as a Heavy Oil Recovery Method; *Journal of Canadian Petroleum Technology, Vol. 13, pp. 54-68, January-March 1974.*

Farouq-Ali S. M. and Abad B., Bitumen Recovery from Oil Sands, Using Solvents in Conjunction with Steam; *Journal of Canadian Petroleum Technology, Vol. 15, pp. 80-90, July-September 1976.*

Farouq-Ali S. M., Is There Life After SAGD?; *Journal of Canadian Petroleum Technology, Vol. 36, pp. 20-24, June 1997.*

Gates I. D., Kenny J., Hernandez-Hdez I. L. and Bunio G. L., Steam-Injection Strategy and Energetics of Steam-Assisted Gravity Drainage; *SPE Reservoir Evaluation & Engineering, Vol. 10, pp. 19-34, February 2007.*

Gates I. D., Adams J. and Larte S.,The Impact of Oil Viscosity Heterogeneity on the Production Characteristics of Tar Sand and Heavy Oil Reservoirs. Part II: Intelligent, Geotailored Recovery Processes in Compositionally Graded Reservoirs; *Journal of Canadian Petroleum Technology, Vol. 47, pp. 40-49, September 2008.*

Gates I. D. and Chakrabarty N., Design of the Steam and Solvent Injection Strategy in Expanding Solvent Steam-Assisted Gravity Drainage; *Journal of Canadian Petroleum Technology, Vol. 47, pp. 12-20, September 2008.*

Gates I. D. and Leskiw C., Impact of Steam Trap Control on Performance of Steam-Assisted Gravity Drainage; *Journal of Petroleum Science and Engineering, Vol. 75, pp. 215-222, December2010.*

Geological Survey, Oil Sand Recovery 2013; *Available at http://www.ags.gov.ab.ca/energy/oilsands*

Gotawala D. R. and Gates I .D., A Basis for Automated Control of Steam Trap Subcool in SAGD; *SPE Journal,Vol. 18, pp. 680-686, September2012* .

Govind P. A., Das S., Srinivasan S. and Wheeler T. J., Expanding Solvent SAGD in Heavy Oil Reservoirs; *SPE-117571, Presented at International Thermal Operations and Heavy Oil Symposium, 20-23 October 2008, Calgary, Alberta, Canada.*

Gupta S., Gittins S. and Picherack P., Field Implementation of Solvent Aided Process; *Journal of Canadian Petroleum Technology, Vol. 44, pp. 8-13, November 2005.*

Gupta S. C. and Gittins S. D., Christina Lake Solvent Aided Process Pilot; *Journal of Canadian Petroleum Technology, Vol. 45, pp. 15-18,September 2006.*

Hamm R. A. and Ong T.S., Enhanced Steam-assisted Gravity Drainage: A New Horizontal Well Recovery Process For Peace River, Canada; *Journal of Canadian Petroleum Technology, Vol. 34, pp. 33-40, April 1995.*

International Energy Agency, World Energy Outlook 2012; *Available at http://www.strategywest.com/downloads/ERCB_ST98_2012.pdf*

Ito Y. and Suzuki S., Numerical Simulation of the SAGD Process In the Hangingstone Oil Sands Reservoir; *Journal of Canadian Petroleum Technology, Vol. 38, pp. 27-35, September 1999.*

Ito Y. and Ipek G, Steam Fingering Phenomenon During SAGD Process; *SPE-97729, Presented at SPE/PS-CIM/CHOA International Thermal Operations and Heavy Oil Symposium, 1-3 November 2005, Calgary, Alberta, Canada.*

Ivory J., Zheng R., Nasr T., Deng X., Beaulieu G. and Heck G., Investigation of Low Pressure ES-SAGD; *SPE-117759, Presented at SPE/PS/CHOA International Thermal Operations and Heavy Oil Symposium held in Calgary, Alberta, Canada, 20-23 October 2008.*

Jha R. K., Kumar M., Benson I. and Hanzlik E., New Insights into Steam-Solvent Co-injection Process Mechanism; *SPE-159277, Presented at SPE Annual Technical Conference and Exhibition, 8-10 October 2012, San Antonio, Texas, USA.*

Jiang H., Deng X., Huang H., Beaulieu G., Heck G., Akinlade O. G., and Nasr T. N., Study of Solvent Injection Strategy in ES-SAGD Process; *SPE-157838, Presented at SPE Heavy Oil Conference Canada, 12-14 June 2012, Calgary, Alberta, Canada.*

Kendal J. and Monroe K. P.,The Viscosity Liquids. II. The Viscosity-Composition Curve for Ideal Liquid Mixtures; *The Journal of the American Chemical Society, Vol. 39, pp. 1787-1802, September 1917.*

Keshavarz M., Okuno R. and Babadagli T., Optimal Conditions for Steam-Solvent Coinjection. *SPE-165471, Presented at SPE Heavy Oil Conference held in Calgary, Alberta, Canada, 11-13 June 2013.*

Khan M. A. B., Mehrotra A. K. and Svrcek W. Y., Viscosity Models for Gas-free Athabasca Bitumen; *Journal of Canadian Petroleum Technology, Vol. 23, pp. 47-53, May-June 1984.*

Kisman K. E. and Yeung K. C, Numerical Study of the SAGD Process in the Burnt Lake Oil Sands Lease; *SPE-30276, Presented at SPE International Heavy Oil Symposium, 19-21 June 1995, Calgary, Alberta, Canada.*

Law D. H. S., Nasr T. N. and Good W. K., Lab-Scale Numerical Simulation of SAGD Process in the Presence of Top Thief Zones: A Mechanistic Study; *Journal of Canadian Petroleum Technology, Vol. 42, pp. 29-35, March 2003a.*

Law D. H. S., Nasr T. N., and Good W. K., Field-Scale Numerical Simulation of SAGD Process With Top-Water Thief Zone; *Journal of Canadian Petroleum Technology, Vol. 42, pp. 32-38, August 2003b.*

Lederer E. L., Viscosity of Binary Mixtures; *Nature, Vol. 139, pp. 27-28, Jabuary 1937.*

Li W. and Mamora D. D, Solvent-Type and Ratio Impacts on Solvent-Aided SAGD Process; *SPE Reservoir Evaluation & Engineering, Vol. 14, pp. 320-331, June 2011.*

Li Z., Wollen C., Yang P. and Fustic M., Potential Use of Produced Oil Sample Analysis to Monitor SAGD Performance; *SPE-117822, Presented at International Thermal Operations and Heavy Oil Symposium, 20-23 October 2008, Calgary, Alberta, Canada.*

Mehrotra, A. K. and Svrcek W. Y., Correlations for Properties of Bitumen Saturated with CO2, CH4, N2, and Experiments with Combustion Gas Mixture; *Journal of Canadian Petroleum Technology, Vol. 21, pp. 95-104, July 1982.*

Mehrotra A. K., A Generalized Viscosity Equation for Liquid Hydrocarbons: Application to Oil-Sand Bitumens; *Fluid Phase Equilibria, Vol. 75, pp. 257-268, 1992.*

Miadonye A., Doyle N. L., Britten A., Latour N. and Puttagunta V. R., Modelling Viscosity and Mass Fraction of Bitumen-Diluent Mixtures; *Journal of Canadian Petroleum Technology, Vol. 40, pp. 52-57, July 2001.*

Mohebati M. H., Maini B. B. and Harding T. G., Numerical Evaluation of Hydrocarbon Additives to Steam in the SAGD Process; *Journal of Canadian Petroleum Technology, Vol. 49, pp. 45-53, September 2010.*

Mohebati M. H., Maini B. B., and Harding T. G., Numerical-Simulation Investigation of the Effect of Heavy-Oil Viscosity on the Performance of Hydrocarbon Additives in SAGD; *SPE Reservoir Evaluation & Engineering, Vol. 15, pp. 165-181, April 2012.*

Moini B, and Edmunds N., Quantifying Heat Requirements for SAGD Start-up Phase: Steam Injection and Electrical Heating; *Presented at World Heavy Oil Congress, Edmonton, Alberta, 2011.*

Nasr T. N., Law D. H. S., Golbeck H. and Korpany G., Counter-current Aspect of the SAGD Process; *Journal of Canadian Petroleum Technology, Vol. 39, pp. 41-47, January 2000.*

Nasr T. N., Beaulieu G., Golbeck H., Heck G., Novel Expanding Solvent-SAGD Process 'ES-SAGD'; *Journal of Canadian Petroleum Technology, Vol. 42, pp. 13-16, January 2003.*

Nasr T. N. and Ayodele O. R., New Hybrid Steam-Solvent Processes for the Recovery of Heavy Oil and Bitumen; *SPE-101717, Presented at Abu Dhabi International Petroleum Exhibition and Conference held in Abu Dhabi, UAE, 5-8 November 2006.*

Orr B., ES-SAGD; Past, Present and Future; *SPE-129518, Presented at SPE Annual Technical Conference and Exhibition, 4-7 October 2009, New Orleans, Louisiana, USA.*

Parmar G., Zhao L. and Graham J., Start-up of SAGD Wells: History Match, Wellbore Design and Operation; *Journal of Canadian Petroleum Technology, Vol. 48, pp. 42-48, January 2009.*

Perkins T. K. and Johnston O.C., A review of Diffusion and Dispersion in Porous Media; *SPE Journal,Vol. 3, pp. 70-84, March 1963.*

Redford D. A. and McKay A. S., Hydrocarbon-Steam Processes for Recovery of Bitumen from Oil Sands; *SPE-8823, Presented at SPE/DOE Enhanced Oil Recovery Symposium, 20-23 April 1980, Tulsa, Oklahoma.*

Redford D. A., The Use of Solvents And Gases With Steam in the Recovery of Bitumen From Oil Sands; *Journal of Canadian Petroleum Technology, Vol. 21, pp. 45-53, January-February 1982.*

Robinson B., Kenny J., Hernandez-Hdez I. L., Bernal A. and Chelak R., Geostatistical Modeling Integral to Effective Design and Evaluation of SAGD Processes of an Athabasca Oilsands Reservoir, A Case Study; *SPE-97743, Presented at SPE/PS-CIM/CHOA International Thermal Operations and Heavy Oil Symposium, 1-3 November 2005, Calgary, Alberta, Canada.*

Sasaki K., Akibayashi S., Yazawa N., Doan Q. T. and Farouq Ali S. M., Experimental Modeling of the SAGD Process - Enhancing SAGD Performance with Periodic Stimulation of the Horizontal Producer; *SPE Journal,Vol. 6, pp. 89-97, Match 2001.*

Satyro M. A. and Yarranton H. W., Expanded Fluid-Based Viscosity Correlation for Hydrocarbons Using An Equation of State; *Fluid Phase Equilibria, Vol. 298, pp. 1-11, November 2010.*

Sharma J. and Gates I. D, Dynamics of Steam-Solvent Coupling at the Edge of an ES-SAGD Chamber; *SPE-128045, Presented at SPE Oil and Gas India Conference and Exhibition held in Mumbai, India. 20-22 January 2010.*

Sheikha H., Pooladi-Darvish M. and Mehrotra A. K., Development of Graphical Methods for Estimating the Diffusivity Coefficient of Gases in Bitumen from Pressure-Decay Data; *Energy & Fuel, Vol. 19, pp. 2041-2049, August 2005.*

Sheikha H., Mehrotra A. K. and Pooladi-Darvish M., An Inverse Solution Methodology for Estimating the Diffusion Coefficient of Gases in Athabasca Bitumen from Pressure-Decay Data; *Journal of Petroleum Science & Engineering, Vol. 53, pp. 189-202, September 2006.*

Shin H. and Polikar M., Review of Reservoir Parameters to Optimize SAGD and Fast-SAGD Operating Conditions; *Journal of Canadian Petroleum Technology, Vol. 46, pp. 35-41, January 2007.*

Shu W. R., A Viscosity Correlation for Mixtures of Heavy Oil, Bitumen and Petroleum Fractions; *SPE Journal,Vol. 24, pp. 277-282, June 1984.*

Shu W. R. and Hartman K. J., Effect of Solvent on Steam Recovery of Heavy Oil; *SPE Reservoir Engineering, Vol. 3, pp. 457-465, May 1988.*

Svrcek W. Y. and Mehrotra A. K., One parameter correlation for bitumen viscosity; *Chemical Engineering Research and Design, Vol. 66, pp. 323 -327, 1988.*

Sylvester N. B. and Chen H. L., An Improved Cyclic Steam Stimulation Model for Pressure-Depleted Reservoirs; *SPE-17420, Presented at SPE California Regional Meeting, 23-25 March 1988, Long Beach, California.*

Upreti S. R. and Mehrotra A. K., Diffusivity of CO2, CH4, C2H6 and N2 in Athabasca Bitumen; *The Canadian Journal of Chemical Engineering, Vol. 80, pp. 116-125, February 2002.*

Van der Wyk A. J. A., Viscosity of Binary Mixtures; *Nature, Vol. 138, pp. 845-846, November 1936.*

Vincent K. D. , MacKinnon C. J. and Palmgren C. T. S., Developing SAGD Operating Strategy using a Coupled Wellbore Thermal Reservoir Simulator; *SPE-86970, Presented at SPE International Thermal Operations and Heavy Oil Symposium and Western Regional Meeting, 16-18 March 2004, Bakersfield, California.*

Vogel J. V., Simplified Heat Calculations for Steam flood; *Journal of Petroleum Technology, Vol. 36, pp. 1127-1136, July 1984.*

Walther C., *1st World Petroleum Congress, July 18 - 24, 1933, London, UK.*

Wang J. Y. , Ezeuko C. C. and Gates I. D., Energy (Heat) Distribution and Transformation in the SAGP Process; *SPE-157808, Presented at SPE Heavy Oil Conference Canada, 12-14 June 2012, Calgary, Alberta, Canada.*

Wei W. and Gates I. D., On the Relationship between Completion Design, Reservoir Characteristics, and Steam Conformance Achieved in Steam-based Recovery Processes such as SAGD; *SPE 129694, Presented at SPE Improved Oil Recovery Symposium, 24-28 April 2010, Tulsa, Oklahoma, USA.*

World Energy Council, Natural Bitumen and Extra-Heavy Oil 2010; *Survey of energy resources 22 ed.*

Wright W. A. ASTM Viscosity Index Tables Calculated from Kinematic Viscosity; *American Society for Testing Materials. York, Pennsylvania, U.S.A; 1965.*

Wu C. H., A Critical Review of Steam flood Mechanism; *SPE-6550, Presented at SPE California Regional Meeting, 13-15 April 1977, Bakersfield, California.*

Yazdani A. and Maini B. B., Measurements and Modelling of Phase Behaviour and Viscosity of A Heavy Oil/Butane System. *Journal of Canadian Petroleum Technology, Vol. 49, pp. 9-14,February 2010.*

Yee C. T., and Stroich A., Flue Gas Injection Into a Mature SAGD Steam Chamber at the Dover Project (Formerly UTF); *Journal of Canadian Petroleum Technology, Vol. 43, pp. 54-61, January 2004.*

Zhang W., Youn S. and Doan Q., Understanding Reservoir Architectures and Steam-Chamber Growth at Christina Lake, Alberta, by Using 4D Seismic and Crosswell Seismic Imaging; *SPE Reservoir Evaluation & Engineering, Vol. 10, pp. 446-452, October 2007.*